CHALMERS
UNIVERSITY OF TECHNOLOGY

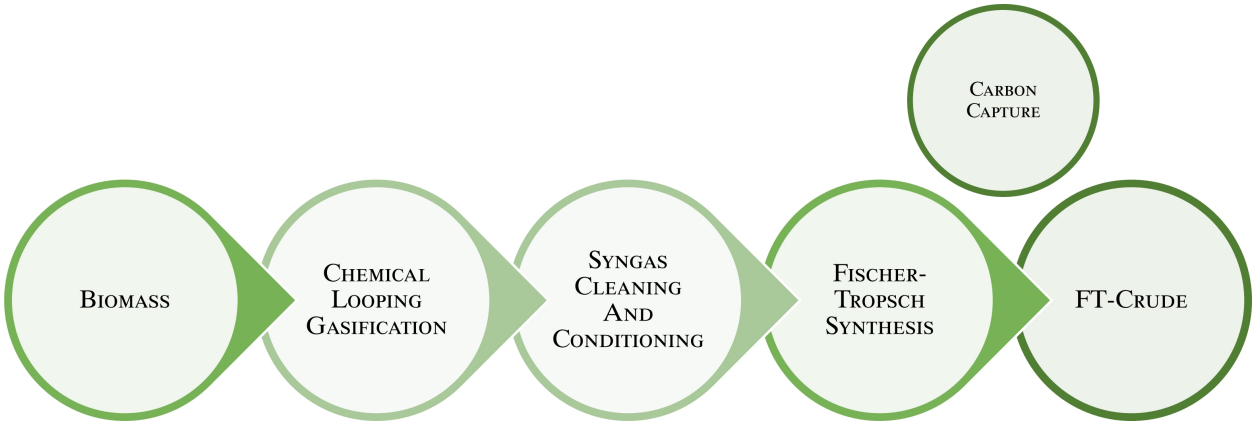

Process analysis of chemical looping gasification (CLG) of biomass for liquid fuel production with net-negative CO_2 emissions

Master's thesis within Nordic Master Programme in Innovative and Sustainable Energy Engineering

THARUN ROSHAN KUMAR

Department of Space, Earth and Environment
CHALMERS UNIVERSITY OF TECHNOLOGY
Gothenburg, Sweden 2019

Master's thesis 2019

Process analysis of chemical looping gasification (CLG) of biomass for liquid fuel production with net-negative CO_2 emissions

THARUN ROSHAN KUMAR

CHALMERS
UNIVERSITY OF TECHNOLOGY

Department of Space, Earth and Environment
Division of Energy Technology
Chalmers University of Technology
Gothenburg, Sweden 2019

Process analysis of chemical looping gasification (CLG) of biomass for liquid fuel production with net-negative CO_2 emissions
THARUN ROSHAN KUMAR

Supervisor: Tobias Mattisson, Department of Space, Earth and Environment
Co-supervisor: Mika Järvinen, School of Engineering, Aalto University
Examiner: Tobias Mattisson, Department of Space, Earth and Environment
Co-Examiner: Ville Vuorinen, School of Engineering, Aalto University

Master's Thesis 2019
Department of Space, Earth and Environment
Division of Energy Technology
Chalmers University of Technology
SE-412 96 Gothenburg
Telephone +46 31 772 1000

Cover: Integrated process chain of biomass-to-liquid fuel production through CLG and Fischer-Tropsch synthesis with carbon capture

Printed by Chalmers Reproservice
Gothenburg, Sweden 2019

Process analysis of chemical looping gasification (CLG) of biomass for liquid fuel production with net negative CO_2 emissions

THARUN ROSHAN KUMAR
Department of Space, Earth and Environment
Chalmers University of Technology

Abstract

Biomass gasification integrated with downstream Fischer-Tropsch (FT) synthesis for the production of liquid biofuel is a potential pathway to decarbonize growing transportation sectors such as aviation and maritime sectors. Chemical Looping Gasification (CLG) is a novel gasification technology that resembles indirect gasification in circulating fluidized bed, but instead of inert bed material (e.g. olivine), so-called oxygen carrier (OC), metal-oxide particles are utilized. The OC particles undergo cyclic oxidation and reduction in the air reactor and the fuel reactors, respectively, providing heat and oxygen for gasification. Thus, the raw syngas produced is more oxidized than in a conventional gasifier, with a lower concentration of tar and a higher concentration of CO_2. Capturing and storage of CO_2 during the subsequent gas cleaning stages would result in FT-crude production with net-negative CO_2 emissions. For evaluating the performance of an integrated biomass-to-liquid (BTL) process with CLG as the primary gasification technology, an integrated process model was developed and analyzed using Aspen Plus® simulation software. The CLG process model was modelled with a thermal input of 100 MW_{th} of waste biomass and was complemented with Fortran statements to calibrate thermodynamic equilibrium deviations, experienced during associated experimental activities or reported in the literature. LD-slag, an inexpensive and readily available by-product from steel production, was used as the primary oxygen carrier in the process models. The core gasification models were validated with experimental data from the chemical looping gasification tests done at Chalmers research boiler/gasifier with wood pellets and LD-slag as bed material. The gasification model predicts syngas composition, energy content and cold gas efficiency in good agreement with published data. Syngas with a high energy content of 12 MJ/Nm^3 (LHV basis) is predicted with an average cold gas efficiency of 56.6%. A high CO_2/CO ratio is also predicted in the syngas produced, which would be suitable for carbon capture. The integrated model estimates an FT-crude production of approximately 359 barrels per day with a CO_2 capture capacity of 138.5 $ktCO_2$/year. The integrated model has an average chemical efficiency, i.e. the conversion efficiency of biomass-to-FT crude of 22.8% with the chosen operating conditions. Heat integration studies show that there are adequate heat recovery possibilities for co-generation of steam and power.

Keywords: chemical looping, biomass, gasification, Fischer Tropsch Synthesis, oxygen carriers, LD-slag

Acknowledgements

This thesis work was carried out under the framework of the project "Kemcyklisk förgasning av biomassa för produktion av biodrivmedel" (CLG of biomass for production of biofuel), financed by Swedish Energy Agency: Project 43220-1

Firstly, I would like to thank *Tobias Mattisson*, *Magnus Rydén* and *Carl Johan Linderholm* for giving me the opportunity to work on this project. I am greatly thankful to my supervisors for their invaluable insights and guidance, without whom this thesis would not have been possible.

Special thanks to *Viktor Stenberg* for his inputs and sharing his knowledge with process modelling on Aspen Plus. I would also like to thank my supervisor, *Mika Järvinenen*, at Aalto University. Thanks to everyone at the Division of Energy Technology and colleagues in the thesis workers room. I would like to express my gratitude towards the OC group for all the interesting discussions during the lunch seminars.

Finally, I would like to thank my friends and family for getting me through this phase of life. Thanks to my brother and my father for their love, support and inspiration. This thesis is dedicated to the memory of my late mother, *Padmaja Menon* for her endless love and for being my constant source of encouragement.

Tharun Roshan Kumar, Gothenburg, September 2019

Contents

List of Figures

List of Tables

Nomenclature

Abbreviations

AEA	Aspen Energy Analyzer
AFR	Air-to-fuel ratio
AGR	Acid gas removal
AR	Air reactor
ASU	Air separation units
ATR	Autothermal reformer
BE-CCS	Bioenergy with carbon capture and storage
BFB	Bubbling fluidized bed
bio-SNG	Biomass-based synthetic natural gas
BTL	Biomass-to-liquid
BTX	Benzene, toluene and xylene
CBTL	Indirect coal-biomass-to liquids
CCS	Carbon capture and storage
CCU	Carbon capture and utilization
CFB	Circulating fluidized bed
CGE	Cold gas efficiency
CLC	Chemical looping combustion
CLG	Chemical looping gasification
CLG-FT	Chemical looping gasification-Fischer-Tropsch
DCOALIGT	IGT coal density model
DFB	Dual fluidized bed
DME	Dimethyl ester
EF	Entrained flow
EU	European Union
FICFB	Fast internally circulating fluidized bed
FR	Fuel reactor
FT	Fischer-Tropsch
FT-crude	Heavier hydrocarbon products from FT synthesis
FT-diesel	Long-chained hydrocarbons with carbon number, ranging from C_{12}-C_{19}
FTS	Fischer-Tropsch synthesis
GCC	Grand composite curve
GHG	Greenhouse gas
GoBiGas	Gothenburg Biomass Gasification
HCOALGEN	General coal model for computing enthalpy in Aspen Plus
HEN	Heat exchanger network

HHV	Higher heating value	
HP	High pressure	
HTFT	High temperature Fischer-Tropsch	
IEA	International Energy Agency	
IGT	Institute of Gas Technology	
ILUC	Indirect land-use change	
IPCC	Intergovernmental Panel on Climate Change	
LD	Linz-Donawitz	
LDS-57	LD-slag with 43% inert sand dilution	
LDS-80	LD-slag with 20% inert sand dilution	
LHV	Lower heating value	
LP	Low pressure	
LTFT	Low temperature Fischer-Tropsch	
MDEA	Methyldiethanolamine	
MC	Moisture content	%
MDEA/PZ	Methyldiethanolamine/piperazine	
MEA	Monoethanolamine	
MP	Medium pressure	
Naphtha	Long-chained hydrocarbons with carbon number ranging from C_5-C_{11}	
OC	Oxygen carrier	
OL-AA	Olivine – artificially activated	
OTC	Oxygen transport capacity	
PG	Purge gas	
PR-BM	Peng-Robinson equation of state with Boston-Mathias modifications	
RME	Rapeseed methyl ester	
SF	Split fractions	
S/B	Steam-to-biomass ratio, (mass-basis)	
SNG	Synthetic natural gas	
SYN-CLN	Syngas cleaning model	
WGS	Water-gas shift	
Symbols		
$\dot{m}$	Mass flow	kg/s
ΔH	Heat of reaction	$kJ/mole$
ΔTmin	Minimum approach temperature	K
G_v	Total syngas flow	Nm^3/s
MeO	Metal oxides	–
n_i	Mole fractions	–
R_o	Oxygen ratio	–
X	Conversion	%
α	Mechanism factor	–
η	Efficiency	%
Indices/Exponents/Subscripts		
$biomass$	Biomass feed on a dry ash-free basis	
ch	Chemical	

co	Carbon monoxide	
$comb$	Combustion	
ct	Tar species	
$d.b$	Dry basis	
daf	Dry ash-free basis	
$e, consumed$	Electricity consumed	
e, net	Net electricity	
$e, produced$	Electricity produced	
el	Electricity	
f	Feed	
$fuel$	Biomass fuel	
i	Gas species	
in	Inlet	
is	Isentropic	
m	Hydrogen atoms	
min	Minimum	
n	Carbon atoms	
ox	Oxidized	
p	Oxygen atoms	
$product$	FT-crude products	
red	Reduced	
sg	Syngas	
sys	System	
$temp$	Temperature	$°C$
v	Standard volume	Nm^3
x	Metal atoms in metal oxides	
y	Oxygen atoms in metal oxides	

1

Introduction

Greenhouse gas emissions (GHG) from human activity are one of the primary reasons for the fateful climate emergency due to global warming. Carbon dioxide (CO_2) emissions from fuel combustion accounted for nearly two-thirds of total GHG emissions in 2015, of which the transportation sector contributes around a quarter of the global CO_2 emissions [1]. Transportation is the third largest contributor to global CO_2 emissions and the road transportation sector accounts for nearly two-thirds of the entire transportation sector [1]. According to the Intergovernmental Panel on Climate Change (IPCC) special report on global warming of 1.5°C [2], limiting global warming temperature rise below 1.5°C would require 45% reduction of CO_2 emissions of the 2010 level by 2030 and net-zero CO_2 emissions by the year 2050. It also states that if significant CO_2 emissions reduction are not achieved by the year 2030, the reliance on CO_2 removal technologies would drastically increase, in addition to this, almost all forecasted pathways to return to a global warming of 1.5°C, indicate a need for CO_2 removal technologies in the future to make up for the remaining emissions and achieve net-negative emissions. Bioenergy with carbon capture and storage (BE-CCS) is one of the CO_2 removal technologies that can potentially achieve net-negative emissions. With rising CO_2 levels in the atmosphere and fast depleting carbon budget, there is an immediate need for deployment of not only CCS technologies but also carbon capture and utilization (CCU) technologies to support growing sectors like aviation, that are still heavily reliant on fossil fuels.

Transport biofuels are one of the promising pathways to decarbonize the transportation sector that is still heavily dependent on petroleum products. It can reduce countries dependence on crude oil imports, reduce price volatility and contribute to the replacement of conventional transport fuels such as diesel and gasoline with little to no changes to the current fuel distribution network. According to IEA's Technology Roadmap: Biofuel for Transport [3], biofuels can potentially provide 27% of the total transport fuel demand in the year 2050. Biofuels such as ethanol derived from food crops are used mainly as additives or blends with gasoline to tackle rising crude oil prices and lower vehicular- GHG emissions. However, there are uncertainties regarding the actual GHG emissions savings from these biofuels, while considering the GHG emissions over its full life cycle of production [4]. It is estimated that the actual GHG emissions from corn-based ethanol could increase emissions as opposed to the previous estimates of a 20% savings in emissions, as a result of land-use change patterns [5]. In contrast to this, sugarcane ethanol is estimated to have a lower impact of indirect land-use change (ILUC) and hence, relatively higher GHG emissions savings, making it a feasible alternative to corn-based ethanol [6], [7]. Biodiesel derived from plants were estimated to have no GHG savings and in most cases had higher GHG emissions compared to fossil fuels owing to ILUC. However, bioethanol and biodiesel from waste woods were estimated to have the highest GHG savings. Uncertainties concerning the impact of land-use change and its plausible effect on

food prices, make it imperative to utilize sustainable biomass to produce advanced biofuels such as methanol, synthetic natural gas (SNG), and synthetic liquid fuels from Fischer-Tropsch synthesis (FTS) process. Waste biomass could include both agricultural, forest or industrial waste streams.

Fluidized bed systems could either be a bubbling fluidized bed (BFB) or a circulating fluidized bed (CFB), based on the fluidization regimes. A BFB generally has a low fluidization velocity, that mainly uses solid-solid heat transfer whereas circulating fluidized bed (CFB) utilizes higher fluidization velocities, that circulates bed particles from the reactor through a cyclone and a loop-seal [8]. Liquid fuel synthesis from biomass gasification requires syngas with high calorific content and little to no contaminants. Syngas is mainly composed of hydrogen and carbon monoxide with some fractions of CO_2 and steam, depending upon the gasification conditions. Syngas with high calorific value is preferable in any downstream fuel synthesis processes and to achieve this nitrogen dilution of syngas must be minimized. In order to prevent dilution of fuel gases with air, the required oxygen required for gasification can be provided with pure oxygen or by preventing direct contact between the fuel and air through reactor design measures. To produce syngas with higher calorific value compared to conventional gasification with air, pure oxygen is proposed as an alternative fluidizing medium along with steam; however, this requires expensive air separation units (ASU) like pressure swing adsorbers or cryogenic distillation to supply pure oxygen to the gasifier.

Indirect gasification of biomass is another technology capable of producing high energy-content syngas, relatively free of diluents using internally circulating fluidized bed system, as first proposed by H. Hofbauer et al. [9]. This technology, however, emits CO_2 from its combustor, as shown in Figure 2.4, and would require CO_2 compression units to capture the CO_2 in the air-diluted flue gas, which would result in severe economic and energy penalty on its overall process. Gothenburg Biomass Gasification (GoBiGas) plant is the only industrial-scale advanced fuel production plant that employs indirect gasification; using a 32 MW_{th} dual fluidized bed (DFB) boilers for woody-biomass gasification. It uses a bubbling fluidized bed (BFB) boiler as the gasifier and a circulating fluidized bed (CFB) boiler for heat generation and has a biomethane production capacity of 20 MW [10].

Chemical looping gasification (CLG) of waste biomass for syngas production is a potential technological pathway to produce high-quality syngas for downstream carbon-neutral fuel production such as dimethyl ether (DME), methanol, SNG or FT-diesel. This process is based on the technology: chemical-looping combustion (CLC) where interconnected circulating fluidized beds (CFB) are used to combust solid fuels in fuel reactor (FR) with the help of oxygen carriers (OC), as shown in Figure 1.1.

OC are usually metal oxide particles that undergo a reduction in the FR and provides enough oxygen for combustion. The OC particles are then oxidized with air in the air reactor (AR), and this cyclic oxidation-reduction cycles of the OC pre-

vents direct contact of fuel with air, resulting in a concentrated stream of CO_2 from the FR and nitrogen-rich air from the AR. This process can significantly reduce costs and energy penalties associated with carbon sequestration [12]. In addition to this, there are no costs associated with ASU as in the oxyfuel combustion process. CLC with biomass as fuel can potentially remove CO_2 from the atmosphere, hence achieving net-negative emissions at low cost.

Chemical looping gasification process is based on indirect gasification to produce syngas while employing the benefits of replacing sand bed material with oxygen carrier particles as done in CLC operations. The oxygen carriers will add an additional pathway for fuel conversion in the fuel reactor, generating combustion and gasification products. In addition, the oxygen carrier will be reduced to some extent. In comparison to indirect gasification,this results in a more oxidizing environment in the gasifier; hence, tar formation is expected to be lower with higher conversions of fuel in the FR. Further, as the heat necessary for heating the oxygen carrier particles is generated by the exothermic oxidation of the metal in the air reactor, no carbon needs to be transferred to the air reactor. CO_2 can, therefore, be restricted to the fuel reactor. Thus, a raw syngas with just CO_2 as the diluent is achieved.The CO_2 in the syngas stream is however at a higher concentration than conventional biomass gasification systems, making it amiable for capture. Nitrogen dilution of the product gas is avoided and restricted to the AR, and this stream can ideally be cooled down to ambient temperature for heat recovery as it is free from any other contaminants. Lower volumes of diluents and tar in the syngas can reduce costs related to carbon capture and gas cleaning, respectively.

Using sustainable waste biomass as fuel in CLG operation with CCS can potentially enable the production of high-quality syngas for liquid fuel production with net-negative emissions for the overall biomass-to-liquid (BTL) fuel production process. This could bring a breakthrough to attain a carbon-free transportation sector while replacing the demand for conventional transportation fuels up to some extent.Thereby preventing expected future CO_2 emissions with the possibility to

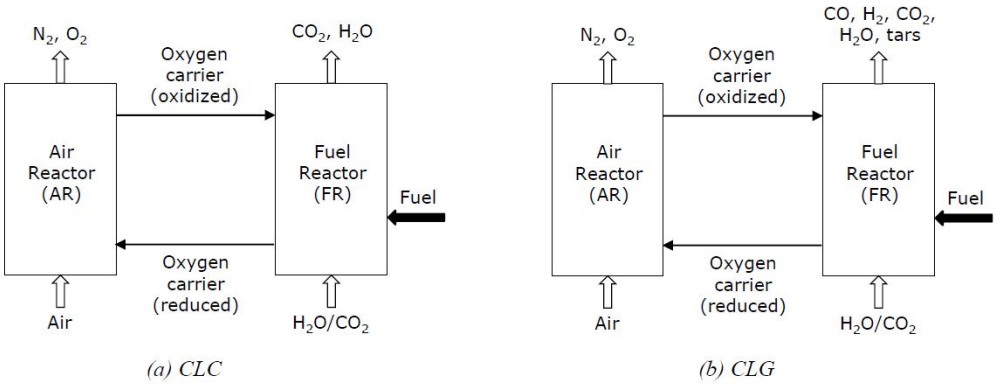

Figure 1.1: Process schematic of (a) chemical looping combustion and (b) chemical looping gasification(CLG) [11]

replace fossil fuels and at the same time achieve net negative emissions through its production process, that could be a highly climate-efficient endeavour. More specifically, liquid fuel production through CLG is a potential pathway to decarbonize growing transportation sectors such as aviation and maritime sectors, where electrification is technologically challenging. Thus, FT-crude production through Fischer-Tropsch synthesis is the primary fuel synthesis process chosen in this thesis. Therefore, depending on the system boundary, ideally, the produced biofuel through this integrated process can potentially be carbon negative to carbon neutral. An integrated process model of a CLG plant for liquid fuel production through FTS is developed, and heat integration of the overall plant is performed in this thesis.

1.1 Project Objectives

The project objectives of this master thesis are to study the production of FT-crude from biomass using chemical looping gasification as the primary process for gasification. More specifically the aim is to,

- Develop a process model of a chemical looping gasification plant and its subsequent gas cleaning steps in Aspen Plus® software
- Conduct a thermal evaluation of the gasification process to determine optimal process parameters for gasification
- Integrate an existing Fischer-Tropsch synthesis model to the developed gasification model for the downstream utilization of produced syngas
- Heat integration of the overall process components in the integrated model
- Determine essential parameters such as cold gas efficiency, overall process efficiency, fuel production capacity and CO_2 capture potential
- Identify process constraints and the future key areas of research

2

Background

A typical biomass-to-liquid (BTL) fuel chain involves five stages, namely, biomass pre-processing or pretreatment, gasification, gas cleaning, gas processing and fuel synthesis stage, as shown in Figure 2.1. It is a multi-stage process that employs the thermochemical conversion route of biomass to produce synthetic fuels.

Depending on the source and the type of biomass, feedstock pretreatment steps are decided. The composition of produced syngas depends on the various operational parameters of the gasification process, the gasifying agent used and reactor technology. The degree of syngas cleaning and syngas processing is dependent on the desired fuel product in the downstream fuel synthesis stage. Each stage of the BTL fuel chain is described more in detail in the following sections with CLG as the primary gasification technology with FTS as the downstream fuel synthesis stage.

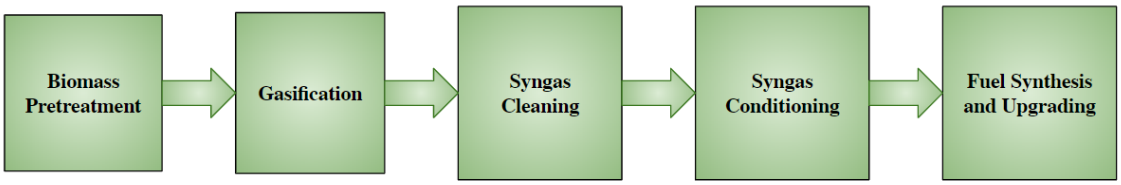

Figure 2.1: Overview of the biomass-to-liquid fuel chain

2.1 Biomass as fuel

Biomass is defined as any organic material obtained from plants and animals and it mainly consists of carbon (C), hydrogen (H), oxygen (O), nitrogen(N) and minute amounts of sulphur (S). Plants through photosynthesis convert atmospheric CO_2 to organic compounds, and it could be considered carbon-neutral, as it captures atmospheric CO_2 and releases it back into the atmosphere by combustion or by wood decay [13]. Biomass can be classified based on the source – primary and waste biomass. Primary biomass includes biomass-derived directly from wood, plants and crops. Waste biomass includes municipal solid wastes, wastes from agriculture, forest residues and industrial wastes [8].

Waste biomass, as a potential source of energy for heat and power generation, is seen as an attractive alternative to fossil fuels to mitigate climate crisis and achieve emissions reduction targets. This is mainly because of its costs and the only renewable energy source that reduces lifecycle GHG emissions with no or low attached social, economic or environmental impacts.

In addition to this, waste biomass such as forest residues has a high theoretical utilization potential in countries such as Finland and Sweden with large forestry industries. The utilization potential of biomass, in general, remains highly contentious as it depends on local conditions, the source of biomass, and with respect to forest residues, the sustainability of forest management and harvesting. According to the World Bioenergy Association, a global biomass potential of 150 EJ is estimated globally by the year 2035 increasing from 52.6 EJ in 2012 and roughly 52% of it coming from forests that include forest residues, wood fuel and forest industry by-products [14]. Agricultural waste streams also have excellent potential as these residues are generally burnt in open fields, causing more pollution. Demand for agricultural waste could also give the rural communities an added source of income. In comparison with woody biomass, agricultural waste biomass, generally have lower LHV with higher nitrogen and ash content [15]. In Table 2.1, proximate and ultimate analyses of forest residues and agriculture wastes are listed, on a dry-basis. On an as-received basis, wheat straw tends to have lower moisture content ranging from 10-15% as compared to 30-50% in the forest residues [15], [16]. More information on biomass feedstock in relation to CLG can be found in [16].

Table 2.1: Ultimate and proximate analyses of forest and agricultural waste streams [15]

	Forest residues[1]	**Forest residues**[2]	**Wheat straw**
Proximate analysis (wt. % d.b)			
Volatile Matter	79.3	74.1	77.7
Fixed Carbon	19.37	21.85	17.59
Ash	1.33	4.05	4.71
Ultimate analysis (wt. % d.b)			
C	51.30	51.00	47.30
H	6.10	5.80	5.87
O	0.40	0.90	0.58
N	40.85	38.21	41.49
S	0.02	0.04	0.07
Ash	1.33	4.05	4.71
HHV (MJ/kg d.b)	20.67	20.54	18.94

[1]*Sweden*, [2]*Denmark*

In Table 2.1, the higher heating value (HHV) is given on dry basis, and the lower heating value (LHV) of forest residues chips is roughly between 18-19 MJ/kg on a dry basis. Biomass accounted for approximately 9% of the world primary energy supply in 2015 [3]. Consumption of biomass in the energy sector shows that it is predominantly consumed as a traditional source of energy in the developing countries, followed by the heat generation industry and co-generation of heat and power, which accounts for nearly 16% and 13% respectively [3]. Forest residues from sustainable forestry are considered as a low-risk biofuel feedstock due to its abundance and utilization potential in EU [17]. The current forest industry infrastructure in northern Europe can complement a biomass-to-fuel chain in the future and provide integration possibilities and minimize costs related to logistics and biomass pre-processing.

2.1.1 Biomass in the transportation sector

Biofuels or fuels derived from biomass can be categorized based on the source of biomass. Biofuels currently in use, are predominantly conventional biofuels such as bioethanol and biodiesel from vegetable oils. Bioethanol is mainly derived from food crops with high sugar content, grown on agricultural land. They are coming under increased scrutiny in recent years as they could cause agrarian land-use change and increase food prices [5]. Advanced biofuels are derived from lignocellulosic biomass, agricultural and forest residues that do not have any impact on land-use patterns. Fuels such as FT-diesel, DME, alcohols and SNG are some examples of advanced biofuels.

Utilization of biomass as feedstock to produce transportation fuels either for blending or direct replacement will enable a low carbon transportation sector in the future. Approximately 96% of the total energy consumption in the transportation sector in 2012 was petroleum products [18], and it was estimated that it would reduce to 88% in the year 2040. In 2016, only a meagre 3% of the total road transportation was met with biofuels [3]. In addition to road transportation, biomass-derived liquid fuels could be a potential pathway to decarbonize sectors such as aviation and maritime sectors.

In this thesis, forest residue from Sweden is chosen as the primary feedstock for the CLG plant model developed and its ultimate, and proximate analysis are listed in Table 2.1. Waste biomass such as forest residues is especially interesting in a gasification process for fuel production as it contains higher volatile matter and relatively lower sulphur and ash content. Chemical looping gasification is highly applicable for biomass fuel since there are several oxygen carrier materials developed for gaseous fuels, such as methane, natural gas, thus highly applicable for high-volatile fuels such as biomass [19], [20].

2.2 Biomass pre-processing

Biomass pre-processing or pretreatment is an essential step before its utilization as feedstock in a gasifier and especially crucial for a gasification process integrated with downstream fuel synthesis. Waste biomass streams tend to have an inherent drawback, its inconsistency in composition, and this negatively impacts the downstream gasification and fuel synthesis process. An extensive review of feedstock variability and its impact on biofuels production was done by Williams et al. [21]. For an efficient gasification and fuel synthesis process, it must undergo a series of pre-processing steps before it can be used in the gasifier. These steps could either be chemical, physical or thermal treatment processes that can reduce the feedstock particle size and composition to a more uniform homogeneous feedstock that can be fed into the system with ease. Biomass pretreatment is imperative to achieve an efficient gasification process, although the extent is not completely clear as it depends on various factors, including economic and technical. The pretreatment method and its specifications vary depending on the type of feedstock and the type

of gasifier used in the process, respectively. The impact of various pretreatment methods was studied by Isaksson et al. [22] for a biomass gasification plant with an entrained flow (EF) gasifier and downstream FT crude production plant that was integrated with a pulp and paper mill. The different FT production routes with different pretreatment alternatives that were examined are shown in Figure 2.2.

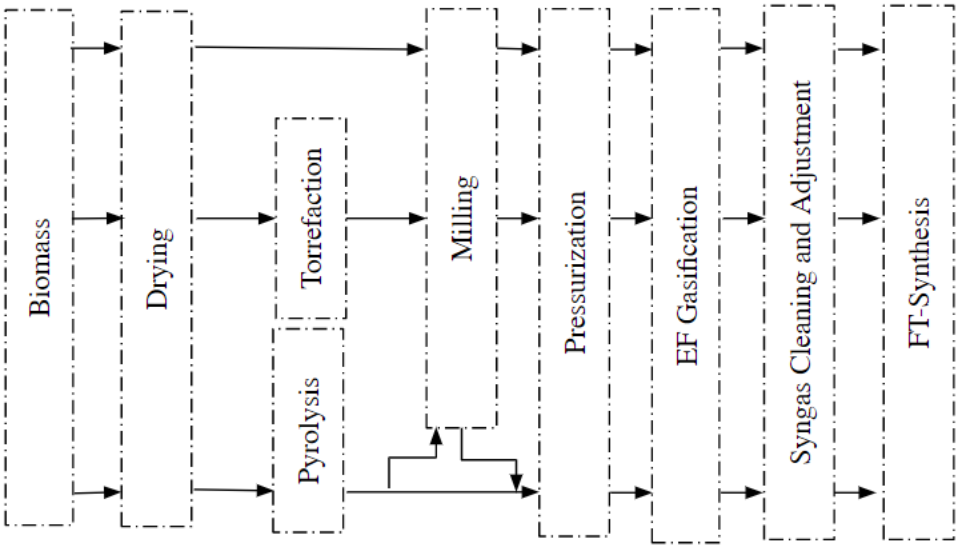

Figure 2.2: Syngas transformation routes to alternative fuels

Although the study was done for an EF gasifier, their results on FT production efficiencies, give an indication on how an overall biomass-to-liquid fuel integrated plant could be affected with different pretreatment methods, which is relevant with respect to the integrated CLG-FT plant modelled in this thesis. For a thermal input of 300 MW_{HHV}, FT-crude energy yield (%) or chemical efficiency (%) of roughly 43% and 52% was reported for the once-through FTS case and recycling FTS case, respectively [22]. However, a relatively high CO conversion (X_{co} of 90% per pass is assumed in their FT synthesis stage. CLC and CLG are based on fluidized bed technology, commonly used for conversion of waste fuels, the degree of pretreatment needed may be less than in other technologies. For example, in the GoBiGas plant, the main objective was to achieve feasible gasification operation with minimal pretreatment for forest residues with high moisture content (≈30-50%). Methane production with high conversion efficiencies (>75% on a higher heating value basis) was achieved with wood pellets that generally has a lower moisture content compared to forest residue [10], [23]. However, based on their experience, an on-site fuel drier was recommended to alleviate problems arising due to the varying moisture content of different forest residues received on site.

Drying is a critical step for gasification processes that are sensitive to the high moisture content in the biomass feedstock. Milling and grinding are generally necessary to reduce the particle size of biomass, that ensures a smooth feeding operation into the gasifier. In this thesis, the pretreatment steps like drying are not considered while modelling, as CLG is expected to tolerate fuel with high moisture content. How-

ever, surplus heat is expected in the integrated process plant that could be used for integrating a fuel drier before the gasifier. The only prerequisite is that there must be considerable technical and operational benefits that outweigh economic aspects associated with the integration of a drier unit to the CLG plant.Problems associated with biomass ash can also be expected during CLG operations, such as ash sintering in the FR. This is due to the generally lower ash melting point (≈800°C) of biomass ash [24]. This potential problem can be limited through certain pretreatment methods. In addition to this, likely ash interactions with the oxygen carriers are also expected, that requires selection of OC particles that are compatible with ash.

2.3 Chemical Looping Gasification

2.3.1 Background

Chemical looping gasification (CLG) is a promising gasification process that incorporates the chemical looping concept to convert low-value carbonaceous feedstock such as biomass to produce high-value products such as syngas. Syngas can be further processed downstream to produce fuels like synthetic natural gas, hydrogen or even liquid fuels like dimethyl ether, methanol and FT-crude through the Fischer-Tropsch process. Along with H_2 and CO, CO_2 is also produced, that is restricted to the fuel reactor, which will be captured in the acid gas removal (AGR) process downstream and the CO_2 removal unit in the FT plant, hence an opportunity to achieve net-negative CO_2 emissions from the overall production process.

In the recent past, chemical looping combustion (CLC) of solid and gaseous fuels has been extensively investigated, as a potential breakthrough technology for power production that avoids substantial economic and energy penalties associated with carbon capture and storage [12], [25], [26]. In the 100 kW CLC plant at Chalmers, a CO_2 capture efficiency of 98-99% was achieved, and an efficiency penalty of less than 3% was estimated when compared to similar CFB plants[27]. It is, therefore estimated to have high carbon capture efficiencies along with high solid-fuel conversion; however, the only challenge is achieving a high degree of gas conversion [25]. CLG works on the same principle as CLC; however, with a different objective, shown in Figure 2.3.

Complete oxidation of fuel is considered undesirable, unlike the CLC process. However, the characteristic feature of both the processes is the inherent ability to avoid nitrogen dilution, along with high carbon conversion in the fuel reactor (FR) that restricts CO_2 only to the FR for downstream carbon capture. CLG, although based on CLC, its operation is similar to indirect gasification process, as shown below in Figure 2.4. Indirect biomass gasification involves gasification of biomass using steam and prevents nitrogen dilution by reactor design measures and thus preventing fuel and air contact, as shown in Figure 2.4. The inert bed material in these reactors acts as the heat carrier which provides the heat required in the gasifier from the combustor, where a portion of the fuel is combusted. A product gas with low nitrogen content close to 2.5% and calorific content more than 13 MJ/Nm^3 was achieved in

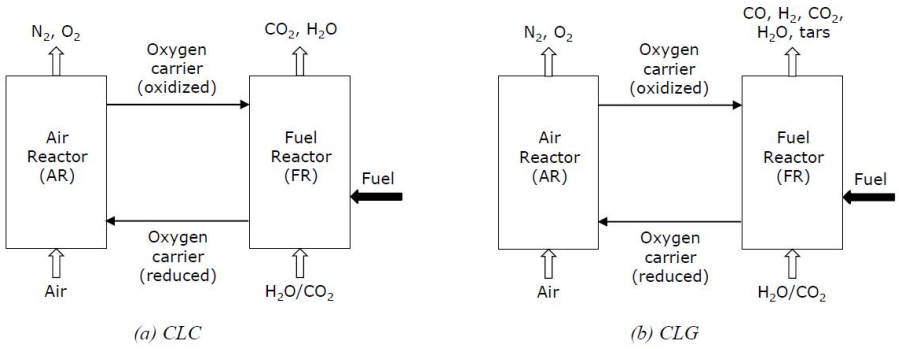

Figure 2.3: Process schematic of (a) chemical looping combustion and (b) chemical looping gasification(CLG) [11]

the fast-internally circulating fluidized bed (FICFB) demonstration plant in Vienna [9]. Although this process generates a high energy content syngas from gasification, it still emits a significant amount of CO_2 from the combustor and would require a post-combustion CCS plant to capture the CO_2 emissions from the combustor. It is important to note here, that the CO_2 produced in the combustion zone is diluted with air, hence larger volumes of gas that needs to be handled for carbon capture process which in turn increases the carbon capture costs.

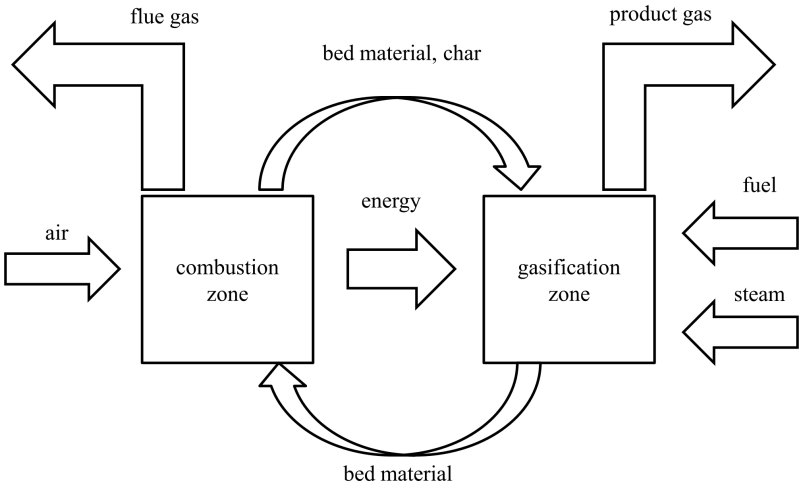

Figure 2.4: Process schematic of indirect gasification process [9]

In contrast to this, CLG employs metal oxide particles as the bed material, instead of inert bed material, that undergoes cyclic oxidation and reduction reactions in the gasifier and the combustor, respectively. The combustor here is generally referred to as the air reactor (AR), where the reduced metal oxide particles are regenerated with air. The heat required in the highly endothermic gasification reactions in the fuel reactor is provided by the circulating oxygen carrier (OC) particles from the air reactor where the exothermic oxidation of oxygen carriers takes place. This results in a nitrogen-rich air from the air reactor and product gas with minimal diluents from the fuel reactor. CLG of a low-value carbonaceous feedstock such as biomass is possible without it coming in direct contact with air; thus a concentrated stream

of gasification gases is produced, mainly consisting of H_2, CO, CO_2 and H_2O [11]. Gas contaminants such as H_2S, NH_3 and other tar components is also expected to be present along with the product gas that would require downstream cleaning processes to utilize the syngas for fuel production. The syngas composition would, however, depend on various operational parameters such as gasification temperature and pressure, including the kind of OC particle used in the process.

In CLG, all the carbon is converted in the FR, see Figure 2.3, and thus the syngas of CO and H_2 will be diluted with a somewhat higher CO_2 concentration than in the indirect gasification process. However, a lower volume of gases that is amiable for carbon capture, when compared to indirect gasification. Hence, it is believed that CLG could be more efficient and feasible with respect to the combination of fuel production with carbon capture. A higher CO_2/CO ratio is expected in CLG when compared to indirect gasification indicating the higher oxidizing environment, that may limit tar formation in the FR. Additionally, replacing inert bed material with metal oxide particles will have added advantages such as the catalytic effect towards tars and improved char gasification rates due to lattice oxygen uncoupling and lowered species that inhibit char gasification rates [26], [28], [29]. Ideally, CLG must have high yields of high-quality syngas, low tar yields and high carbon-conversion in the FR with no leakage to the AR [30].

In comparison with other gasification technologies, syngas produced from air-blown gasifiers usually contains high volumes of nitrogen (>40% by volume) with a lower heating value generally between 3-8 MJ/Nm^3 that makes it unsuitable for any downstream fuel synthesis process and is generally preferred for power production applications. Steam/oxygen-blown gasifiers can produce syngas with comparatively higher energy content, ranging from 10.3-13.5 MJ/Nm^3, as it avoids nitrogen dilution by using a mixture of steam and pure oxygen to provide sufficient oxygen for gasification. Table 2.2 shows the different gas compositions resulting from biomass gasification using different gasifying agents. Syngas from steam/O_2 gasification, with relatively higher energy content, requires high energy-consuming ASU to supply pure oxygen. In this regard, CLG basically eliminates the need for pure oxygen from ASU, as a result of using oxygen carrier particles as the circulating solids in an interconnected CFB with steam as the gasifying agent.

CLG operations have been experimentally investigated using different reactor configurations, various oxygen carriers and feedstocks in recent years. Gasification of rice husks with natural hematite as oxygen carrier performed by Ge et al. [32] in a 25 kW BFB where it was demonstrated that stable operation with sand was attained when the iron ore content in the bed material was increased above 40 wt.%. They reported an optimum gasifier temperature of 860°C where the syngas yield was the highest with a carbon conversion efficiency around 85% and the corresponding raw syngas mainly consisted of H_2, followed by CO, CO_2 and with a hydrocarbon (CH_4 + C_2H_6) concentration of around 13.8%. Other CLG investigations include gasification of pine sawdust in a DFB gasifier with iron ore as oxygen carrying material for hydrogen production [33], CLG of pine sawdust in a BFB gasifier with

Table 2.2: Gas compositions of biomass-derived syngas for different gasifying agents [31]

Gasifying agent	Air	Steam-O_2	Steam[1]
Operating Conditions			
ER	0.18-0.45	0	0.24-0.51
S/B (kg/kg_{daf})	0.08-0.066	0.53-1.10	0.48-1.11
T (°C)	780-830	750-780	785-830
Gas Composition (vol%)[2]			
H_2	5.0-16.3	38-56	13.8-31.7
CO	9.9-22.4	17-32	42.5-52.0
CO_2	9.0-19.4	13-17	14.4-36.3
CH_4	2.2-6.2	7-12	6.0-7.5
C_2H_n	0.2-3.3	2.1-2.3	2.5-3.6
N_2	41.6-61.6	0	0
H_2O	11-34	52-60	38-61
Yields			
Tars (g/kg_{daf})	3.7-61.9	60-95	2.2-46
Char (g/kg_{daf})	-	95-110	5-20
Gas Yield (Nm^3/kg_{daf})	1.25-2.45	1.3-1.6	0.86-1.14
LHV (MJ/Nm^3)	3.7-8.4	12.2-13.8	10.3-13.5

[1] *Pure* [2] *Dry-basis*

Fe_2O_3/Al_2O_3 (70:30% by weight) as the oxygen-carrying material where a carbon conversion efficiency of 89% and hydrocarbon concentration of 6.8% was reported [34]. Both reported a positive effect of increasing fuel reactor temperature on the H_2/CO ratio, which is an essential parameter with respect to downstream fuel synthesis and is discussed in more detail in section 2.3.2. Huseyin et al. [34] reported a carbon conversion efficiency of 90% and gasification efficiency of around 78% at 900°C in the fuel reactor. CLG operation in the 10 kW Chalmers unit with high volatiles fuel such as wood pellets and black pellets with LD-slag as the OC was investigated in [11], where the estimated raw gas composition mainly comprised of H_2, CO_2, CO and CH_4. C_2-fractions were also detected in their experiments, however only in low concentrations. Hence, these results indicate that a syngas with gas compositions suitable for further downstream processing which could be utilized for fuel synthesis is possible to achieve. In addition to this, CLG operation with LD-slag as the OC was found to be feasible since its regeneration rates considering its fines production and particle lifetime were similar to regeneration rates of bed material in conventional CFB combustors [11].

2.3.2 Oxygen carriers

There has been significant research on the effect of various OC in both CLC and CLG process operations [26], [30], [35]. With respect to CLC, OC with a high rate of reaction and high oxygen ratios or maximum oxygen transport capacity

for a given mass flow of metal oxide is preferred, to fully convert the volatile gases. Whereas in CLG operation, complete combustion of volatile gases is undesired; thus, it is essential to employ specific oxygen transport control strategies as suggested by Pissot et al. [30] in order to achieve CLG behaviour, i.e. to partially oxidize the fuel to produce syngas. Here, oxygen ratio (R_o) or oxygen transport capacity is defined as the maximum oxygen that can be transferred between the two reactors, through cyclic oxidation and reduction, for a given mass flow of circulating OC particles [36] and calculated as shown below in Equation 2.1.

$$R_o = \frac{m_{ox} - m_{red}}{m_{ox}} \tag{2.1}$$

The oxygen carrier of interest in this thesis, is the steel converter slag from the Linz-Donawitz process, a by-product of the steel industry. It is a Fe-based material which is low-cost and is an abundantly available material. There is limited demand for it, for any other purposes. It mainly consists of CaO, Fe_2O_3, SiO_2 and other metal oxides, see Table 2.3. In addition, iron oxides and manganese oxides are known to generally have an oxygen transfer capacity of 3.3% and 7-10% by weight, respectively, depending on what oxides are considered [37]. Based on the tests done on LD-slag by Eliasson, F. [38] at Chalmers, the oxygen transfer capacity of LD-slag was found to be around 1.12%. This is relatively lower compared to other investigated OC for CLC, but it is especially interesting in CLG operations to limit oxygen transfer and volatiles combustion in the FR, up to a certain extent. The elemental composition of LD-slag is listed in Table 2.3.

Table 2.3: Elemental composition of LD-slag (wt.%) [30]

Composition	Fe_2O_3	MnO_2	SiO_2	CaO	MgO	Al_2O_3	TiO_2	K_2O
w/w %	26.6	3.3	11.9	39.8	9.1	1.2	1.3	<0.09

2.3.3 Chemical reactions

The reactions involved in the fuel reactor and the air reactor is described in the section. In chemical looping gasification of biomass, the reaction mechanism involves devolatilization, steam gasification of char and gas-solid reactions between the volatile gases and the oxygen carriers. Firstly, biomass devolatilizes into solid char, tar and volatile gases as shown in Reaction 2.2.

$$C_nH_{2m}O_p \longrightarrow Char + Volatiles(CO, H_2, CO_2, CH_4, C_nH_{2m}) + Tar \tag{2.2}$$

The main reactions during biomass gasification [8], are listed in the Table 2.4, including their enthalpy change at 25°C. In addition to this, Reaction 2.3 and 2.6 can be combined into one equation and written as in Reaction 2.7.

Table 2.4: Main reactions during biomass gasification [8]

Reaction Name	**ΔH** (kJ/mol)	**Reaction**
Steam gasification	+131	$C + H_2O \longrightarrow CO + H_2$ (2.3)
Boudouard reaction	+172	$C + CO_2 \longrightarrow 2\,CO$ (2.4)
Methane formation	-74.8	$C + 2\,H_2 \longrightarrow CH_4$ (2.5)
Water-gas shift reaction	-41.2	$CO + H_2O \longrightarrow CO_2 + H_2$ (2.6)

$$C + \alpha H_2O \longrightarrow (2-\alpha)CO + (\alpha-1)CO_2 + \alpha H_2 \tag{2.7}$$

The α value was experimentally determined for coal-gasification by Lee et al. [39], where the α varied between 1.1 and 1.5 for a gasification temperature between 750°C-900°C. Oxygen carriers provide lattice oxygen that is more likely to partially oxidize the fuel than gas-phase oxygen [32]. The overall reaction in the fuel reactor, i.e. the syngas production from the partial oxidation of biomass ($C_nH_{2m}O_p$) can be written as in Reaction 2.8.

$$C_nH_{2m}O_p + (n-p)Me_xO_y \longrightarrow nCO + mH_2 + (n-p)Me_xO_{(y-1)} \tag{2.8}$$

Volatile gases mainly consist of H_2, CO and CH_4. These gases can easily react with the oxygen carrier due to their redox properties and good gas-solid contact [40], and the volatiles combustion takes place in the fuel reactor as shown in Reaction 2.9. Here, they also react with volatile gases and undergo partial reduction and the overall reaction between the gases and oxygen carrier can be written as:

$$C_nH_mO_p + (n-p)Me_xO_y \longrightarrow nMe_xO_{(y-1)} + H_2O + CO_2 \tag{2.9}$$

Tars generally decompose into lighter hydrocarbons due to higher reactor temperatures and the presence of oxygen carriers such as Fe_2O_3 [32], [41]. This reaction could be written as:

$$Tar \longrightarrow H_2 + CO + hydrocarbons(C_2, C_4...) \tag{2.10}$$

Leftover solid after devolatilization can also react with the oxygen carriers, as shown in reaction 2.11. However, this solid-solid reaction is reported to be negligible as there is inadequate contact between the two in a fluidized bed gasifier and steam as a gasifying agent is deemed to be necessary for improved char conversion in the fuel reactor [42], [43].

$$Char + Me_xO_y \longrightarrow 2Me_xO_{(y-1)} + CO_2 \tag{2.11}$$

Thus, the most applicable reaction for the conversion of char, C, would be Reaction 2.3 as given above, although CO_2 could also be employed as a gasification agent instead of H_2O.

2.4 Syngas Cleaning and Conditioning

2.4.1 Syngas cleaning processes

Syngas from biomass gasification generally contains tars, particulate matter, alkali compounds and minute amounts of contaminants, such as sulphur and nitrogen compounds. The amount of impurities present in the syngas depends on the type of biomass used in the gasifier. For example, woody biomass tends to have lower amounts of sulphur, nitrogen and chlorine in them when compared to agricultural residues and by-products [44]. Independent of which biomass is used, they could still be present in sufficient amounts in the raw syngas, that they could hinder any downstream fuel synthesis process.

Syngas cleanup technologies have been extensively reviewed in [45], where the technologies are classified based on the range of process temperatures. In comparison with hot gas cleanup and warm gas clean up technologies, cold gas cleanup technology is mostly considered as the conventional cleanup approach because of its demonstrated removal efficiency and reliability [46]. Although reliable, it is known to impact the thermal efficiency of the overall process plant due to lower operating temperatures [45].

Particulate matter mainly consisting of elutriated solid particles from the gasifier, is usually captured with conventional cyclones, electrostatic precipitators, bag filters that generally have high collection efficiencies. In the GoBiGas plant, a textile bag filter coated with limestone is used to separate the particulate matter. However, such filters can tolerate gas temperatures only up to a specific limit; in this case, 230°C [10].

Tars can be cracked to CO and H_2 either by thermal cracking at high temperatures or by RME-based scrubbing. The latter is a widely used option for tar removal, where the tar components get dissolved in the scrubbing agent. An RME-based scrubber uses rapeseed methyl ester (RME) as the scrubbing liquid to absorb the tars from the raw syngas. This tar cleaning process was used in the Güssing gasification plant and the GoBiGas plant [10], [47]. However, it was recommended that RME scrubbers must be replaced with a cheaper alternative as the RME scrubber agent accounted for 5-10% of their operational cost at the GoBiGas plant [10]. With respect to chemical looping gasification operation, fewer tars are expected due to the higher oxidizing environment in the fuel reactor and oxygen carriers' catalytic effect towards tars. Several OCs like LD-slag, manganese ores and artificially activated olivine (OL-AA) were experimentally investigated with varying levels of dilution with inert silica sand, in the Chalmers DFB gasifier, as an oxygen transport control strategy [30]. In their experiments, tar yield was found to be the highest for silica

sand, approximately 55 g/kg$_{daf}$, including benzene, toluene and xylene compounds (BTX). It was the lowest for OL-AA that had approximately 15 g/kg$_{daf}$ (including BTX). LD-slag with 20% dilution (LDS-80) was found to have slightly lower tar yield ($\approx$ 24 g/kg$_{daf}$) compared to LDS-57 ($\approx$ 26 g/kg$_{daf}$) at similar test conditions; gasifier temperature of 825°C and steam-to-fuel mass flow ratio of 0.8.

Acid gases such as H_2S and CO_2 are removed either by chemical or physical regenerative solvents. Chemical solvents such as alkanolamines are used to absorb the acid gases from the raw syngas in an absorber unit, followed by a stripper unit that regenerates the chemical solvent and releases a rich stream of acid gases. Other process acid gas removals (AGR) processes such as Rectisol® or Selexsol™ unit uses regenerative physical solvents like methanol or DME, respectively [44], [46]. Compared to AGR processes with physical solvents, amine-based AGR is cheaper owing to lower capital and solvent costs. However, physical absorption AGR processes are preferred for downstream fuel synthesis and other processes that need high purity syngas free of acid gases [45]. In addition to this, zinc oxide-based guard beds are also widely used for H_2S removal with high efficiencies [44], [48].

Syngas cleaning costs are known to significantly increase due to high sulphur and ash content in the fuel [49]. However, for CLG, H_2S content in the raw syngas is expected to be minimal due to low sulphur in the waste biomass. In addition, high concentrations of CO_2 in the raw syngas is expected from the fuel reactor, that must be captured. In conventional biomass gasification, fuel-bound nitrogen typically gets converted to mainly NH_3 and N_2 [50]. Although nitrogen dilution by the gasifying agent is prevented in CLG, fuel-bound nitrogen in waste biomass can get converted to nitrogen compounds such as NH_3. Along with NH_3, NO_x compounds are also expected in the raw syngas as a result of the likely oxidation of ammonia by the oxygen carriers in the fuel reactor. Nitrogen compounds such as ammonia are highly soluble in water and are generally removed in wet scrubbers, where leftover solid particles in the raw syngas also get completely removed.

Gas cleaning is considered as one of the most vital steps for an FTS plant as variability in biomass feedstock fed to the gasifier is expected. Hence, a raw syngas with varying amounts of contaminants is produced. The catalysts used in FT reactors are extremely sensitive to these gas contaminants, resulting in stringent gas purity requirements. Apart from FT catalyst poisoning, some of the other problems that can occur are fouling and corrosion [51]. The tolerable limits of contaminants for FTS are listed in Table 2.5, along with other fuel synthesis processes for comparison.

2.4.2 Syngas conditioning

After the gas cleaning stages, the clean syngas must undergo gas processing or so-called conditioning steps to achieve a desirable gas composition to meet the end-use fuel synthesis process requirements. The desired gas composition can be defined by the H_2/CO molar ratio of the syngas that varies for different fuel synthesis routes. For example, methanol synthesis requires a clean syngas with an H_2/CO ratio of 2,

Table 2.5: Syngas purity requirements based on the downstream fuel synthesis process [52]

Contaminants	**Methanol Synthesis** *(mg/Nm^3)*	**Fischer-Tropsch Synthesis** *(ppmv)*	**Hydrogen**	**SNG** *(ppmv)*
Particulate Matter	<0.02	0	0	0
Tars	<0.02	<0.01	<2-5*	<2-5*
Alkali	<0.005#	<0.01	-	-
Nitrogen	<0.1	<0.02-10	<1-10	<30
Sulphur	<1	<0.01-1	<1-50	<0.1
Halides	<0.1	<0.01	-	<10

*g/Nm^3, #*ppmv*

whereas a typical FTS process requires an H_2/CO ratio of 2.05-2.15 [49]. However, with respect to FTS, this ratio depends on the chosen FT process temperatures, the catalyst used in the FT reactor and the type of FT reactor used [49]. Table 2.6 shows the different H_2/CO ratios required for methanol synthesis and different FT-synthesis processes.

Table 2.6: Desired H_2/CO ratio for methanol synthesis and different FTS processes [49]

	Methanol Synthesis	**Low-temperature FT**		**High-temperature FT**
Catalyst	-	Iron-based	Cobalt-based	Iron-based
H_2/CO	2	≈ 1.65	≈ 2.05-2.15	1

Desirable H_2/CO ratio is achieved by a catalytic water-gas shift (WGS) reactor where a portion of carbon monoxide is converted to hydrogen and carbon dioxide using steam. It undergoes a reaction, as shown in Reaction 2.6. This shift reaction can be done before or after the AGR process, depending on the catalyst used in the WGS reactor. Catalysts resistant to acid gases like H_2S would enable WGS reaction before the AGR process; it is then said to have undergone a sour WGS reaction [52]. The carbon dioxide generated in the step is considered as an undesired inert for FT synthesis, depending on the catalyst used in the reactor, and thus must be removed before the FT reactor. It is, therefore, imperative to identify and design the process parts of the syngas cleaning stage in the most economical manner without compromising on the clean gas composition required for a downstream FT-synthesis.

2.5 Fuel Synthesis

Biomass-derived syngas that has undergone gas cleaning and conditioning can be utilized to produce various advanced biofuels such as FT-crude, methanol, synthetic natural gas, or pure hydrogen, as shown in Figure 2.5. Here, FT-crude obtained from FTS process requires further refining or product upgradation stage to obtain FT-diesel and other useful hydrocarbons. Syngas is predominantly used in the chemical industry; however, there is growing in interest in utilizing syngas to produce

advanced biofuels. The primary transformation route chosen for this thesis is FT-synthesis and discussed in the following section.

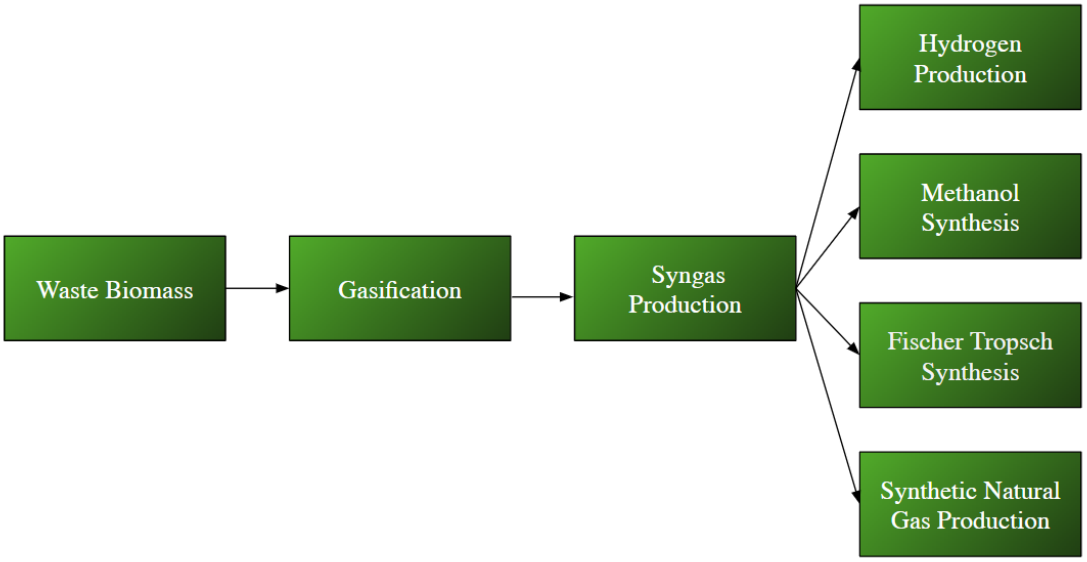

Figure 2.5: Syngas transformation routes to alternative fuels

2.5.1 Fischer-Tropsch synthesis

In FT-synthesis, the H_2 and CO-rich cleaned syngas from the gasification process is utilized and converted into liquid hydrocarbons using cobalt or iron-based catalyst [49]. Apart from hydrocarbons, other products include olefins, paraffins and alcohols as shown in Reaction 2.12-2.14.

$$nCO + (2n+1)H_2 \longrightarrow C_nH_{2n+2} + nH_2O \tag{2.12}$$

$$nCO + 2nH_2 \longrightarrow C_nH_{2n} + nH_2O \tag{2.13}$$

$$nCO + 2nH_2 \longrightarrow C_nH_{2n+1}OH + (n-1)H_2O \tag{2.14}$$

These hydrocarbons can be further converted to transportation fuels and other chemicals, through product upgrading steps. FT-synthesis has two main operating modes, low-temperature mode (LTFT) and high-temperature (HTFT) mode. LTFT (200-240°C) is suitable for the production of diesel and wax hydrocarbons and HTFT (300-360°C) for gasoline and middle distillate hydrocarbons [49]. A more detailed description of FT-reactor types, process description, catalysts and product upgrading can be found in [49], [53], and is not described in this section for brevity.

Viability of a biomass-to-liquid fuel chain is significantly dependent on the syngas gasification technology and its efficiency, syngas cleaning and conditioning energy

requirements, FT conversion efficiency and subsequent product upgrading efficiency. It is especially interesting when it comes to integration with CLG, as a significant portion of costs related to gas cleaning, ASU and carbon capture are either avoided or abated when compared to other gasification technologies. In addition to this, FT synthesis plants generally have excess heat available for recovery. Hence it could potentially have exciting heat integration possibilities with upstream processes such as steam generation for gasifier and to meet the steam demand in the solvent regenerators of the AGR units.

3

Methodology

A chemical looping gasification (CLG) model is developed using Aspen Plus® software [54]. Forest residues are considered as the waste biomass feedstock for the model. Based on the feedstock and a thermal input of 100 MW_{th}, a maximum flow rate of fuel was set for the CLG plant. LD-slag, a steel industry by-product is the primary oxygen carrier used in in the model. It is, however, challenging to choose and design a specific gas cleanup stage technology in the early stages of process modelling as it clearly depends on the downstream FTS technology and its operating conditions and the upstream gasification process parameters, gasifier type and fluidizing agent. Therefore, in this thesis, the gas cleaning model is done using mature technologies such as wet scrubbers and other processes used in the cold gas cleanup method. Due to the uncertainty regarding the extent of gas cleaning required in an actual CLG plant, the base case models with the gas cleaning stage is adapted from the gas cleaning model developed by Arvidsson et al. [55] for the GoBiGas plant. This is deemed suitable as the GoBiGas plant is a useful reference, that is currently the only large-scale biofuels production plant, where bio-SNG is produced from woody biomass. A Fischer-Tropsch synthesis model developed by Maddalena & Madeline [53], at Chalmers, is integrated with the CLG model to investigate and estimate the overall plant performance and process efficiencies. Additionally, carbon capture capacity and the FT-crude production capacity of the integrated chemical looping gasification-FT (CLG-FT) plant is evaluated. In this thesis, the various sections of the integrated plant, namely, CLG, syngas cleaning and FTS models, are modelled in hierarchy blocks to simulate the overall process flow diagram. These hierarchy blocks are built within the main parent block i.e. FTS and Figure 3.1 only depicts the transfer of stream data from one submodel to the subsequent submodels.

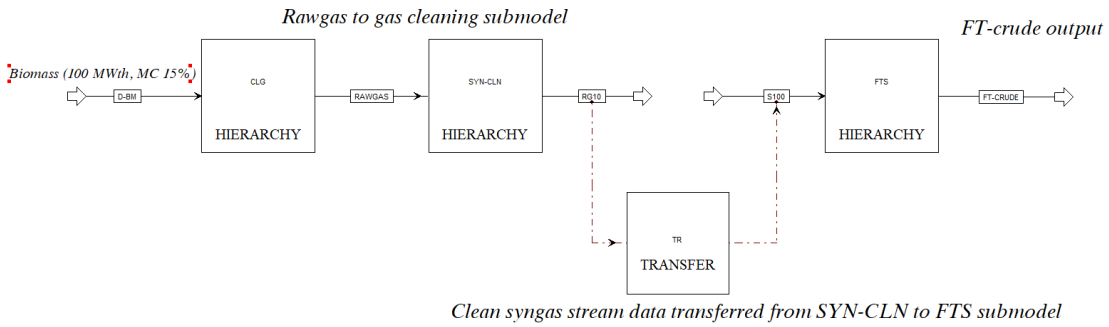

Figure 3.1: Overall process flow diagram of the integrated sub-models

Here, the raw syngas output from the CLG block is taken as input for the syngas cleaning block, SYN-CLN and the resulting cleaning syngas from this block is taken as input in the FTS hierarchy block and a *Transfer* manipulator block, *TR* is used for this purpose. This is followed by a pinch analysis of the integrated model, targeting

for maximum heat recovery in the process to estimate the co-generation potential and other process efficiencies.

4

Process Modelling

This chapter describes the process modelling of the chemical looping gasification submodel and its subsequent gas cleaning and FTS submodel. The steady-state process models are developed using Aspen Plus® V10 software. The chemical components used in the models with their corresponding substream class are specified in the software. Different unit operators are used to simulating the various stages of the overall process plant. Calculator blocks and design specification blocks in the software enables setting important user-defined process parameters and relations to define any boundary conditions and analyze the model by varying specific parameters. The calculator and design specification blocks used in this thesis are described in the Appendix A.2 and A.3, respectively. The global stream class in the model is set as MIXCINC as this enables modelling with three substreams, namely, MIXED, CISOLID and NC. The MIXED substream includes all streams that are fluid and aqueous, CISOLID substream includes all homogeneous solid components and NC, or non-conventional substream includes all non-conventional heterogeneous solid components such as biomass or coal with user-defined compositions. This function, however, excludes size distribution information, as the particle size distribution of solids is not considered in the model.

4.1 Chemical Looping Gasification Model

The process model setup and assumptions made in the model are discussed in this section. It is assumed that the fuel is converted in the fuel reactor, see Figure 1.1, while the oxygen carrier is oxidized in the air reactor.

Model assumptions

- Reactions reach an equilibrium state
- Reactor heat losses are not considered
- Pressure drops in the system are neglected
- Fuel-bound S completely converts to H_2S
- Char is assumed to be 100% carbon (Solid)
- Instantaneous devolatilization of biomass in the FR
- Complete conversion of char in the FR
- Complete oxidation of OC in the AR
- Fe_2O_3/Fe_3O_4 are assumed to be the active species

In the CLG submodel, Peng-Robinson equation of state with Boston-Mathias or PR-BM is chosen as the property method for calculating thermodynamic properties of various components used in the simulation. This property method is chosen as it is generally recommended for gas-processing, refinery and petrochemical applications,

and it also commonly used by researchers developing gasification process models [56], [57]. Biomass and ash are defined as non-conventional components, and the HCOALGEN method [58] is used to calculate the enthalpy of biomass based on its ultimate and proximate analysis. DCOALIGT method [58] is used to calculate the densities of biomass and ash. The proximate and ultimate analysis of the forest residues used in the model is listed in Table 4.1. Forest residues generally have high moisture content, roughly 30-50% on an as-received basis with low commercial value. In this model, the biomass is assumed to have undergone drying in a low-temperature air dryer before being fed into the gasifier, and a minimum moisture content of 15% is assumed. Further, the corrosive element, chlorine, is neglected, see Table 4.1. Char is assumed as 100% carbon-graphite as a solid component in the model.

Table 4.1: Proximate and ultimate analysis of biomass fuel used in the model [15]

Ultimate Analysis	**w/w%$_{d.b}$**
Ash	1.33
Carbon	51.30
Hydrogen	6.10
Nitrogen	0.40
Sulphur	0.02
Oxygen	40.85
Chlorine	-
Proximate Analysis	**w/w%$_{d.b}$**
Moisture	15
Volatile Matter	79.3
Fixed Carbon	19.37
Ash	1.33
LHV (MJ/kg)	19.34

The main oxygen carrier particles studied in this thesis is LD-slag, and its constituent elements are also defined as solid components in the model. The mass compositions of iron oxides and silicon oxides in LD-slag are calibrated by difference to compensate for the impurities in LD-slag, that are not reported in [30], and this calibrated mass composition of LD-slag is used in the CLG submodel and are listed below in Table 4.2.

Table 4.2: Mass compositions of LD-slag used in the CLG model

Composition	Fe_2O_3	MnO_2	SiO_2	CaO	MgO	Al_2O_3	TiO_2	K_2O
w/w %	28.8	3.3	14.1	42.0	9.1	1.2	1.3	<0.09

A CLG plant with a thermal input of 100 MW_{th} biomass is modelled, which corresponds to a maximum fuel flow rate of 5 kg/s. The process flow diagram of the CLG submodel is shown in Figure 4.1.

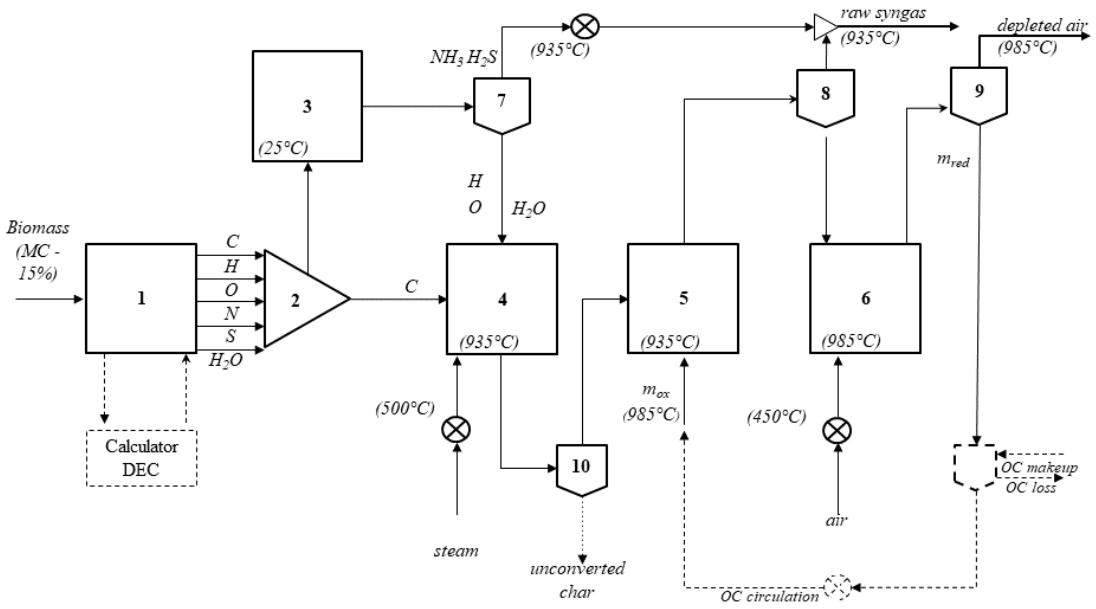

Figure 4.1: Process schematic of the chemical looping gasification model

The unit operators used in the CLG submodel and given in Figure 4.1 are listed and described further in Table 4.3. Stream summaries and block IDs used in the this are shown in the Appendix A.1. Since the reactions taking place in the fuel reactor is rather complicated, the fuel reactor was modelled with four unit-operators. The fuel decomposition, char-steam gasification, conversion of fuel nitrogen and sulphur and finally, the gas-solid reactions of the volatiles and oxygen carriers. The gas-solid reactions take place in the *RGibbs* block **5**, referred here as volatiles combustion, see Table 4.3. Two *RStoic* blocks (Block **3** & **4**) are used to simulate the char-steam gasification and NS conversion, and this can be reduced to one *RStoic* block; however, this has been done for simplicity, to understand the process flow diagram, shown in Figure 4.1.

4.1.1 Fuel Decomposition

In this model, the biomass is defined as a non-conventional (NC) component with its ultimate and proximate analysis directly given as input in the inlet stream, D-BM. A calculator block is used to set the mass flow rate of the input fuel to the desired thermal input based on its lower heating value on a dry basis; in this case, a thermal input of 100 MW and an LHV of 19.6 MJ/kg. In previous modelling efforts using biomass, the fuel has been represented using a stream of conventional gas, that is defined as a MIXED substream with its corresponding mass composition as $C_nH_{2m}O_p$ calculated from its ultimate and proximate analysis [59], [60] The former

Table 4.3: Main unit operations in the CLG Model

Block	Unit Operation	Aspen Model	Description
1	Fuel decomposition	*RYield*	Yield distribution specified by calculator block *DEC*
2	Elements separation	*Sep*	Separation of char (CISOLID) from other conventional elements (H, O, N, S, H_2O)
3	N, S Conversion	*RStoic*	Fractional conversion for N is set as 0.5; for S set as 1
4	Char-steam gasification	*RStoic*	α taken as 1.1, as reactor temperature 900°C
5	Volatiles combustion	*RGibbs*	Adiabatic reactor
6	Air reactor	*RStoic*	Adiabatic reactor
7	Gas-separation	*Sep*	Separation of gas contaminants
8	Solids-separation	*SSplit*	Solids-raw gas separation at FR outlet
9	Solids-separation	*SSplit*	Solids-raw gas separation at AR outlet
10	Char separation	*Sep*	Separation of unconverted char from combustible gases

technique is chosen, as the model could be used in the future to analyze various other biomass in CLG operation with ease. An *RYield* reactor, block **1** in Figure 4.1, simulates the decomposition of the non-conventional biomass into its constituent elements on a mass basis, and this block does not require any chemical reaction, or kinetic data as its input and its output simply depends on the yield distribution defined in the block. The yield distribution in this block is calculated and set by Fortran statements written in a calculator block, *DEC* and these statements used in the calculator block is described in the Appendix A.2.1. It is a standard modelling approach used to decompose unconventional heterogeneous solids into its constituent elements [57]. Instantaneous devolatilization of biomass is assumed, and it decomposes into volatile gases, ash and char as depicted in reaction, 2.2. Apart from its constituent elements, the yields from the reactor also include the fixed carbon and ash in the biomass, which is defined as CISOLID and NC substreams, respectively. The change in enthalpy in this step must be integrated into the FR. Hence a heat stream, QDEC is used for this purpose. A *Sep* block, **2** is used to separate the conventional components, ash and solid-char. The conventional components (H, N, O, S) and ash are directed to the *RStoic* block, **3**. Char is sent to the *RStoic* block, **4** where it undergoes char-steam gasification reactions as in Reaction 2.7.

4.1.2 Nitrogen and Sulphur Conversion

Sulphur is assumed to undergo 100% conversion to H_2S. In case of nitrogen, in CLG operations, it is assumed to get converted to NH_3 predominantly, however, some fuel-bound nitrogen is estimated to be oxidized to nitrogen oxides, due to the higher

oxidizing environment in the fuel reactor in comparison to conventional gasification systems. The raw gas is also expected to have minute amounts of nitrogen, possibly due to using sweep gas in the fuel feeding system to prevent any backflows. This has not been considered in this model. The fractional conversion of the fuel bound nitrogen is adjusted to simulate the N_2 coming out of the fuel reactor. The fate of fuel nitrogen in the conventional biomass gasification shows that two-thirds of it typically converts to NH_3 and the rest to N_2 [50]. Since very little information was found on the fate of nitrogen in a CLG operation, a fractional conversion of 0.6 is assumed in the block **3**, which would result in an outlet gas with mainly NH_3, N_2, H_2S and other conventional gases, including ash. The outgoing stream is split using a separator block, **7** in Figure 4.1. The ash and gas contaminants are directed to a heater and the second stream from block **7** consistes of conventional gas which are directed to block **4**. The outgoing gas contaminants stream is heated to the fuel reactor temperature and a mixer block, **11** is used to mix the contaminants stream with the gases from block **5**. This is done to obtain a raw syngas including its contaminants as the input stream for the subsequent gas cleaning submodel.

4.1.3 Char-steam gasification

Char-steam gasification reactions take place in the *RStoic* block, **4**, with steam at 500°C and 1 bar pressure as the input stream and its mass flow rate is calculated based on the steam-to-biomass (S/B) ratio specified in the calculator block, *STB*. For the baseline process models, an S/B ratio on a mass flow basis, 0.8 is chosen. Steam is heated to the required temperature by heat exchangers recovering heat from exit gas streams; however, for the preliminary models, a heater block is used instead to calculate the required heat duty for steam heating. This block is defined as an isothermal reactor operating at 935°C and 1 bar pressure, i.e. the operating conditions of the fuel reactor. This temperature is set based on the chosen temperature difference of 50°C between the fuel and air reactor. Char undergoes gasification with steam as per Reaction 2.7. Since steam is used as the gasifying agent in the CLG process, thus 2.4, the gasification of char with carbon dioxide is not considered, and the combined equation of water-gas reaction and water-gas shift reaction is used, as shown in Reaction 2.7. The mechanism factor, α, varies from 1.5 – 1.1 for a temperature varying from 750°C – 900°C in the gasifier [39]. The α value is chosen as 1.1 here, since the operating temperature of the FR is above 900°C, and the corresponding equilibrium reaction 2.7, is given as input in the block, **4**.

Other equilibrium reactions specified in the *RStoic* block **4** are hydrogasification of carbon, Reaction 2.5, and the tar formation reactions based on Reaction 2.10. There is very limited information available in the literature currently, on the tar yield in a CLG operation; however, it is expected to be lower than conventional biomass gasification technologies. The CLG experiments done by Pissot et al.[30] on a high-volatiles fuel estimated a tar yield of roughly 30g/kg_{daf}, including BTX, where LD-slag with 20% fraction of sand (LDS-80) was used as the oxygen carrier [29]. Here, the experiments were done at a gasifier temperature of 825°C with an S/B ratio of 0.79. Huang et al. [61] estimated a tar yield of 6.49 g/Nm^3 with a gas

yield of approximately 1.32 Nm^3/kg biomass for CLG of pine sawdust with natural hematite as the oxygen carriers. Experiments were done on DFB gasifiers with ilmenite as OC by Larsson et al. [62], indicated lowered tar yields due to the presence of a higher oxidizing environment and its catalytic effect on tars; however, an increasing trend of heavier tars were also noticed. Using these finding, as the basis for tar formation in CLG, tar components such as phenol (C_6H_6O), naphthalene($C_{10}H_8$) and toluene (C_7H_8) were consider simulating the tar formation in the CLG model. The fractional conversion of these tar components in block **4** is controlled by a calculator block, *TAR-CONV*, where the expected tar yield is set as a constant value, this has been explained in more detail in the following Section 4.1.4 on volatiles combustion. Since the fuel reactor temperature in the model is higher, close to 935°C, even lower tar yields can be expected compared to available data, however, due to the various assumptions mentioned above, a conservative approach has been taken, and higher expected tar yields corresponding to lower reactor temperatures are considered.

Apart from the water-gas shift reaction, which is slightly exothermic, the other reactions specified in block **4** are highly endothermic gasification reactions. Therefore, the required heat duty in this reactor is integrated into the adiabatic *RGibbs* block, **5** using a heat stream. This is done to simulate the temperature drop in block **5** and to calculate the total reactor duty of the FR. Although CLG model, complete conversion of char is assumed, however in block **4**, the char conversion is dependent on the incoming mass flow of steam, or the S/B ratio. The unconverted char from this block is separated in the separator block, **10**. This block can be used to simulate the carbon leakage into the air reactor. However, in this model, it is assumed that there is no carbon leakage into the air reactor, owing to high carbon conversion in the FR and a carbon leakage of less than 1% reported in pilot unit operations [11].

4.1.4 Volatiles combustion

An *RGibbs* block is used to model the complex gas-solid reaction between the volatiles and the oxygen carriers. This block is generally used when detailed stoichiometric reactions or if the reaction kinetics are unknown and calculations are done by minimization of Gibbs free energy of all components in the system [54]. LD-slag, the oxygen carrier mainly consists of CaO, followed by Fe_2O_3, SiO_2, MgO, MnO in that order by weight. It is assumed that only Fe_2O_3 in the LD-slag provides lattice oxygen for the gasification reactions and the corresponding gas-solid reactions that take place in the fuel reactor are listed below, see Reaction 4.1-4.7. However, these reactions are not specified in the *RGibbs* block, **5**, see Table 4.3. Hydrocarbons could react with OC in the fuel reactor to form CO and H_2, apart from CO_2 and H_2, as shown in Reaction 4.7. It is important to note here that the redox reactions in the *RGibbbs* reactor are limited to Fe_2O_3/Fe_3O_4 oxide couple, by defining the expected oxide products from block **5**. This is done as the redox reactions for the lower iron oxides such as Fe_3O_4/FeO, FeO/Fe couple are thermodynamically limited [63], [64].

$$CO + 3\,Fe_2O_3 \longrightarrow 2\,Fe_3O_4 + CO_2 \tag{4.1}$$

$$CO + Fe_2O_3 \longrightarrow 2\,FeO + CO_2 \tag{4.2}$$

$$H_2 + 3\,Fe_2O_3 \longrightarrow 2\,Fe_3O_4 + H_2O \tag{4.3}$$

$$H_2 + Fe_2O_3 \longrightarrow 2\,FeO + H_2O \tag{4.4}$$

$$CH_4 + 3\,Fe_2O_3 \longrightarrow 2\,Fe_3O_4 + CO_2 + 2\,H_2 \tag{4.5}$$

$$CH_4 + 4\,Fe_2O_3 \longrightarrow 8\,FeO + CO_2 + 2\,H_2O \tag{4.6}$$

$$C_2H_4 + 6\,Fe_2O_3 \longrightarrow 12\,FeO + 2\,CO_2 + 2\,H_2O \tag{4.7}$$

The inherent drawback is using equilibrium reactors such as *RGibbs* for gasification, is that it assumes infinite time for the reaction that results in overestimation and underestimation of specific compounds. Some of the examples being, the complete conversion of CH_4 in the reactor, or the complete reduction of oxygen carriers in the fuel reactor, resulting in notable thermodynamic equilibrium deviations [60]. This deviation is observed in numerous process models developed by modellers and researchers in the past, and there are some ways to control or regulate this. Biomass gasification with steam, modelling done by Pala et al. [65], uses the restrict chemical equilibrium option in the *RGibbs* reactor module, by defining the reactions taking place in the reactor and adjusting the temperature approach of either the overall reactor or for each reaction. A temperature approach of 0°C would mean the reactor calculates the equilibrium constant of reactions at the specified reactor temperature. Since, in this model, the *RGibbs* block is taken as an adiabatic reactor operating at atmospheric pressure, this modelling approach is deemed unsuitable.

Another approach is modified-equilibrium models, where pre-processing of expected tar yield, carbon conversion and other components is done. For example, to achieve restricted methane conversion in the *RGibbs* reactor, the expected yields of CH_4 from the process is set as a constant value using a calculator block to vary carbon conversion in a stoichiometric reactor prior to the *RGibbs* reactor. This method has been used by Arvidsson et al. [55] for a biomass-based syngas production plant. This technique has been used in this thesis and Fortran statements adapted from Arvidsson et al. [55] is written in calculator blocks, *CH4-CONV* and *TAR-CONV*

for CH_4 and tar components, respectively. The calculator blocks, based on the set values for the expected yields of CH_4 and tar components, it manipulates the fractional conversion of char in the previous block, **4** and thus set as inert components in **5**, in order to avoid complete conversion in the Gibbs reactor.

The gasification gases and the oxygen carriers from the fuel reactor are separated in a cyclone, **8**. Here, an *SSplit* block is used instead of the *Cyclone* block available in the Aspen Plus® software, as the cyclone, solid separation efficiency is assumed to be 100%. A cyclone block would be more appropriate to model accurate gas-solid separation based on appropriate cyclone separation efficiencies. The produced gasification gases separated in **8**, is mixed back with gas contaminants from block **3** in a mixer, **11**. The reduced oxygen carriers are directed to the air reactor, **6**.

4.1.5 Air reactor

This block is modelled as an adiabatic *RStoic* reactor **6**, at 1 bar pressure. The exothermic oxidation reactions in the air reactor are generally spontaneous with low residence times; thus a 100% conversion of reduced oxygen carrier is assumed in the model. Oxidation reactions, Reaction 4.8 and Reaction 4.9, of the oxygen carrier particles and air are specified in **6** with a fractional conversion of 1. Reaction 4.9, although specified in block **6**, only Reaction 4.8 takes place in block **6**, as the reduction of iron-oxides are limited to Fe_3O_4 in block **5**, and no FeO compounds are expected. The highly exothermic oxidation reactions in the air reactor are shown in Reaction 4.8 and 4.9.

Reaction	Δ**H** (kJ/mol)
$4\,Fe_3O_4 + O_2 \longrightarrow 6\,Fe_2O_3$ (4.8)	-479
$4\,FeO + O_2 \longrightarrow 2\,Fe_2O_3$ (4.9)	-560.66

Excess air is usually supplied for solid circulation control in actual operation, however in this model, only sufficient air required for complete conversion of oxygen carriers is supplied, and this is specified using a design specification block, AFR. The air is assumed to be heated to roughly 450°C, recovering the heat from AR flue gases. The resulting oxygen-depleted air and solids are separated in a cyclone, **9**. Since the depleted air typically has no contaminants, heat can be recovered using heat exchangers, and its temperature can be brought close to ambient temperatures. In the baseline CLG model, heater blocks are used instead of a heat exchanger unit and the model can be updated based on HEN design with maximum heat recovery. The outlet solid stream composition from block **6** is matched with the inlet OC stream to **5**, and hence, the closing of the solids circulation loop is not considered, for simplicity, in this model. Unconverted char in the FR generally gets transported to the AR with the OC. However, it has been experimentally estimated in a 10 kW unit, that this carbon leakage to the fuel reactor is typically below 1% for fuel

with high volatile content [11]. However, some uncertainties regarding the same were also reported. For larger reactors, this carbon leakage is estimated to be even lower. Hence the unconverted char stream from block **10** is not connected to block **6**. Based on more information on carbon leakage to the air reactor in the future, the unconverted char separation specification in **10** can be modified, and the stream can be connected to the air reactor to estimate the CO_2 emissions from the air reactor.

4.1.6 Oxygen carrier circulation

The oxygen carrier inlet stream is defined with the mass compositions of LD-slag mentioned in Table 4.2. LD-slag is estimated to have a maximum oxygen transport capacity of 1.12%. However, in real CLC/CLG operations, it is reported that after several redox cycles, the oxygen transport capacity of the OC, generally reduces and is lower than the maximum OTC. In this thesis, a conservative value of 0.06% oxygen transport is chosen and calculated by Equation 2.1. Assuming lattice oxygen is only provided by Fe_2O_3 in LD-slag, would require complete conversion of Fe_2O_3 in the *RGibbs* equilibrium block, **5**. However, Fe_2O_3 generally reduces to Fe_3O_4 and does not completely convert in the fuel reactor in the presence of steam. This is also observed when CLG experiments were conducted on biomass char using iron ores as oxygen carrier [40]. Thus, indicating that lattice oxygen for a maximum oxygen transport of 1.12% could also be provided by other elements in LD-slag other than Fe_2O_3. Since there are no studies on the elemental composition of LD-slag after its reduction in the FR, the inert specification of iron and manganese oxides are considered flexible assuming manganese oxides present in the LD-slag also provide lattice oxygen for volatiles combustion, the inert specification of Mn and Fe oxides in **5** is adjusted to achieve an oxygen transport capacity of 0.06% across block **5**. This is calculated by a calculator block, *OTC* in the CLG submodel, described in the Appendix A.2.1. The other elements of LD-slag are assumed to be inert. By iterative calculation, an inert specification of 0.95 for the manganese oxide and 0.4 for iron oxide is given as input in **5**. The heat streams from the blocks representing the fuel reactor are integrated to the *RGibbs* block **5**, and since it is set as an adiabatic reactor, the temperature drop due to the highly endothermic reactions in the FR is observed, after block **5**.

The temperature in block **5** is dependent on the oxygen carrier input mass flow rate. The mass flow rate of the OC stream, OC-FR-IN, see Figure A.1 in the Appendix, must be controlled to achieve an auto-thermal operation. The input OC stream is defined with the mass compositions of fully oxidized OC with a temperature of 985°C at 1 bar pressure. This input mass flow rate of OC is controlled by a calculator block, *ART*, in order to reach the predefined AR outlet temperature of 985°C. Generally, oxygen carriers with low oxygen transport capacity would require very high circulation rates to achieve auto-thermal operation, which is in the case of LD-slag, that has only 28.8% of hematite by weight and an overall oxygen transport capacity of 1.12% by weight [38]. In the current CLG model, however the OTC has been taken as 0.06% compared to 1.12%, which would result in a slightly higher OC circulation rate to achieve an autothermal operation, along with a lower level

of volatiles oxidation. The OTC of 0.06% is rather conservative, and this could be updated in the model in the future, with data from future CLG experiments with LD-slag as the primary OC. The inlet OC stream composition and operational conditions are matched with the returning solids stream from the *SSplit* block, **9**. However, this oxygen carrier recirculation loop is not modelled for simplicity, shown as dotted lines in Figure 4.1.

4.2 Syngas Cleaning Model

This model has been adapted from the gas cleaning process model developed by Arvidsson et al. [55]. The main purification stages in this submodel are particulate removal, tar removal, acid gas removal and trace contaminant removal, as shown in Figure 4.2. Stream summaries and block IDs used in the SYN-CLN sub-model are shown in the Appendix A.1. However, a water-gas shift (WGS) reactor for syngas conditioning is not included in this submodel as a WGS reactor was modelled in the previously developed FTS model where a sweet shift reaction is considered assuming a clean syngas inlet stream as input.

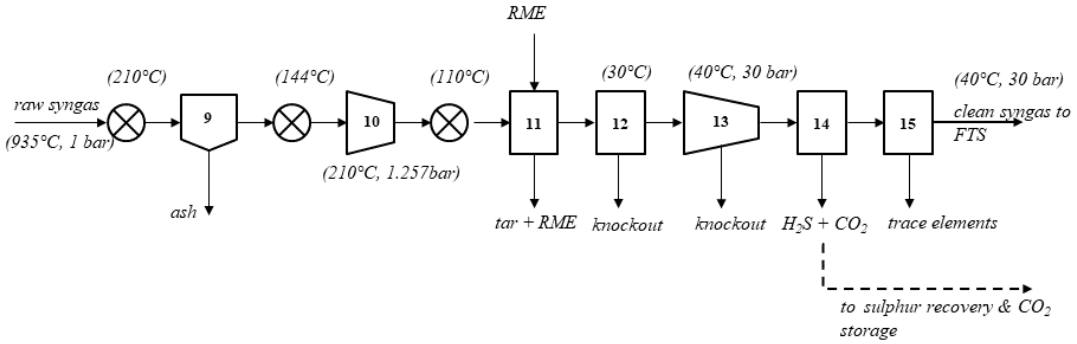

Figure 4.2: Process flow diagram of the syngas cleaning submodel

Firstly, a considerable amount of heat can be recovered from the hot syngas from the fuel reactor. For the baseline process model, a cooler is used instead to simulate the heat recovery process and cooled down to 210°C. This cooler can be replaced with a set of heat exchangers based on the optimum heat exchanger network design obtained from pinch analysis of the integrated model. Ash and other particulate matter are separated in a fabric filter, for this an *SSplit* block, **9** is used to separate the ash and solid particles. After the solids separation step, the syngas is further cooled down to 144°C for heat recovery. The cooled syngas is then compressed in

block **10** to compensate for the expected pressure loss in the RME scrubber, **11**. After the gas compression, it is further cooled down to 110°C prior to **11** to compensate for the heat of compression in **10**. The main unit operations in the syngas cleaning submodel are listed below in Table 4.4.

Table 4.4: Main unit operations in the syngas cleaning submodel

Block ID	Aspen Model	T_{out} (°C)	ΔP (bar)	Description
9	*SSplit*	210	- 0.2	Slag stream: NC split fraction set as 1
10	*Compr*	209	0.425	Set to compensate for pressure drop in the RME-scrubber
11	*Sep*	109	-0.2	100% tar and RME removal: split fractions set as 1. Mass flow of RME inlet adjusted by a calculator
12	*Flash2*	30	0	-
13	*MCompr*	40	30	3 stages, cooler outlet temp: 80°C,80°C, 40°C; No dP in coolers
14	*Sep*	40	-0.2	MDEA-S absorber- Split fractions set based on removal % calc. in [66], [67]; 96% H_2S, 62% CO_2, 100% NH_3, 0.0738% CH_4, 0.058% CO, 0% H_2O
15	*Sep*	40	-0.2	Guard-bed model – 100% S removal assumed

Tars are removed in an rapeseed methyl ester (RME) based scrubber, modelled using a *Sep* block, **11** by specifying the split fraction of components to be removed. In the gas cleaning model developed by Arvidsson et al. [55], RME consumption was assumed to be around 2.4% of energy rate (HHV basis) of product gas and this assumption is used with FT-crude as the final product. As lower tar yields are expected from CLG of biomass, this assumption could be overestimating the actual RME consumption in this process and in reality, it could be much lower than what is assumed here. This gas is then scrubbed and compressed to 30 bar pressure in a multi-stage compressor block, **13** and sent to an amine absorber, modelled here with a *Sep* block, **14**. Separation efficiencies of H_2S ($\approx 96\%$) and other gas impurities are based on conventional amine scrubber technology, and their corresponding split fractions are specified in **14**. A major portion of CO_2 also gets removed in this scrubber that can sent for storage, shown as dotted line in Figure 4.2. The specific energy demand for acid gas removal step is also assumed to be same as in the previously developed model and is set as 3.3 MJ/kg of absorbed H_2S and CO_2. Furthermore, a techno-economic study done by Jiang et al. [68] for an indirect coal-biomass-to liquids (CBTL) plant model compared different sulphur removal technologies and it was reported that MDEA/PZ based amine scrubber had the lowest energy penalty when compared to other technologies such as Selexsol™ or MEA solvents. Thus, a conventional amine scrubber with an MDEA solvent modelled previously was left unchanged and replacing it with other solvents with different separation efficiencies was not considered. The syngas, now free of sulphur and nitrogen contaminants, is

then sent to a zinc oxide guard bed, **15** where remaining contaminants are assumed to be completely removed. A clean syngas, free of impurities at a temperature of 40°C and 29.6 bar pressures is obtained at the outlet. However, this stream must be heated and brought to pressures favourable for a subsequent high temperature sweet WGS reaction, which is modelled in the FTS model and discussed in detail in the following section.

4.3 Fischer-Tropsch Synthesis Model

4.3.1 Overview of the developed FTS Model

In this thesis, low-temperature Fischer Tropsch (LTFT) synthesis models previously developed at Chalmers, is used for downstream fuel synthesis integration with the CLG and gas cleaning process models. A more detailed description of the process modelling approach for the FTS model and its analysis can found in the thesis written by Maddalena and Madeline [53]. In their thesis, two basic configurations were modelled with two different purge gas (PG) stream utilization methods, one by burning the PG in a boiler for electricity and steam generation and the other with a gas turbine for electricity production. In addition to this, advanced configurations were also modelled where unconverted gases from the FT reactor was recycled through the auto-thermal reformer (ATR), shown as block **27** in Figure 4.4.

In this thesis, since the primary objective is to maximize the FT-crude production capacity and heavier products suitable for the aviation and maritime sector, for the integrated CLG-FT plant, the most suitable basic and advanced configurations are chosen for integration based on the parametric study done in their thesis. In addition to the configurations, operating conditions of the FT-reactor such as pressure, temperatures and CO conversion (X_{co}) that are conducive to maximizing FT crude production are chosen. Here, the CO conversion is a rate based equation, that calculates the amount of CO converted for each hydrocarbon reaction in the FT reactor [53]. The chosen FTS-model process configuration and operating conditions for integration are referred to as the baseline FTS model in this section.

It is well known that higher FT reactor temperatures aid in lighter hydrocarbon production and vice versa, heavier hydrocarbons such as FT-diesel and waxes are produced at a lower reactor temperature range. Therefore, the lowest reactor temperature of 220°C in an LTFT operation mode is chosen. Based on this fixed reactor temperature, variation in pressure and catalyst amount play a significant role in increasing the FT-crude yield. In Figure 4.3, the colour-coded representation of the variation of FT products yield (kg/s) can be seen with varying pressure and X_{co}, considering the two suggested advanced configurations; i.e. with and without a reformer. In Figure 4.3, the colour green depicts the higher range of FT-product flows (kg/s) and red depicts the lower output or lower yield of FT-crude. Note, that the values shown here are from the old FT-model with a much higher syngas input to the FTS model. This parametric study is used only as an indicator to choose suitable operating conditions for the baseline FTS model for integration in this thesis.

	without reformer			*with reformer*		
FT-pressure (bar)	*Xco = 0.5*	*Xco = 0.6*	*Xco = 0.7*	*Xco = 0.5*	*Xco = 0.6*	*Xco = 0.7*
20	3.04	3.17	3.28	3.21	3.78	4.42
22	3.07	3.20	3.30	3.24	3.82	4.43
24	3.09	3.22	3.33	3.26	3.88	4.46
26	3.11	3.24	3.35	3.29	3.91	4.49
28	3.13	3.26	3.37	3.31	3.95	4.52
30	3.14	3.28	3.39	3.33	3.96	4.58

Figure 4.3: Color-coded representation of FT-crude yield (kg/s) for a clean syngas input of 1.5 kmol/s; with varying pressure and catalyst amount at a constant FT reactor temperature of 220°C [53]

From Figure 4.3, clearly increasing reactor pressure and catalyst amount has a positive impact on FT-crude production. The highest FT-crude yield was achieved with an FTS process with a reformer, operating at 30 bar pressure with an X_{co} of 70%, see Figure 4.3. CO conversion is directly related to the catalyst amount needed in the reactor, block **22** in Figure 4.4 and thus their corresponding reactor volume. Based on their parametric analysis [52], it was seen that the catalyst amount significantly increased at lower temperatures for higher X_{co}. Additionally, the model without reformer required relatively less amount of catalyst for at lower temperature ranges. However, the model with reformer requires significantly less catalyst above 220°C. Based on their parametric studies, the baseline FTS model operating conditions are at 20 bar pressure, and a constant reactor temperature of 220°C is chosen for the integration with CLG model.

Regarding the X_{co}, the economic trade-off between increased catalyst amount/reactor volume and the inclusion of a reformer for unconverted gas recycling in the FTS plant is not clear at this point. This uncertainty can only be cleared after a thorough techno-economic assessment relating to this aspect of the FTS plant is done. Thus, the baseline FTS model used in this thesis includes a reformer that considers a CO conversion case of 50%. As a lower reactor temperature (220°C) is chosen, including a reformer, in order to get high CO conversion of 70%, the catalyst required in the reactor is in significant amounts which in turn increases the reactor volume. Thus, a moderate X_{co} of 50% is justified for the baseline FTS model. Considering certain catalysts, occasionally in some studies, the CO conversion assumed in the FT reactor, is as high as 90% [22]. In Table A.1, the chosen reactor operating conditions for the baseline FTS model are listed.

4.3.2 FTS Model description

A brief description of the developed FTS model is given in this section with some model modifications. Majority of the existing model conditions are left unchanged, and only minor modifications are made to the developed models, in order to make

Table 4.5: Chosen operating conditions in the FT-reactor for the baseline FTS-model used in this thesis

Temperature	Pressure	CO conversion (X_{co})
220°C	20 bar	0.50

the FTS model compatible for integration with the CLG model. The process flow diagram of the low-temperature Fischer-Tropsch (LTFT) synthesis plant is shown in Figure 4.4. The main unit operations used in the FTS model are described in Table A.9 and stream data are listed in the Appendix A.1.

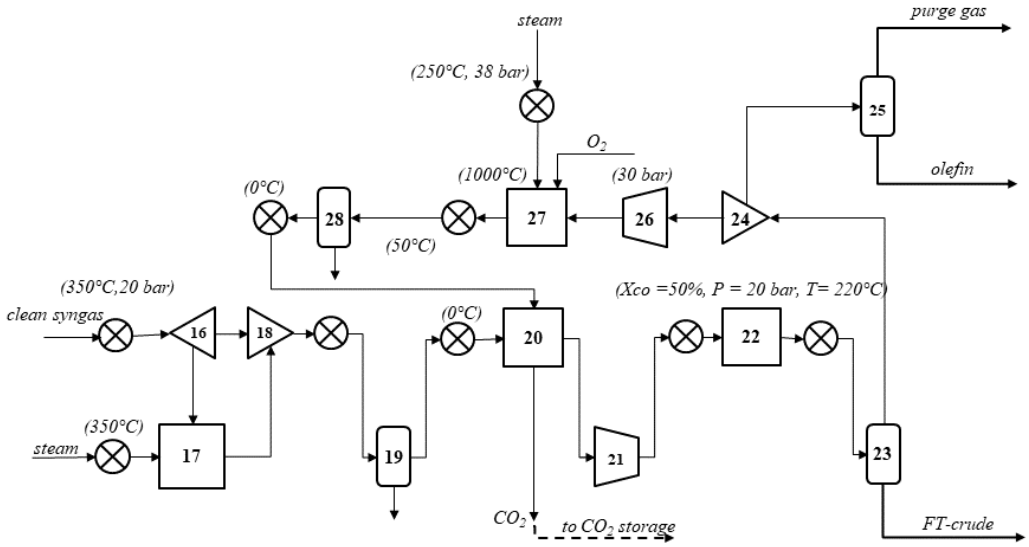

Figure 4.4: Process flow diagram of the Fischer-Tropsch synthesis model

In the previously developed FTS process model [53], a clean syngas stream with set composition was assumed as input, that had already undergone flue gas desulphurization and other gas cleaning processes. However, in the integrated CLG-FT model, the syngas input stream composition is dependent on the cleaned syngas coming from the syngas cleaning submodel. In order to adjust the incoming syngas to an H_2/CO ratio, suitable for FT-synthesis (≈2.05-2.15), a high-temperature WGS reactor, **17** is used prior to the FT reactor, **22**, as shown in Figure 4.4. A typical syngas stream conditions prior to a high-temperature WGS is a temperature of 350°C and 20 bar pressure. However, the incoming syngas from gas cleaning submodel is at a lower temperature of roughly 40°C with a higher pressure of 29.6 bar pressure, due to the cold gas cleanup steps upstream. Thus, a heater block is placed prior to separator block **16** to match the required stream conditions for low-temperature WGS reactor. This heater is used in the preliminary model, however, the heat required is usually provided by recovered heat in the overall process in a

heat exchanger.

Based on the optimum heat exchanger network design for the integrated model, considering economic and technical constraints, this heater duty can be minimized or completely satisfied. Steam is supplied to block **17** at 350°C and 20 bar pressure. An *SSplit* block, **16** splits the incoming syngas stream so that only a specific amount of syngas undergoes water-gas shift reaction in **17**, to achieve a suitable H_2/CO ratio of 2, after mixing in the mixer block, **18**. This is done by using a calculator block that adjusts the split fraction in **16**. Another calculator block calculates the amount of steam required in the WGS reactor **17** by setting an H_2O/CO ratio equal to 3 for the syngas stream entering **17**.

This is followed by a flash separator, **19** and then a Rectisol® unit, **20** for CO_2 removal prior to the FT-reactor, **22**. Rectisol® units operate at low temperatures; thus, the shifted syngas is cooled to 0°C before **20**. A compressor, **21** compensates for the pressure loss in **20**. The FT-Reactor, **22**, is modelled as an *RStoic* reactor with the equilibrium reactions, implemented in an MS-Excel file, see [53] for more information. A flash separator, **23** separates the incoming stream of unconverted hydrocarbon gases and heavier hydrocarbons from the FT-reactor. The heavier hydrocarbons are the FT-crude or the final product obtained from this process, and this can be further upgraded or refined to obtain various FT-products such as naphtha (C_5-C_{11}), FT-diesel (C_{12}-C_{19}) etc. The product upgrading stage is not included in this thesis.

90% of the unconverted hydrocarbon gases are recycled back to the FT-reactor in the model after reforming in the auto-thermal reformer. The split fraction of the recycle stream from flash separator block **23** is specified in *Sep* block, **24**. The unconverted hydrocarbon gases are compressed to 30 bar in **26** and then reformed in an auto-thermal reformer that operates at 1000°C, with an input stream of steam and oxygen. However, the flow rate of required oxygen for this reactor is an insignificant amount, that is set by a calculator block in order to maintain the reactor temperature of the ATR, block **27** at 1000°C. The remaining unconverted gases, the purge stream is separated in a flash separator, block **25**, where heavier olefins are obtained and a stream of PG that can be utilized downstream in a gas turbine, boiler or flared. The PG utilization blocks modelled previously in [53], are removed for the baseline integrated model in this thesis. However, the fate of the PG is decided based on the overall process requirement of heat and electricity, and this is discussed in detail in Section 5.

4.4 Performance Indicators

4.4.1 Data evaluation

Thermodynamic evaluators are calculated to estimate the thermodynamic performance of the stand-alone CLG plant and the integrated CLG-FT plant. Product gas from the CLG fuel reactor mainly consists of H_2, CO, CH_4 and CO_2.

To validate the model with experimental data, different carbon species in the product gas was calculated based on their carbon fractions, as shown in Equations 4.10-4.13 below.

$$f_{CO_2} = \frac{n_{CO_2,sg}}{n_{CO,sg} + n_{CO_2,sg} + \sum_x (x \cdot n_{C_nH_m,sg})} \tag{4.10}$$

$$f_{CO} = \frac{n_{CO,sg}}{n_{CO,sg} + n_{CO_2,sg} + \sum_x (x \cdot n_{C_nH_m,sg})} \tag{4.11}$$

$$f_{CH_4} = \frac{n_{CH_4,sg}}{n_{CO,sg} + n_{CO_2,sg} + \sum_x (x \cdot n_{C_nH_m,sg})} \tag{4.12}$$

$$f_{ct} = \frac{n_{ct,sg}}{n_{CO,sg} + n_{CO_2,sg} + \sum_x (x \cdot n_{C_nH_m,sg})} \tag{4.13}$$

Here, n_i is the mole fractions of each species in the product gas where i represents CO, CH_4, CO_2 and C_xH_y. Equivalence ratio (ER), the ratio of oxygen required to gasify the biomass to the oxygen required for complete combustion, is calculated by the Equation 4.14.

$$ER = \frac{n_{O_2,AR_{in}}}{n_{O_2,comb}} \tag{4.14}$$

Oxygen for gasification is provided by the reduction of oxygen carriers in the fuel reactor, and complete oxidation of oxygen carrier particles is assumed in the air reactor. Although excess air may be provided for solid circulation control in the actual operation of the reactors, in the model, excess air is not considered. Therefore, the moles of oxygen required to oxidize reduced oxygen carries completely, $n_{O_2,AR_{in}}$, is considered as the oxygen required for gasification. *O2-COMB* property data is used to calculate the moles of oxygen required for complete combustion of fuel stream into the fuel reactor. In the CLG model, this is the stream with volatiles coming from the block **4**, see Figure 4.1.Steam-to-biomass ratio (S/B, kg/kg_{daf}) is an important parameter for steam-based gasification technologies and is calculated as the ratio of mass flow of steam input to the mass flow of biomass fuel, on a dry-ash free basis, into the fuel reactor, as shown in Equation 4.15.

$$S/B = \frac{\dot{m}_{steam}}{\dot{m}_{biomass}} \tag{4.15}$$

4.4.2 Process efficiencies

The gasification performance is evaluated by the cold gas efficiency (CGE) calculated as the ratio between the energy content of the product gas (LHV basis) to the energy content in the dry ash free biomass fuel input, as shown in Equation 4.16.

$$CGE = \frac{LHV_{sg} \cdot G_v}{LHV_{fuel,daf} \cdot \dot{m}_{fuel}} \tag{4.16}$$

The energy content of the product gas is the product of the combined lower heating value of the combustible gases to the total syngas flow (G_v). Here, G_v is the standard volume (Nm^3/s) of syngas at 0°C and 1 atm. Here, the LHV_{sg} of the product gas is calculated on a volume basis where the sum of LHV of gas components is calculated, as shown in Equation 4.17, where V_{H_2},V_{CO},V_{CH_4} are volume fractions of gas components in the syngas [69]. Note, that C_2-species and C_3-species are not included while calculating the LHV_{sg} (MJ/Nm^3), this is mainly because no C_2-species are considered in the model, although it is expected in small amounts in the syngas. C_3-species are also not considered as they are generally not detected during CLG operations [11].

$$LHV_{sg} = 12.67V_{H_2} + 12.63V_{CO} + 39.72V_{CH_4} \tag{4.17}$$

Chemical efficiency is calculated as the ratio of the total energy content of the FT-products to the biomass fuel input to the CLG plant, including the net energy consumption in the scrubber feeds (Q_f), as shown in Equation 4.18. The energy content of the FT-products is evaluated on an HHV basis. This is evaluated by stoichiometric combustion of the FT-products stream in a Gibbs reactor model and considering the heat released in the reactor and accounting for the convection heat flow, by cooling the flue gas stream. A more detailed explanation of this technique can be found in [53].

$$\eta_{ch} = \frac{HHV_{product} \cdot \dot{m}_{product}}{(HHV_{biomass} \cdot \dot{m}_{biomass}) + \sum Q_f} \tag{4.18}$$

Energy efficiency is defined here as the ratio of the sum of the net useful energy products and net electricity production to the net required energy input, according to Equation 4.19 shown below.

$$\eta_{sys} = \frac{Q_{product}}{Q_{biomass} + \sum Q_f + W_{e,net}} \tag{4.19}$$

The electricity balance is an important indicator for evaluation of the integrated models, as it gives an indication if the process plant is electricity deficit or surplus. Steam cycle integration to recover maximum possible surplus heat in the plant is considered and is discussed in more detail in the following section.

$$W_{e,net} = \sum W_{e,produced} - \sum W_{e,consumed} \tag{4.20}$$

Electricity balance is calculated as in Equation 4.20, where a positive or negative outcome would indicate a net electricity surplus or deficit, respectively.

5

Heat Integration

Pinch analysis of the integrated process is done to evaluate potential heat and power production opportunities. Pinch analysis is defined as a systematic method for energy targeting and process network integration, where a minimum approach temperature (ΔTmin) is chosen for heat exchange to avoid large heat exchanger surface areas [70]. Heat integration is done by analyzing the GCC (Grand Composite Curve) of the integrated model and by targeting maximum heat recovery from the process. A GCC depicts the heat cascade of hot and cold streams in the process network graphically and shows the heat and cooling utility demands at different temperature levels [70]. The minimum hot and cold utility requirement can also be determined based on the GCC.

The integrated CLG-FT process requires heating and cooling of streams at different temperature levels. Several regions for steam generation can be identified by analyzing the integrated process model. Firstly, the gas cooling required, subsequent to the auto-thermal reformer, operating at a fixed temperature of 1000°C, can potentially generate high pressure (HP) steam. In addition to this, the highly exothermic reactions occurring in the FT-reactor that operates at a fixed reactor temperature of 220°C can produce medium pressure (MP) steam. The hot air from the air reactor could potentially be cooled down to ambient temperature as it is free of any gas contaminants.

Aspen Energy Analyzer (AEA) software is used to evaluate the heat recovery potential by generating a grand composite curve (GCC) for the integrated model. The AEA considers all the streams in the Aspen model while generating the GCC; however, it is imperative to remove certain streams that are not relevant to the GCC. For example, the stream heating of gas impurities before their mixing with FR raw syngas, see Figure 4.1, is not relevant as it is used only for modelling purposes and in reality, it is a single stream of gases coming from the FR. It is also important to specify streams that undergo a phase change. The relevant process streams considered for generating the process GCC are listed in the Appendix A.4.

To meet the steam demand of the gasification plant, solvent reboilers, WGS reactor and the ATR in the FT plant, a heat recovery steam cycle is integrated to recover excess heat available in the overall process and produce electricity. A split-GCC graphical analysis is done for the steam cycle integration to the integrated CLG-FT model, where GCC of the heat recovery steam cycle is plotted against the GCC of the integrated model. In this analysis, a global minimum temperature difference (ΔT_{min}) of 10°C is chosen.Maximum heat integration potential can be achieved by activating at least one pinch point between the background process (CLG-FT) and the foreground (steam cycle) GCCs [70]. As a rule of thumbs, heat pockets in the background process GCC must be large enough, spanning at least two steam

pressure levels, in order to justify maximum integration through heat cascading, otherwise, for smaller heat pockets, it can be isolated where internal heat exchange can be assumed [71].

Assuming an input steam conditions of 500°C and 60 bar pressure to the steam turbine, the steam extraction pressure levels are chosen iteratively to meet the steam demands of the background GCC of the integrated model, by activating one of its pinch points. Based on this, steam extraction pressure levels of 38, 5 and back-pressure of 1.5 bar are chosen. The isentropic efficiency (η_{is}) of each turbine stage is assumed to 0.75. In addition to this, a superheat of 20°C is taken in each steam header in order to avoid condensation. The resulting heat recovery steam cycle GCC is matched with the process GCC to estimate electricity generation potential.

The steam demand in the integrated CLG-FT plant is mainly from the gasification section, the WGS reactor, ATR, and the reboilers in the AGR units. The gasifier requires LP steam at 500°C and 1 bar pressure that corresponds to a heat demand of 13.92 MW. In the ATR and WGS reactor, steam is required at 38 and 20 bar pressure respectively. Instead of introducing another intermediate steam pressure level at 20 bar, the combined heat demand of both these reactors is extracted at 38 bar pressure level. Heat demands in the gasifier, the WGS reactor and ATR are known; however, in the case of reboilers, assumptions are made based on specific heat demand for similar AGR technologies, reported in the literature. The MDEA amine scrubber in the syngas cleaning section is assumed to have a specific energy demand of 3.3 MJ per kg of H_2S and CO_2 absorbed [55], [72]. Approximately 65% of this energy demand in a typical MDEA scrubber is from the LP steam requirement in the reboilers [73]. However, in this analysis, the resulting energy demand of 8.96 MW in the amine scrubber is assumed to be entirely from the LP steam demand in the reboilers and a reboiler temperature of 120°C is assumed. LP Steam is extracted to meet the heat demands in the gasifier and the reboilers at 5 bar pressure.

The Rectisol® unit in the FTS model is assumed to have a specific steam demand of 6.97 kg per kmol of H_2S and CO_2 absorbed [74]. Typically, LP steam at 5 bar pressure is required for solvent regeneration in a Rectisol® unit. This unit is placed after the WGS reactor in the current model configuration, with the sole purpose of removing excess CO_2 emanating from the WGS reactor prior to the FT-reactor. Therefore, a relatively smaller amount of LP steam demand is estimated in this reactor. The heat demands in the various processes of the integrated model are listed in Table A.1 below.The electricity demand in the integrated CLG-FT model is listed in the Appendix A.4.

In the GoBiGas plant, in order to limit saturation of tar components, a constant flow of RME (0.03-0.035 MW_{RME}/MW_{fuel}) was fed to the tar scrubber [75]. The specific heat demand in the tar scrubber is adapted from bio-SNG production analysis by Arvidsson et al. [55] where a specific heat demand or the net consumption of RME in the tar scrubber is assumed to be 2.4% of the energy content of the produced bio-SNG. This assumption of RME consumption in the tar scrubber is

Table 5.1: Heat demand in different units of the integrated CLG-FT model

Submodels	Units	Heat Demand (MW)
CLG	Gasifier	13.92
SYN-CLN	Amine scrubber	8.96
	WGS reactor	0.27
FTS	Rectisol®	3.16e-4
	ATR	1.254
	Total demand	24.41

rather high, as fewer tars are generally expected in a CLG operation in comparison to indirect gasification of biomass. In the FTS model, 10% of the unconverted gases are purged, and the rest is recycled through the auto-thermal reformer. Heavier olefins are recovered and the off-gases from this step, the PG stream, as shown in Figure 4.4, is not considered while generating the GCC in the heat integration analysis. Two advanced configurations were suggested in the previous FTS study [53], where either boiler or a gas turbine is considered for utilizing this PG stream. In the heat integration analysis, it is assumed that the available process heat, excluding PG stream, is adequate to meet the total heat demand of the integrated plant. The most suitable advanced configuration for PG utilization can be chosen, for example, if the total heat demand of the process is not met, the PG stream can be combusted in a boiler to produce additional steam and power, however, with a small penalty on the overall carbon capture capacity of the plant. This penalty is unavoidable as the air-diluted CO_2 in the flue gas would not be suitable for carbon capture, unlike pure CO_2 stream obtained in the upstream processes.

In the gas turbine configuration, PG stream is co-combusted with an additional input stream of natural gas for electricity production. The exiting hot flue gases from the gas turbine could be further utilized for heat recovery steam generation. At a glance, the latter configuration seems to be the more logical and economical solution. However, the biggest drawback here is that additional fuel is combusted and thus significantly impacting the net-negative CO_2 emissions of the overall process. This configuration is therefore deemed to be not suitable for an integrated CLG-FT process with the objective of achieving net-negative CO_2 emissions. Thus, potential heat recovery from PG utilization is not considered for the heat integration study, and it is therefore assumed to be flared.

6

Results and Discussions

6.1 Chemical Looping Gasification Simulation

6.1.1 Model Validation

The chemical looping gasification model has been validated with experimental investigations done at Chalmers by Moldenhauer et al. [11] on CLG with LD-slag as the OC. In their CLG experiments, tests were done with three different fuels, namely black pellets, wood char and wood pellets. For the model validation, the results with wood pellets were considered as its fuel composition is quite similar to the forest residues feedstock used in the CLG model. However, the wood pellets tend to have much lower MC ($\approx$ 6%) as compared to the forest residues ($\approx$ 15%) used in the model. The experiments were done in a 10 kW unit with fuel reactor temperatures around 980°C-985°C. Three data points of gas compositions based on their carbon fractions were available with varying air-to-fuel ratio for the wood pellet case. For the validating model, the lowest air-to-fuel data point ($\approx$ 2.5 mol/mol) is chosen for comparison. There are two reasons behind this selection of data point; firstly, there is no clear trend observed in carbon fractions reported in the wood pellet case

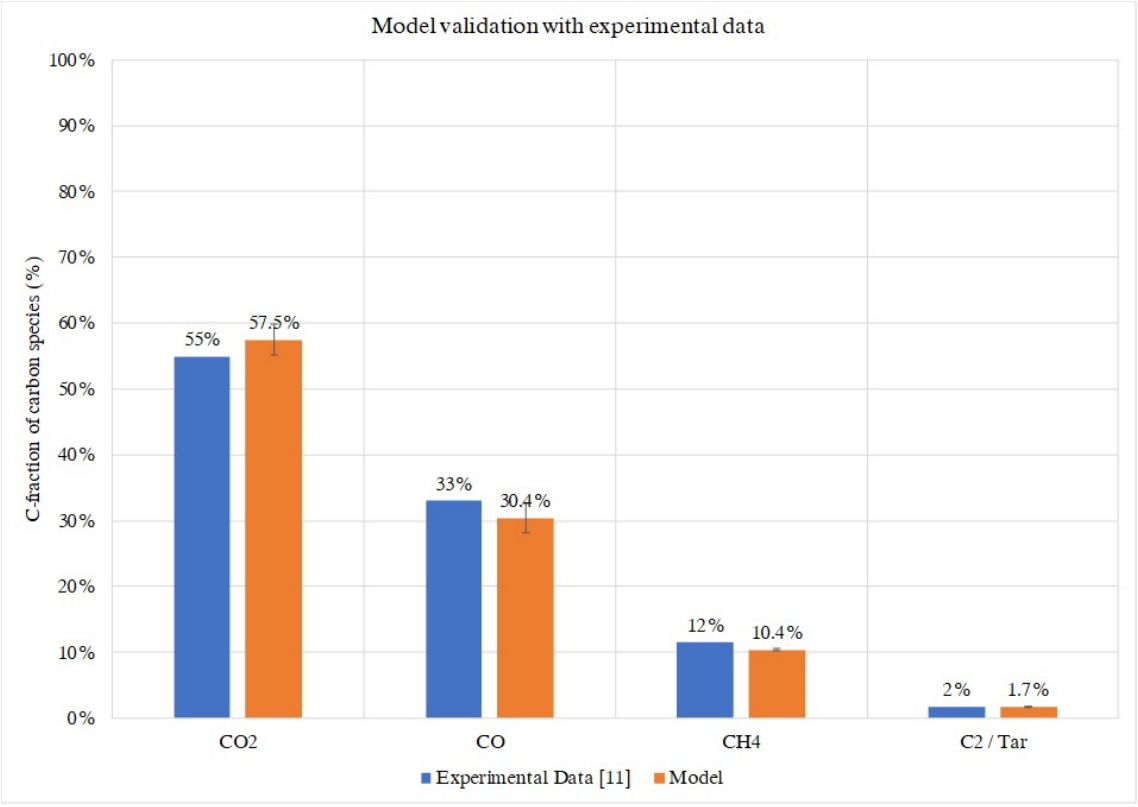

Figure 6.1: Model validation with C-fractions of carbon species in the syngas

with varying AFR, unlike in the black pellet and wood char case. Further, it can be motivated to the assumption made in the CLG model that no excess air is supplied to the AR block. The carbon species in the raw syngas from the FR has been calculated in the model using a calculator block, RG, using Equations 4.10-4.13 and compared with the available published data, as shown in Figure 6.1.

The CLG model predicted the yields of carbon species with a maximum standard error of 2.4% for the CO_2 yield. Here, as no C_2 species were specified in the model, tar content is shown along with C_2 species yield reported in the 10 kW unit tests. The predicted yields of syngas components shown in Figure 6.1, is the mean of the carbon fractions with varying steam-to-biomass ratio at an FR temperature of 985°C. There was no information on the amount of steam used in the tests. The gas composition with the least error was observed in the case with S/B ratio set to 0.8 in the model. Assumptions made in the model could result in variations up to a certain extent. The equilibrium conditions assumed in multiple blocks in the model could be one of the main reasons, followed by differences in operational parameters used during the experimental tests and the model. For example, the biomass compositions although similar, the moisture content (≈15%) of biomass fuel assumed in the model is much higher than of wood pellets (≈6%) used in the 10 kW unit. In addition to this, high carbon conversions (>75%) are estimated in various CLG studies [32]–[34]; however, the assumption of complete char conversion in the FR could be one of the reasons for higher CO_2 yield predicted in the model. No data was reported on hydrogen yield for the wood pellet case in the tests done by Moldenhauer et al.[11]. However, it was reported that there was no clear correlation between hydrogen yield and the fuel type used in the tests, when the hydrogen yields from the three different biomass fuels were compared.

In order to compare the gas compositions including hydrogen, the molar yields (mol/kg_{daf}) predicted by the model was compared with the CLG tests done at Chalmers with LD-slag with varying inert sand fraction [30]. No experiments were conducted with 100% LD-slag, and the gasifier temperature was significantly lower (≈ 800-825°C) in these tests than in the CLG model (≈ 935°C); thus, significant variations can be noted while comparing the model with the tests done with different OC, as shown in Figure 6.2. It is important to note that the model parameters used are significantly different from the ones used in the tests, making it unsuitable for model validation. However, similar trends can be observed, including other CLG syngas compositions reported in the literature. The tests that were done with LDS-57, or LD-slag with 43% inert sand dilution, predicted high yields of CO_2, followed by hydrogen and carbon monoxide. In comparison, the model predicts a similar gas composition, however with a higher yield. This can be attributed to dilution in LDS-57, that results in lower yields compared to the model that uses an oxygen carrier stream with 100% LD-slag. The OL-AA case has the closest match to the model gas composition prediction; however, the OL-AA tends to have high catalytic effect with a low char conversion efficiency reported to be less than 15% [30]. This is unlike the case with LD-slag that generally tends to have significantly higher carbon conversion.

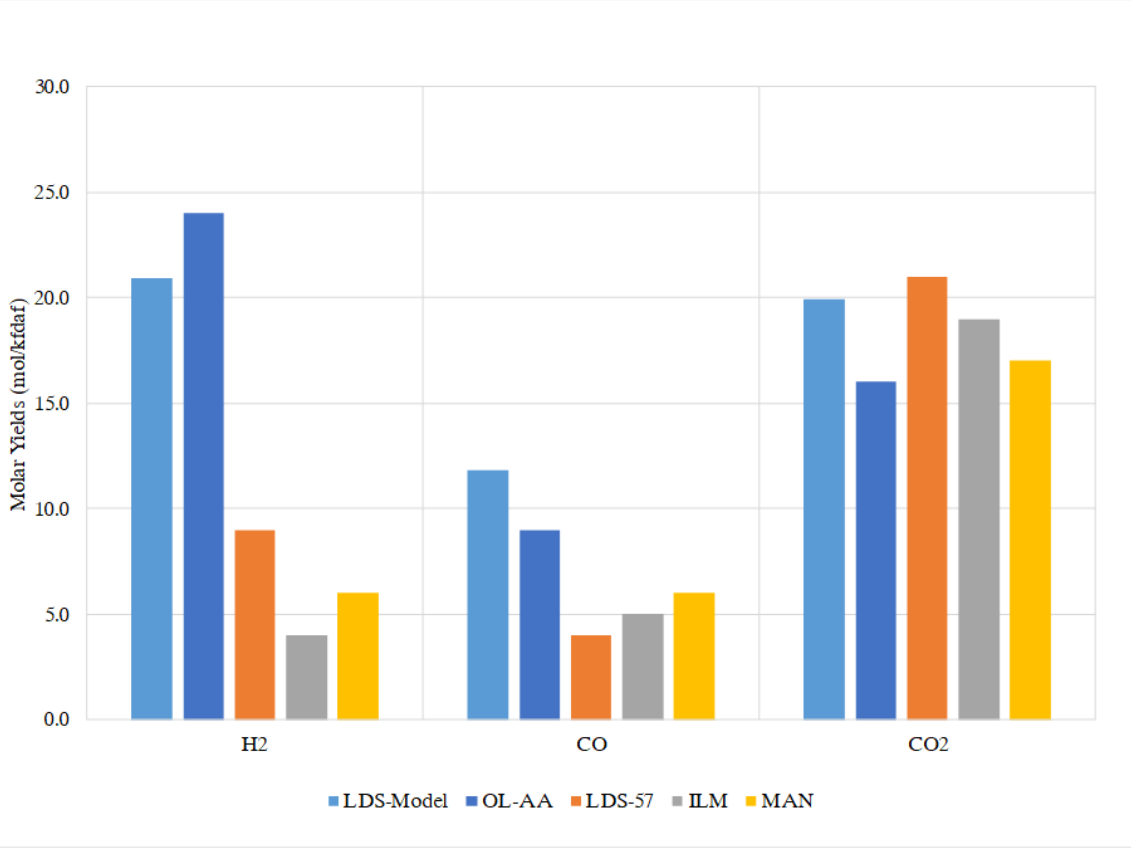

Figure 6.2: Syngas composition predicted by the model at 935°C with S/B ratio of 0.8 compared with CLG experiments with different oxygen carriers

6.1.2 Sensitivity Analysis

As shown in Figure 6.3, a variation of S/B ratio at a set FR temperature of 935°C has a negative impact on the cold gas efficiency (CGE), calculated as in Equation 4.16. The highest CGE (on an LHV-basis) of 59.7% was obtained at an S/B ratio of 0.6 and continues reducing as the steam flow is increased. This indicates an increase in char gasification products with increasing steam flow, producing more CO_2, hence reducing the CGE. The average cold gas efficiency, on an LHV-basis, was approximately 56.6%. Although a 100% char conversion is assumed in the CLG model, char conversion takes place in two different reactor blocks of the FR, in block 4 and 5, see Figure 4.1. Fuel reactor is generally, a well-mixed reactor, however due to the modelling approach used in this thesis, the char conversion is evaluated in each of these reactor blocks by varying the S/B ratio, as shown in Figure 6.4.

The char conversion in block **4** is defined by Reaction 2.7, which is a combined equation of char-steam gasification reaction and water-gas shift reaction. Clearly, as the S/B ratio is increased, more char gets converted in block **4**, and the rest is converted in *RGibbs* block **5**. With S/B ratio above 1, all the char gets converted in block **4** alone. Estimating the most suitable S/B ratio for the process, is however not possible solely based on Figure 6.4, as a complete conversion is assumed and in addition to this, increasing S/B ratio or the steam flow would impact

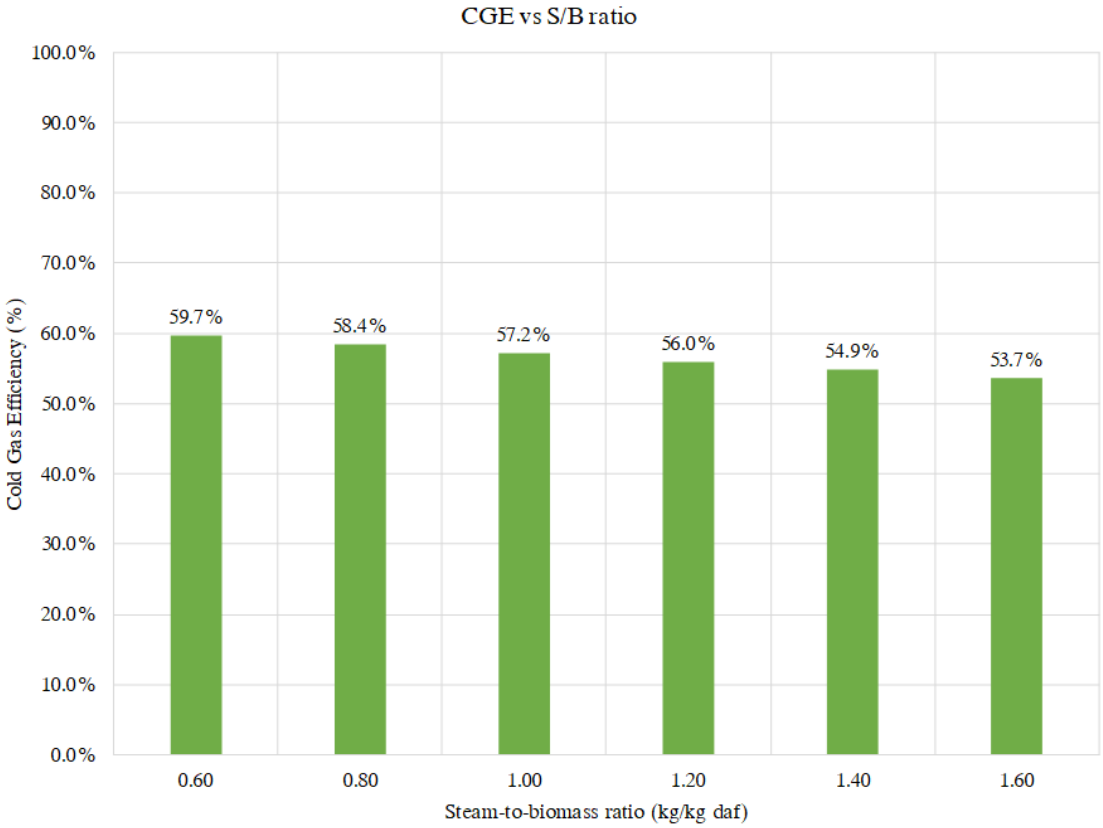

Figure 6.3: Variation of cold gas efficiency with varying S/B ratio at constant FR temperature of 935°C

the thermal efficiency of the plant after a certain point. It is also experimentally shown that char conversion is significantly higher for CLG operation compared to conventional gasification of solid biomass. Thus, a lower S/B ratio between 0.8-1 can be justified. Sensitivity analysis done on various parameters in the following sections is calculated with a set S/B ratio of 0.8. The syngas composition ($vol\%_{d.b}$) is shown with varying S/B ratio at a fuel reactor temperature of 935°C in Figure 6.5.

Here, an increase in hydrogen yield is observed with increasing S/B ratio, and the CO_2 yield in the syngas follows the same trend as H_2, hence indicating water-gas shift reaction, where CO gets consumed, reacting with steam to form H_2 and CO_2. The CH_4 yield remains relatively constant throughout with increasing S/B ratio due to the equilibrium modelling approach taken for methane and tar formation. For an S/B ratio of 0.8, syngas with 47.1% H_2, 26.6% CO, 17.1% CO_2, and 8.9% CH_4 was obtained. Similar gas compositions were reported in the literature. A syngas composition of 40% H_2, 34% CO, 16% CO_2, 7.5% CH_4 and the rest C_2H_4 was reported by Ge et al. [32] for a CLG (FR_{temp}=860°, S/B=0.8) test on rice husk using natural hematite as the OC.

The effect of increasing FR temperature on the syngas composition was also analyzed. This analysis revealed little to changes in the syngas composition, as shown

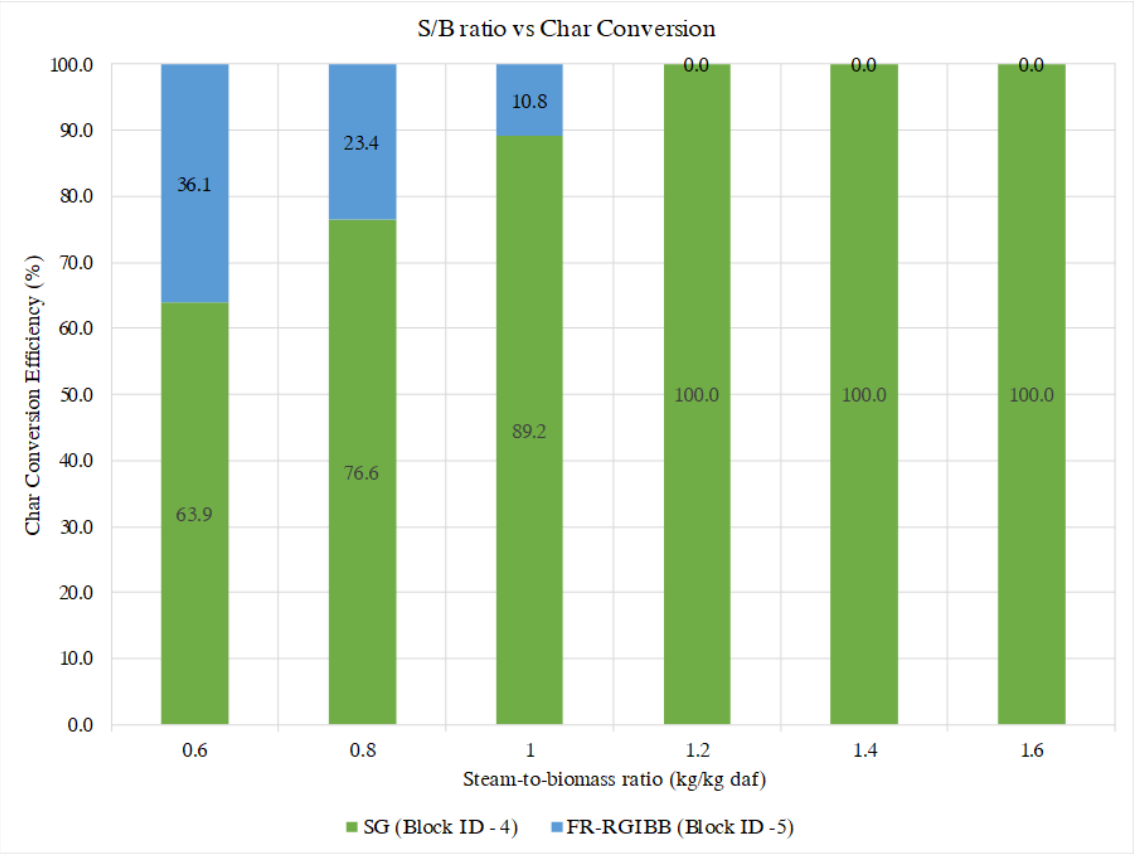

Figure 6.4: Char conversion in the two reactor blocks (4 & 5) of the fuel reactor

in Figure 6.6. However, the higher temperature resulted in a slightly higher OC circulation between the AR and FR in order to maintain an auto-thermal operation. In Figure 6.6, the syngas composition with varying gasifier temperature is shown, along with equivalence ratio, as calculated in Equation 4.14, that depicts the OC circulation between the two reactors in the CLG model.In the case of OC circulation, a conservative value of 0.06% is chosen for the OTC of LD-slag in the model compared to the maximum OTC of 1.12%. This would reflect in a slightly higher mass flow rates of the oxygen carrier particles predicted in the model to maintain an auto-thermal operation between the two reactors. The oxygen carrier transport capacity is known to deteriorate after several redox cycles, and this has been observed in several types of OCs tested; thus, this value is chosen. Based on future CLG experiments with LD-slag, this parameter defined in the model can be corrected for more accurate expected gas compositions and OC mass flow rates.

The impact of varying MC on the cold gas efficiency is shown in Figure 6.6. The moisture content of low commercial value forest residue on an as-received basis is usually between 35-50%. The moisture content of the biomass fuel is varied between 15-35%, in order to evaluate its effect on CGE. It is important to note that, the forest residue composition used in the model, is of pine spruce residue with an assumed minimum MC of 15% and this is higher than the one reported in the literature for pine spruce residue chips, that is close to 6-8% [15].

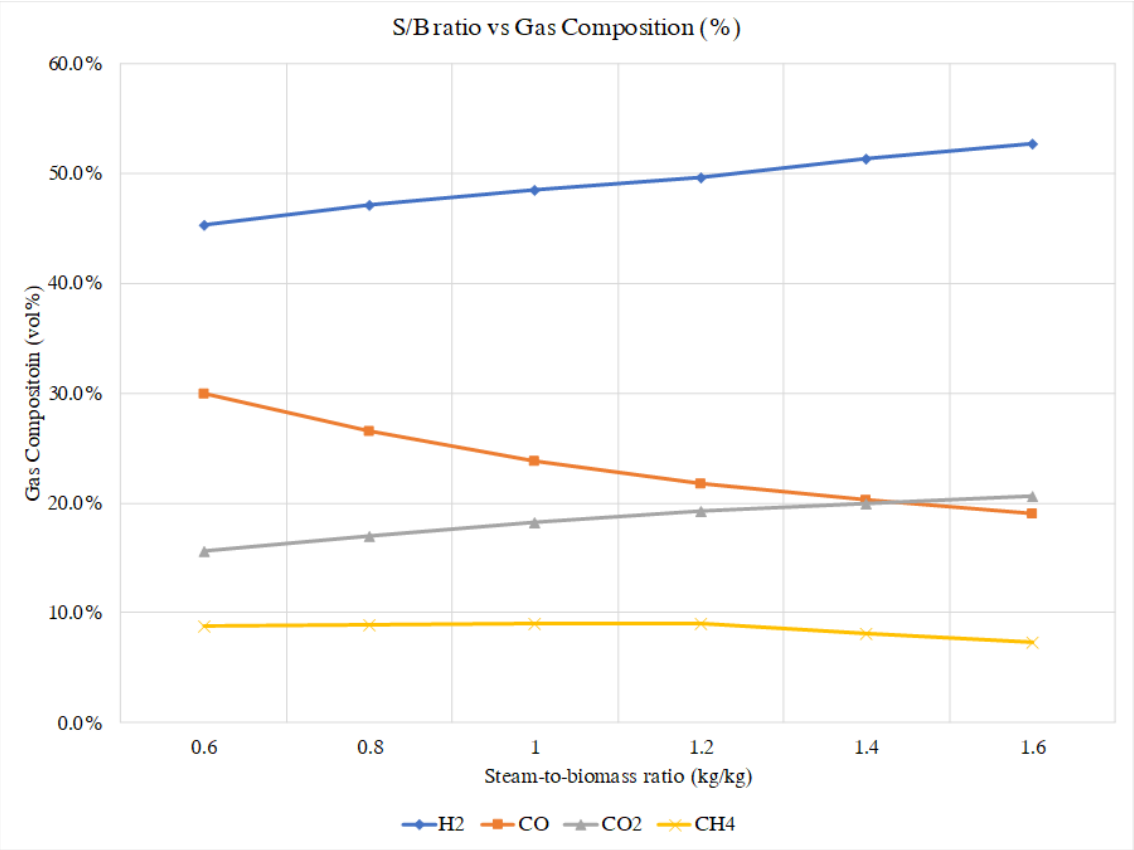

Figure 6.5: S/B ratio vs syngas composition (vol% dry)

As shown in Figure 6.7, for a fixed S/B ratio of 0.8, increasing fuel MC results in reduced CGE or gasification performance. The lowest cold gas efficiency is estimated to be approximately 37.3% for forest residues with an MC of 35%. This indicates a need for an air/steam drier for fuel drying, especially as the MC in forest residue can be as high as 50%. In comparison with the GoBiGas plant, a cold gas efficiency of 71.5% (LHV_{daf}) was reported with a fuel (dried biomass) MC of 8%. Thus, a low MC in the fuel is critical for the gasification performance, especially when it is integrated with a downstream fuel production plant. The hot air from the air reactor could be potentially be utilized for fuel drying, or an excess steam production could be utilized for steam drying of the fuel. However, the most appropriate drying solution can only be decided after an extensive heat integration comparison study.

6.2 Integrated CLG-FTS Model

The performance of the integrated model is evaluated using the performance indicators listed in Section 4.4. The evaluations are done considering a fixed FR temperature of 935°C and an S/B ratio of 0.8. Gasification performance evaluated using Equation 4.16 estimated an average CGE of 56.6%. The produced syngas is converted to FT-products such as paraffins and olefins. Here, long-chained hydro-

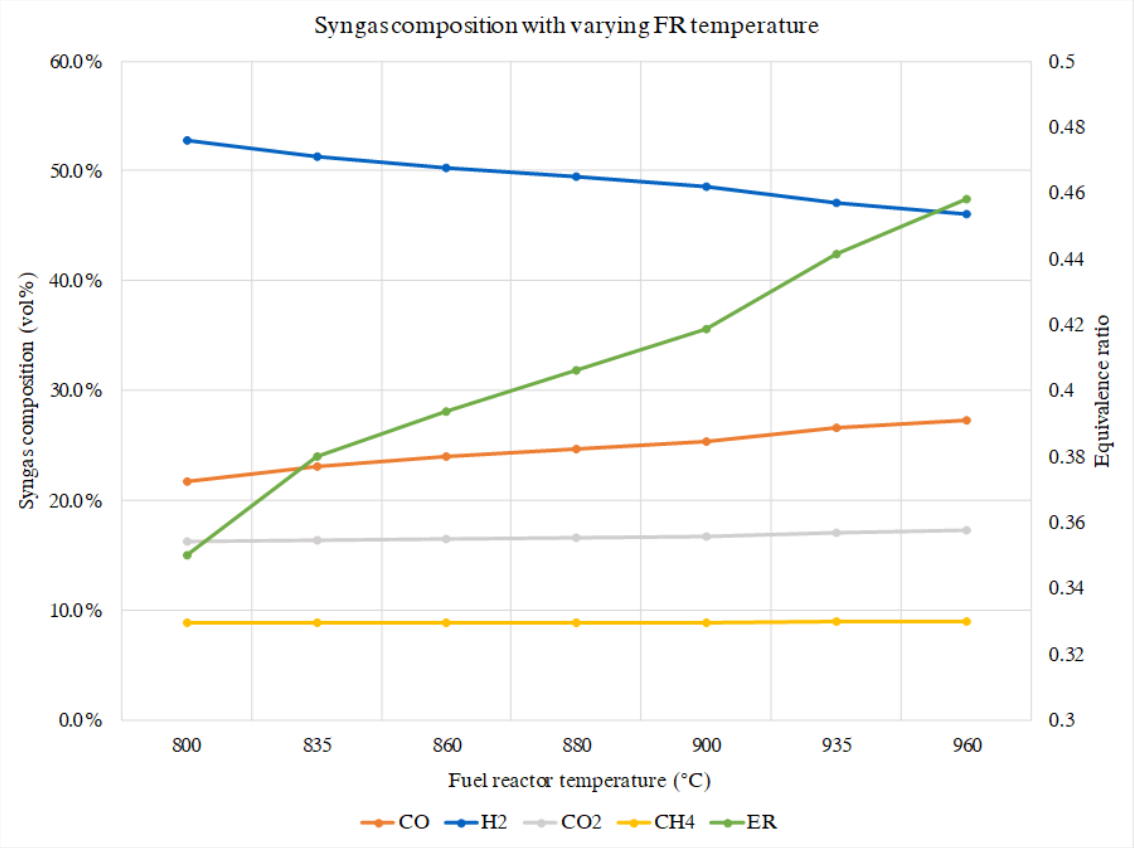

Figure 6.6: Variation in syngas composition with varying FR temperature

carbons ranging from C_5 to C_{11} are grouped as naphtha, C_12-C_19 as FT-diesel or diesel, and hydrocarbons longer than C_20 are grouped as waxes. This approach of distinguishing between paraffins and olefins in the FT-product stream and groupings based on carbon numbers is similar to the previously done thesis on FTS, for more information see [53]. The product distribution of FT-products obtained at these fixed operating conditions of S/B ratio (0.8), FT-reactor operating conditions (220°C, 20 bar, $X_{co} = 0.5$), gasification temperature (935°C) is shown below in Figure 6.7.

In Figure 6.8, the major product obtained is Naphtha ($\approx$ 48%) followed by FT-diesel ($\approx$ 35%), and the remaining products are waxes ($\approx$ 15%), followed by olefin ($\approx$ 1%) and C_1-C_4 products. Higher FT-reactor temperature is conducive to produce lighter hydrocarbons; thus, the product distribution with varying FT-reactor temperatures are not investigated in this thesis as the primary focus with respect to FTS model was to maximize FT-diesel production. Preliminary investigation of total FT-product yield with varying S/B ratio in the gasification section revealed that with higher steam flows, the FT-product decreased slightly. Similarly, when the S/B ratio was reduced to 0.6, FT-product yield slightly increased. However, these variations are quite minimal. Although a WGS reactor is used to set the H_2/CO ratio prior to FT-reactor, the minimal variation in the total FT-product yield can be attributed to the varying syngas input to the FTS model, resulting from variation

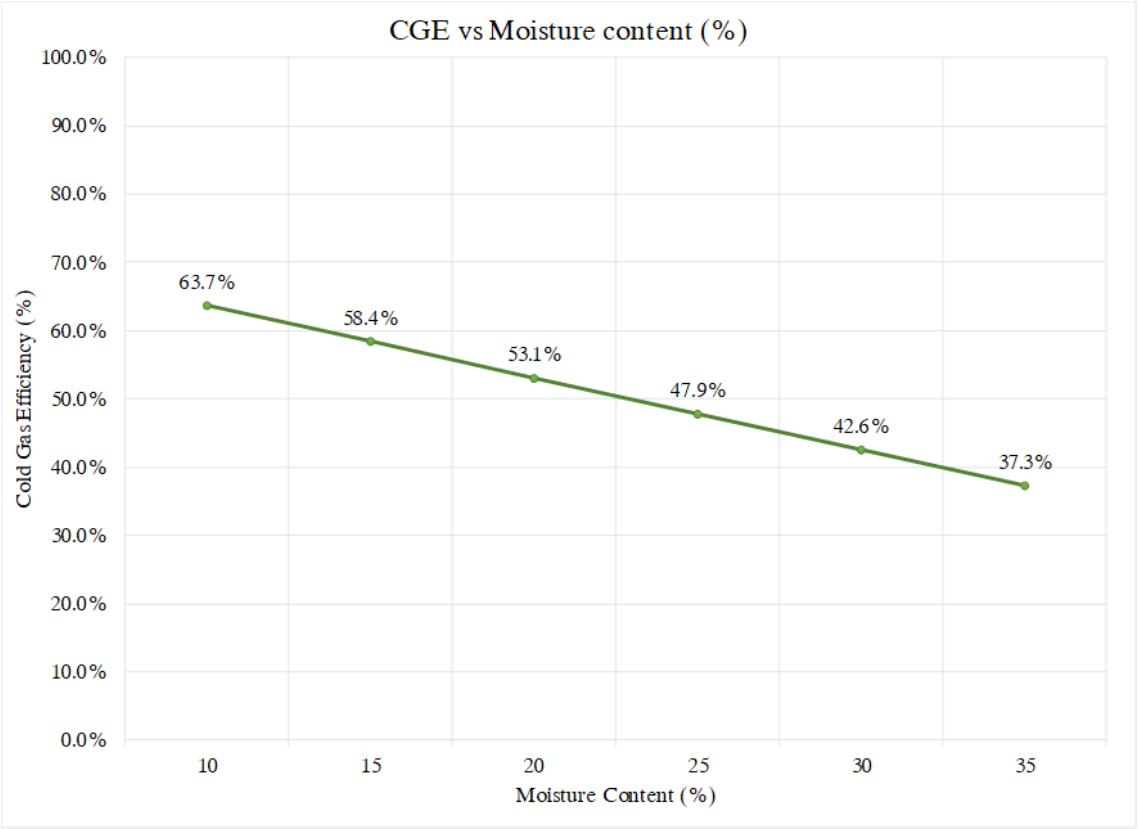

Figure 6.7: Cold gas efficiency (%) variation with increasing moisture content in the biomass fuel

in S/B ratio in the CLG model. Therefore S/B ratio variations and its impact on FT-product distributions are not considered for a sensitivity analysis here, for the sake of brevity. The FT-product distribution is, however, extremely dependent on the FT-reactor process parameters.

The integrated model has two AGR technologies with different operating temperatures and pressures. This is a result of integrating two previously developed standalone models for different purposes. In the integrated model, the amine scrubber acts as the primary AGR unit and the Rectisol® unit is used for capturing the additional CO_2 emanating the WGS reactor and reduce the inert gases in the syngas prior to the FT reactor. Both these AGR units operate at different pressures and temperatures. For example, the Rectisol® unit requires refrigeration for sub-ambient cooling, whereas the amine scrubber operates around 30°C at a higher pressure. This is one of the potential areas for model optimization in the future whereby having a sour WGS reactor with sulphur resistant catalysts, followed by an AGR unit. Thereby needing only one AGR unit for the whole integrated process. Based on this, the current integrated model can be modified in the future to this configuration, which would enable a comparative techno-economic study of the two configurations.

To evaluate, the electricity balance using Equation 4.20, the electricity demand is estimated for the integrated model with fixed operational parameters as mentioned

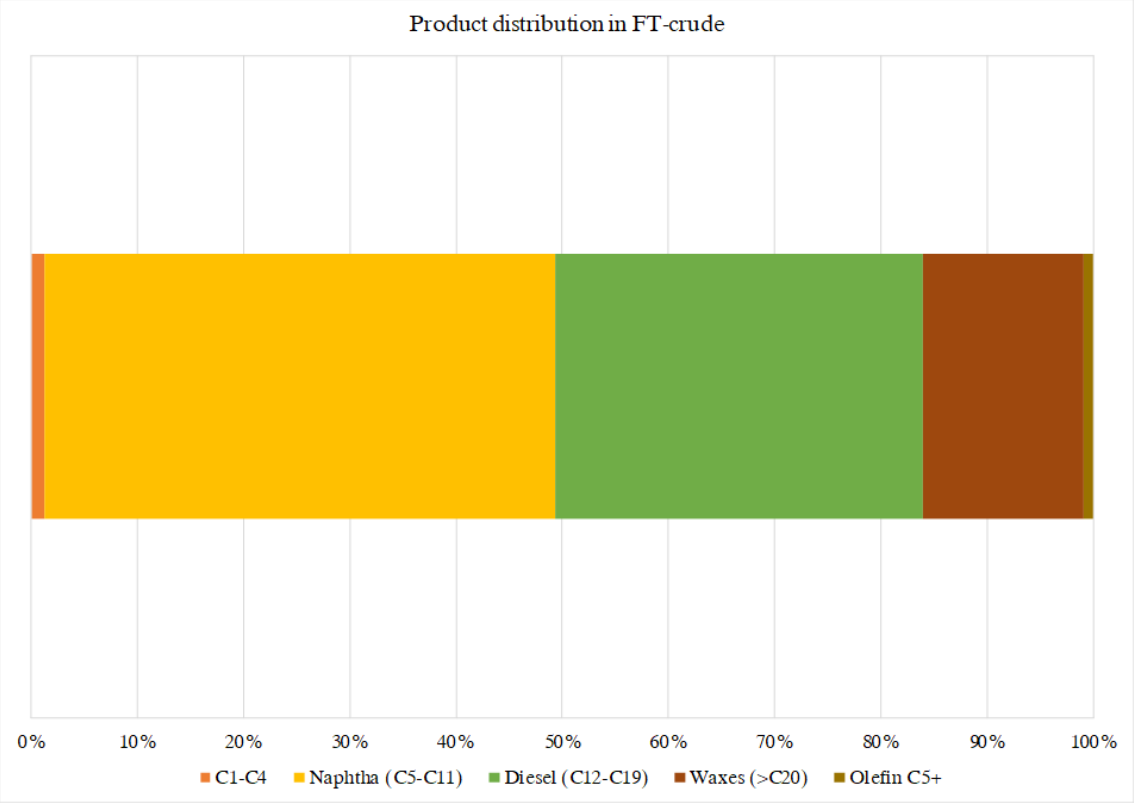

Figure 6.8: Product distribution in FT-crude

before. Several auxiliary units such as compressors and pump are required in the model; however, some are not included in the model, for example, the compressors for carbon capture and the ASU for oxygen supply to the ATR. With respect to electricity balance, it is important to include required compression work for carbon capture as the primary goal of this novel process plant is to produce liquid fuel with net-negative CO_2 emissions. The ASU required for the ATR is used to provide pure oxygen to maintain the reactor temperature at 1000°C. This auxiliary unit is not considered for electricity balance as the required oxygen flows are minimal. In addition to this, the carbon penalty for supplying this oxygen has not been considered.

The Rectisol® unit operates at sub-ambient temperatures and would require refrigeration, and the cooling duty required in this unit is assumed to be 62 kW per MW_{th} of biomass fuel gasified [76]. In a biomass-to-liquid fuel with CCS study by Hannula et al. at VTT [74], the carbon capture compression section is assumed to be done in a three-stage compression train to 150 bar pressure with intercooling to 30°C, with a specific electricity requirement of 0.36 MJ per kg of CO_2 compressed with a compression efficiency of 95%. This specific electricity requirement corresponds to compression from 1.5 bar to 80 bar, and then the supercritical CO_2 is pumped to 150 bar pressure [77]. This available data has been used in this thesis to estimate the compression electricity requirement in the compression train. The CO_2 streams from the AGR and the Rectisol® unit need to be captured; however, the streams are expected to be at different outlet pressures. A typical outlet stream pressures

for a Rectisol® unit is roughly between 3.77-5.1 bar and in a similar range in the amine scrubber unit, hence indicating there could be potential savings in electricity demand for compression. Thus, the assumption of the specific electric requirement of 0.36 MJ/kgCO_2 could be lower in this case; however, to estimate the electricity demand, this is left unchanged. This assumption could potentially lead to slightly overestimation of electricity demand for compression and in turn underestimates the overall system efficiency of the process, calculated as in Equation 4.19. The electricity demand of the integrated model is estimated to be approximately 6.24 MW, excluding refrigeration cooling demand and the total electricity demand, including refrigeration, is roughly 16.9 MW. The electricity demand calculated for each auxiliary unit in the integrated model is listed in the Appendix A.4.

As shown in Figure 6.9, the carbon capture capacity or the net-negative CO_2 emissions of the integrated model is estimated to be roughly 148-160 ktonne per year, depending on the MC in the fuel. Here, the MC of 6% corresponds to dried forest residue chips that tend to be drier when compared to untreated forest residue biomass and the upper bound MC of 15% is the one assumed for the dried forest residue feed in the CLG model. The total carbon capture capacity includes the CO_2 streams from both the AGR units, the amine scrubber and the Rectisol® unit. This estimation, however, excludes the purge gas stream penalty.

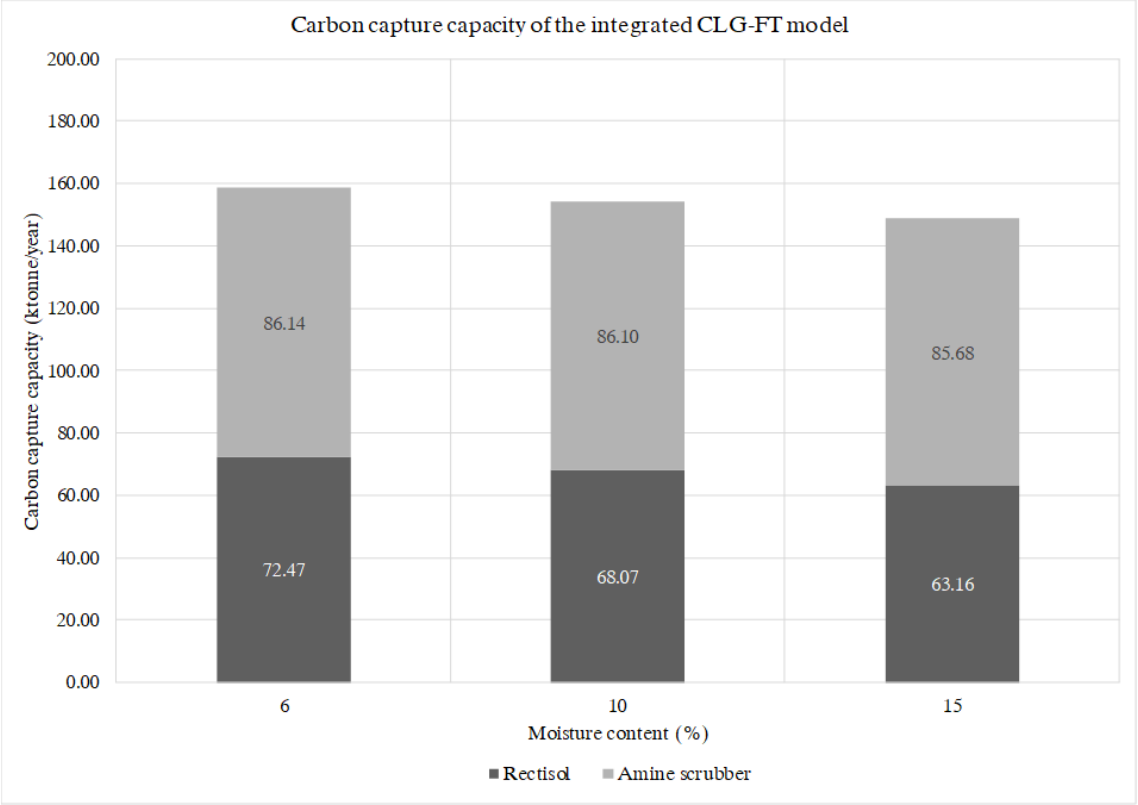

Figure 6.9: Carbon capture capacity of the integrated CLG-FT model from the two gas cleaning units

Considering the PG stream is either burnt in a boiler for heat recovery or flared,

the net-negative emissions are estimated to be between 138-146 ktonne per year, as shown in Figure 6.10. Based on the heat integration study in the following section, an electricity deficit in the integrated plant could lead to another potential penalty on the net-negative CO_2 emissions of the integrated plant that can be attributed to the source of the imported electricity to the plant. Assuming an electricity deficit is met with carbon-free electricity source, this penalty can be avoided. In the case of an electricity surplus in the plant, carbon-free renewable electricity can be exported to generate revenue.

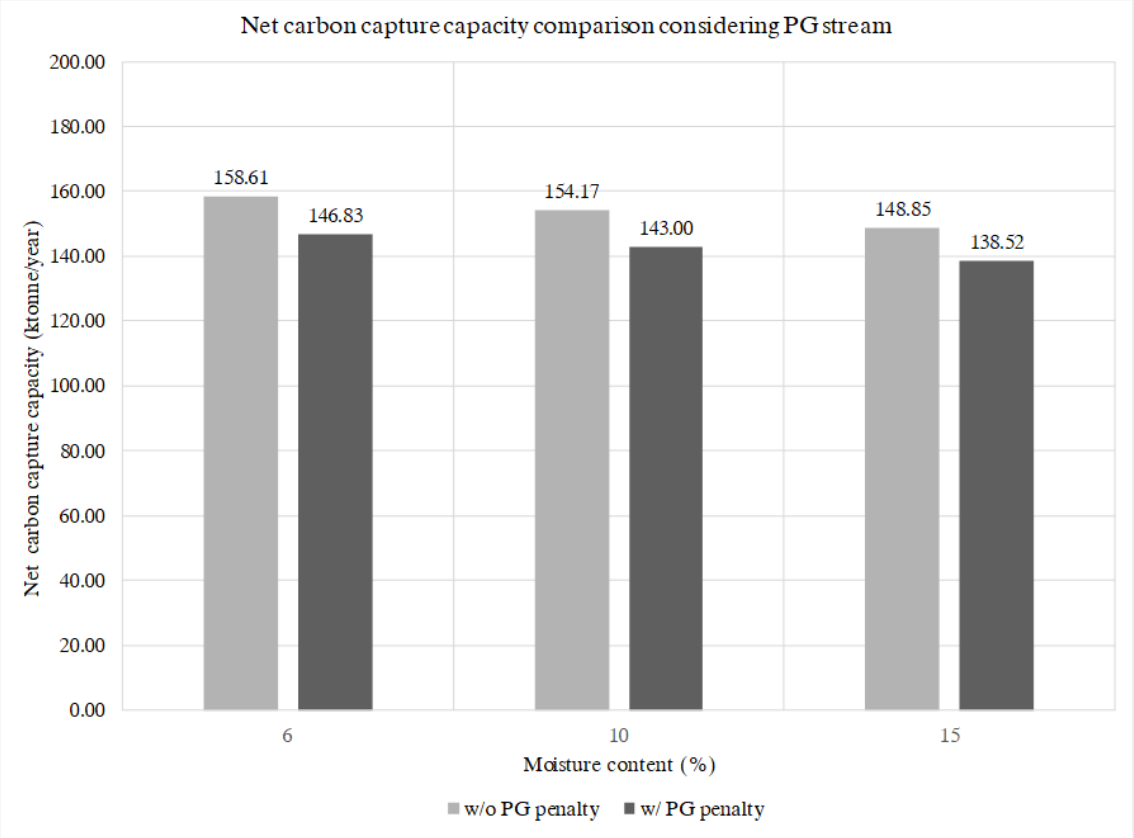

Figure 6.10: Carbon capture capacity comparison of the integrated model with and without the purge gas penalty

The chemical efficiency is calculated using Equation 4.18, and a chemical efficiency of 21.02% is estimated for a 100 MW_{th} of biomass fuel with an MC of 15%, including the energy required for the RME feed in the tar scrubber. This is calculated on an HHV basis, and the resulting HHV for the FT-crude is approximately 46.68 MJ/kg, excluding the other chemical products produced such as olefins. The MC in the waste biomass gasified has a cascading effect on the downstream fuel synthesis process, as a result of lower syngas production, that in turn results in deterioration of chemical efficiency of the overall plant with increasing MC in the biomass fuel, as shown in Figure 6.11.

Overall system efficiency includes the electricity balance of the integrated plant,

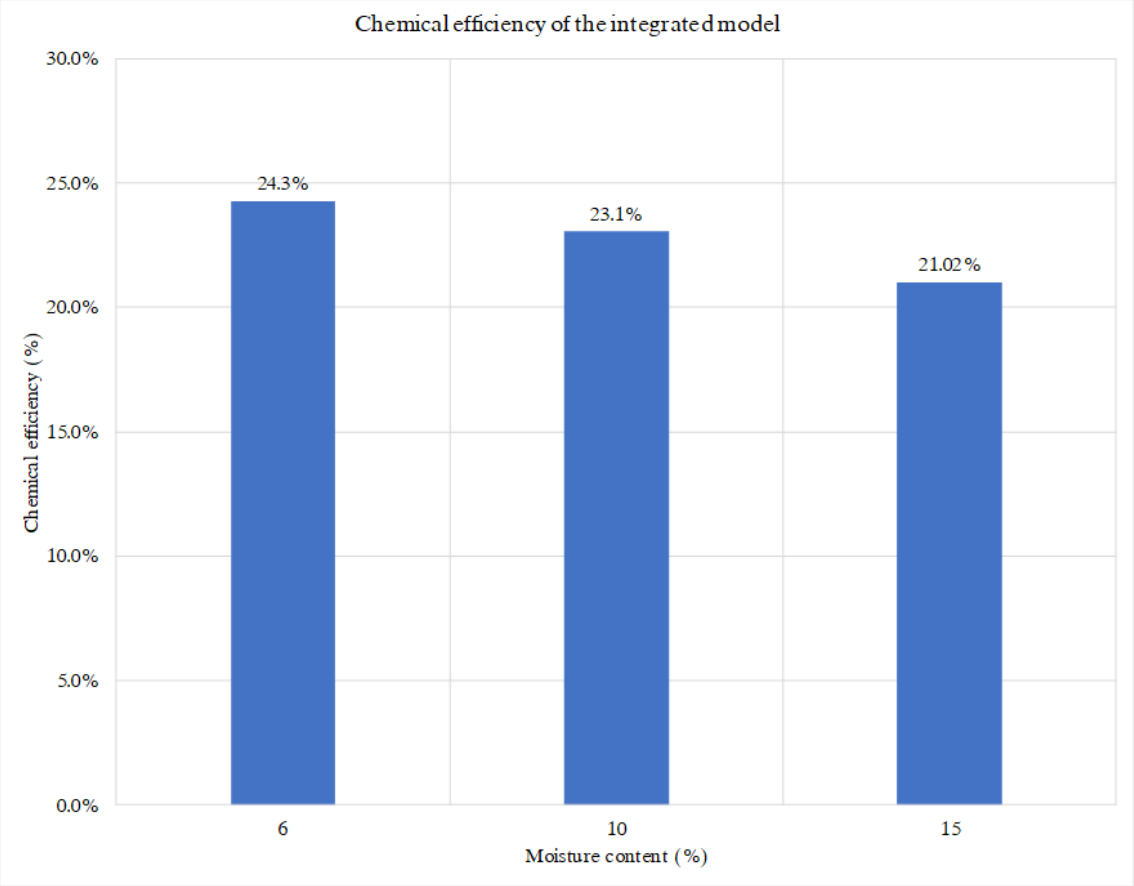

Figure 6.11: Variation in chemical efficiency with increasing moisture content in the biomass fuel

hence depends on the estimated on-site power production after the steam cycle integration. The energy efficiency of the integrated model is, therefore presented in the following section. The overall FT-crude production capacity of the plant is estimated to be between 359-380 barrels per day with the lower limit corresponding to an MC of 15% in the biomass fuel. Clearly, the MC in the waste biomass has a significant impact on the overall process; therefore, procuring dry waste biomass is crucial to the process. Other option would be to integrate an on-site fuel drier system to the integrated model in the future based on heat recovery potential of the plant. With respect to this, the heat recovery or co-generation potential of the integrated model is discussed in the following section.

6.3 Heat Integration Results

The grand composite curve (GCC) for the integrated model at fixed operational conditions, is shown below in Figure 6.12, that includes all the relevant process streams in the integrated model. In Figure 6.12, the solid curve represents the GCC of the integrated CLG-FT process that includes the hot air cooling from the AR, syngas cooling, steam and air preheating. In addition to this, the reactor cooling

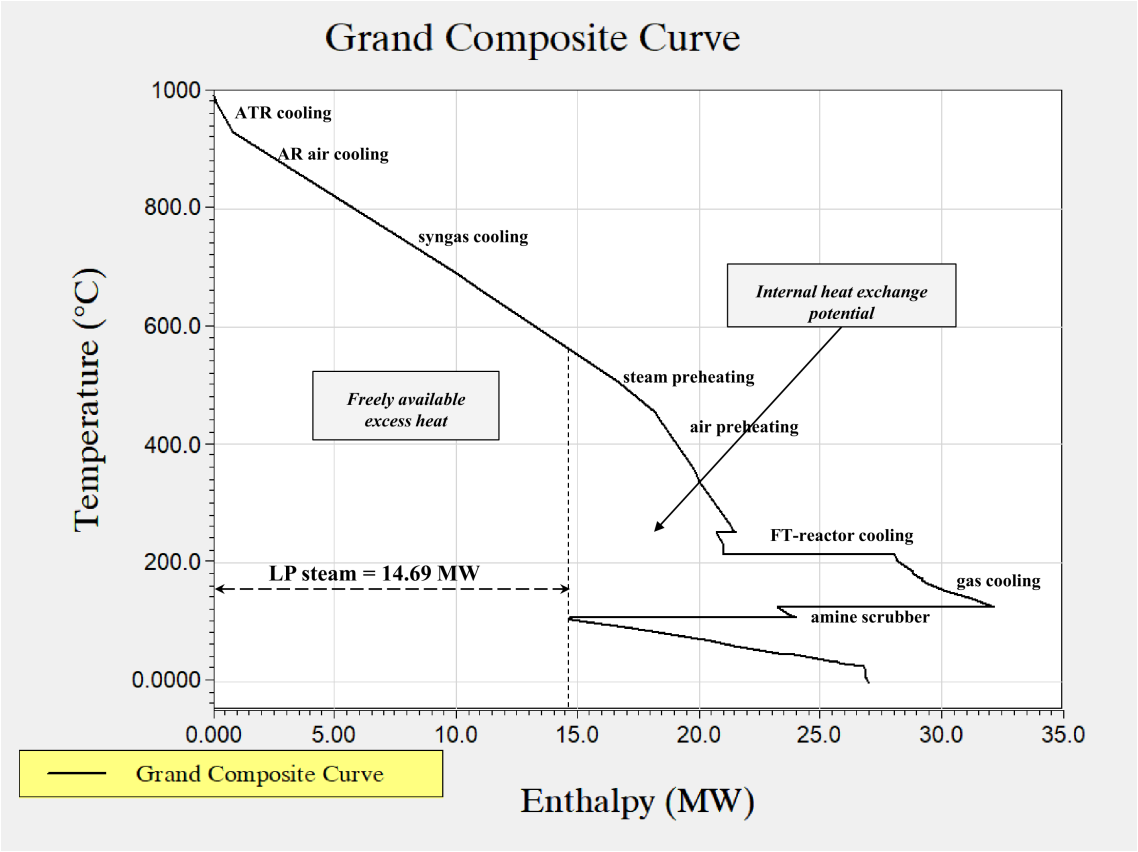

Figure 6.12: Grand composite curve of the integrated model

required to maintain the reactor temperatures in the FT reactor and ATR is also included. The heat demand in the tar scrubber and amine scrubber is included manually in the AEA software, based on the assumed specific heat demands of the scrubbers as mentioned in Section 5.

The GCC of the integrated model is a threshold problem with no heat utility requirement and a minimum cooling duty of 26.9 MW. Pinch analysis clearly shows the considerable amounts of high-temperature surplus heat available in the process above 220°C for heat recovery. External cooling utility with cooling water and refrigerant in the Rectisol® of roughly 12.21 MW is required at certain process steps in the FT plant.Assuming internal exchange within the heat pocket, the excess heat available can be used to generate approximately 14.69 MW of LP steam at 5 bar pressure level as shown in Figure 6.12.

With an increased level of integration, the heat within the pocket can also be utilized to generate additional LP steam along with electricity. The heat pocket here spans between two pressure levels; hence, the pocket is not left isolated assuming process-to-process heat exchange within the heat pocket, and complete exploitation of the heat pocket is preferable. The resulting split-GCC analysis between the two processes is shown below in Figure 6.13, where the dashed line represents the foreground GCC, and the solid curve represents the GCC of the integrated model.

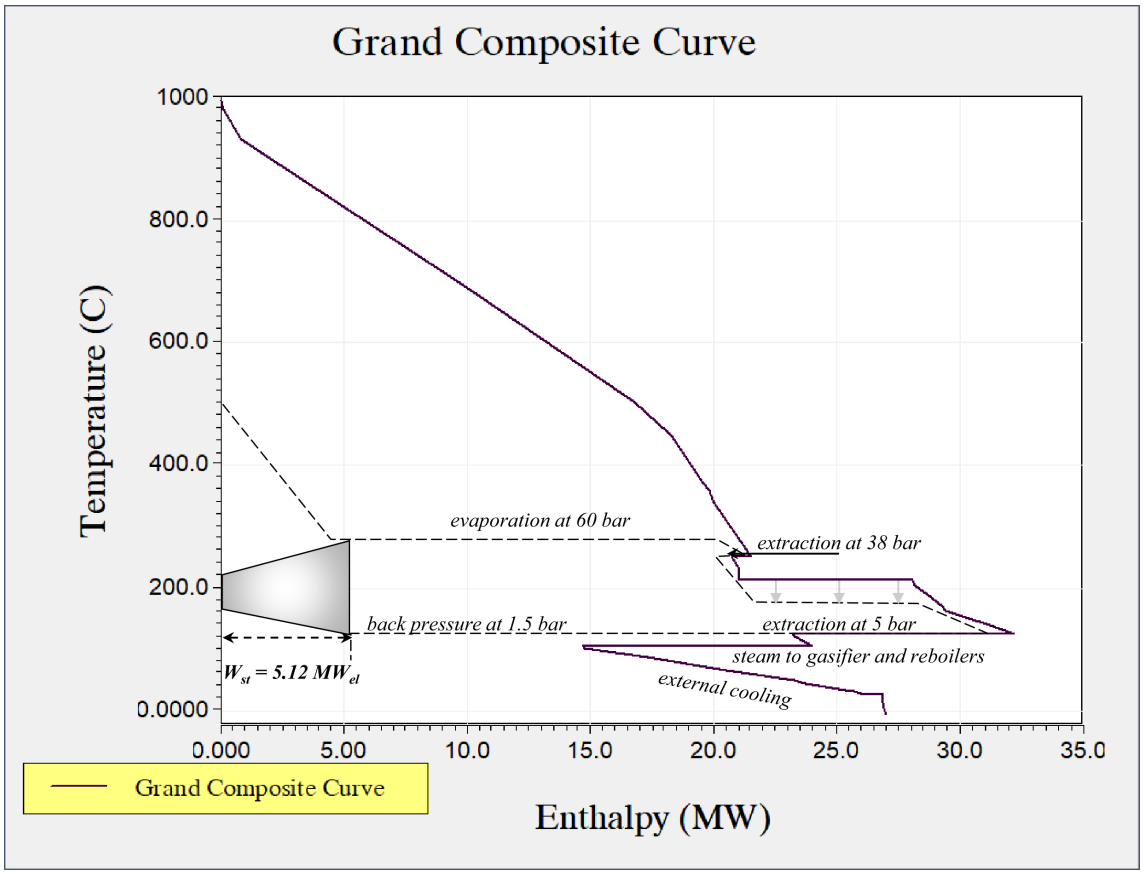

Figure 6.13: Grand composite curves of the integrated model and the heat recovery steam cycle

The electricity generation potential is estimated to be around 5.12 MW_{el} (corresponding to an input steam flow of 9.8 kg/s) while assuming an isentropic turbine efficiency of 0.75 for each turbine stage. This indicates a net electricity deficit in the overall process that has a total electricity requirement of 16.9 MW_{el} (6.24 MW_{el} excluding refrigeration cooling duty). Addition of fuel drier prior to the gasifier would significantly increase LP steam demand of the process, therefore further reducing the electricity generation potential. Based on the current electricity generation potential, the overall system efficiency of the integrated model is shown in Figure 6.14, calculated as in Equation 4.19. Again, this is shown with respect to the MC in the biomass fuel varying from 6% to 15%, for the forest residue chips to the MC taken in the model, respectively.

The overall system efficiency ranges between 21.7-18.8%, as shown in Figure 6.14. It is important to note here that the excess heat in the process is only used for on-site steam consumption and electricity production and no district heating application is considered here. This results in a low system efficiency due to net electricity deficiency. In addition to this, electricity consumption in certain units is overestimated, such as the CO_2 compressor units that are not modelled. Exploring the possibility of using the excess heat in the process for district heating application seems to be the better integration option, and this would result in higher overall

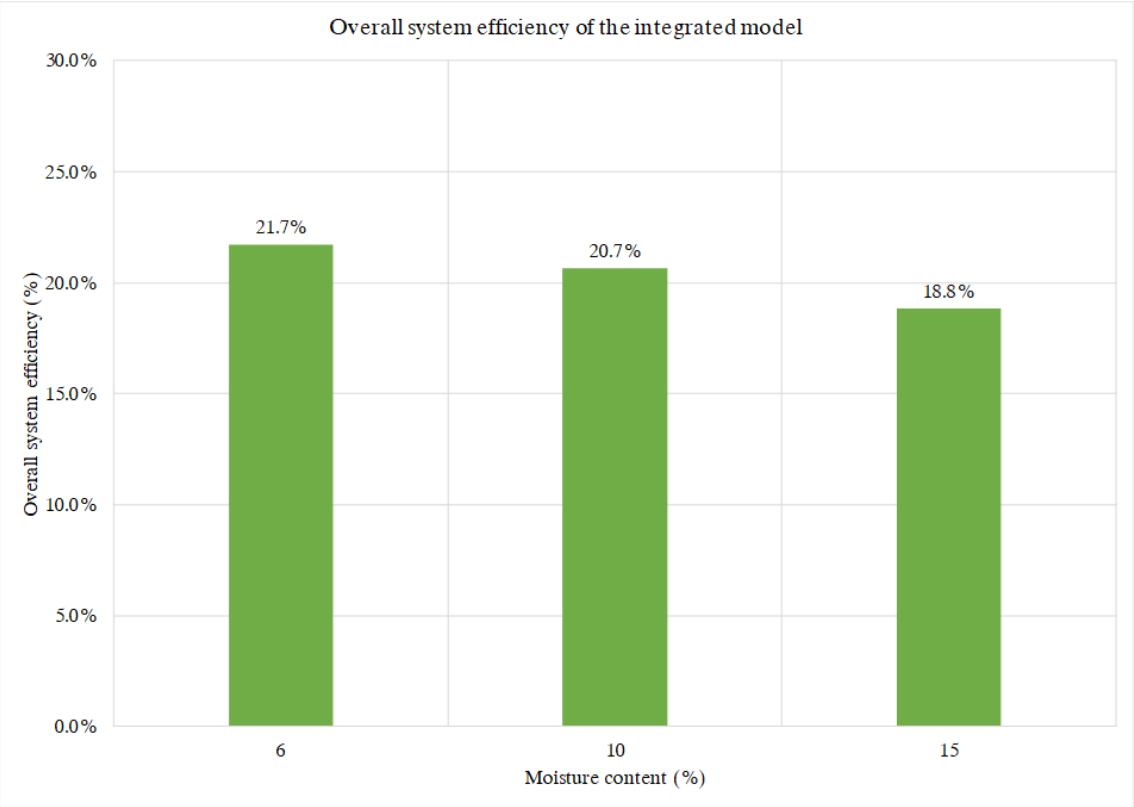

Figure 6.14: Variation in overall system efficiency with increasing moisture content in the biomass fuel

system efficiencies. As discussed before, if the electricity deficit in the integrated plant is met with electricity imported from carbon-emitting sources, it could impact the estimated net-negative CO_2 emissions of the integrated plant. Thus, importing renewable electricity is crucial to maintain the net-negative CO_2 emissions of the overall plant.

7

Conclusion

An integrated model of a 100 MW_{th} chemical looping gasification plant with downstream gas cleaning and Fischer-Tropsch synthesis process was developed and analyzed in this thesis. The CLG simulations have been performed with LD-Slag as the primary oxygen carrier particles in the system. The model has been validated with experimental data available on CLG operations done with LD-slag as the oxygen carrier. Syngas with a high energy content of 12 MJ/Nm^3 (LHV basis) is predicted with an average cold gas efficiency of 56.6%. A syngas composition of 47.1% H_2, 26.6% CO, 17.1% CO_2, and 8.9% CH_4 was obtained with an S/B ratio of 0.8 and fuel reactor temperature of 935°C.

Sensitivity analysis was performed on the CLG model by varying S/B ratio, the moisture content in the fuel and the gasification temperature. A variation in the S/B ratio (0.6-1.6) increases the hydrogen yield in the clean syngas, ranging from 45.3%-52.7% (vol %) which in turn increases the H_2/CO ratio of the syngas. The cold gas efficiency (CGE), however, dipped from a maximum of 59.7% to 53.7% with this increase in S/B ratio, for an FR temperature of 935°C. An optimal S/B ratio is estimated to be in the lower range of 0.6-1 owing to the deterioration of CGE and the penalty on thermal efficiency with increased steam usage for gasification. An increase in the MC of the biomass feed has a significant impact on the CGE, which has an impact on the downstream fuel synthesis process. Varying the moisture content between 10-35% in the biomass feed stream with a fixed S/B ratio (0.8), revealed a significant drop in CGE from 63.7% to 37.3%. The product distribution of the FT-crude is heavily dependent on the FT model process parameters, such as the type of catalyst used, amount of catalyst in the FT reactor, reactor temperature and pressures. The resulting FT-crude in the integrated model, with the chosen FT process conditions (220°C, 20 bar, Xco = 50%), mainly comprised of naphtha (48%), FT-diesel (35%), and waxes (15%).The naphtha, clustered as hydrocarbons ranging from C_5-C_{11}, can be upgraded to gasoline and the FT-diesel (C_{12}-C_{19}) obtained after refining the FT-crude, is a sulphur-free diesel, that can be used in the transportation sector.

The integrated model has been analyzed to estimate its overall process efficiency, chemical efficiency, carbon capture capacity and the total fuel production capacity. The overall chemical and system efficiency of the integrated model is estimated to be approximately 21.02% and 18.8%, respectively. With a lower MC in the biomass fuel of 6%, corresponding to forest residue chips, the chemical efficiency and energy efficiency improves to 24.3% and 21.7% respectively, indicating a need for fuel drier prior to the gasification process. The integrated model has an FT-crude production capacity of roughly 359-380 barrels per day. The FT-crude yield, and therefore the chemical efficiency of the process, is expected to increase with higher CO conversion or higher amounts of catalyst in the FT reactor.

Pinch analysis of the integrated model has been performed for the CLG and FT-synthesis plant to estimate co-generation potential. Approximately 5.12 MW_{el} of electricity can be produced through maximum heat integration that covers roughly 30% of the on-site electricity demand. In addition to this, the on-site heat demands of 24.41 MW is fulfilled. The integrated model is electricity deficit and thus would require electricity import from a carbon-free source to avoid a penalty on the net-negative CO_2 emissions of the process, which is estimated to be around 148.85 ktonne/year for a biomass feed with 15% MC. This drops to 138.5 ktonne/year including the penalty from purge gas stream in the FT-model if flared or combusted in a boiler. The integrated model has an FT-crude production capacity of roughly 359-380 barrels per day. The main result of the integrated CLG-FT plant with a thermal input of 100 MW_{th} biomass with a moisture content of 15% is listed in Table A.3.

Table 7.1: Summary of the main results of the integrated CLG-FT plant with a 100 MW_{th} thermal input of biomass with a moisture content of 15%

Cold gas efficiency (CGE)	**Chemical efficiency (η_{ch})**	**Overall system efficiency (η_{sys})**	**FT-crude production capacity**	**CO_2 capture capacity**
58.4%	21.02%	18.8%	359 barrels/day	138.5 ktonne/year

7.1 Future Work

Some of the limitations of the developed CLG and future process modifications are mentioned in this section. Firstly, the char gasification step is defined based on a combined equation of water-gas shift reaction, and char-steam gasification reaction with a mechanism factor based on the gasification temperature and this factor is estimated from coal gasification experiments. This approach has been previously used in CLC process models with co-combustion of biomass and coal. Based on future CLG experiments with LD-slag, the char-steam gasification could be updated in the model to get more accurate volatile gases composition in the FR, and in turn, improved syngas composition predictions from the CLG model. In addition to this, in the volatile combustion section, the oxygen carrier reduction is restricted to the Fe_2O_3/ Fe_3O_4 oxide couple, and it would be interesting to consider even lower oxide couples such as Fe_3O_4/FeO and evaluate changes in the syngas composition. One of the main compounds of LD-slag, calcium oxide is known to promote water-gas shift reaction. The current model already predicts a high H_2/CO ratio, around 1.77, even with CaO specified as inert in the model. The CLG models can be further improved with additional experimental data regarding these species in LD-slag.

Secondly, concerning the acid-gas removal process, the current integrated model has two acid gas removal units, an MDEA scrubber and a Rectisol® unit. It also employs cold gas cleanup steps prior to the WGS reactor. This could be modified to a hot gas cleanup process with a WGS reactor that is resistant to acid gases, followed by a physical solvent scrubber such as a Rectisol® unit with high separation

efficiencies. This would reduce the AGR units required to one, in the integrated model, and it would also eliminate the need for heating the clean syngas prior to the high-temperature WGS reactor. Further modifications in the CLG model can be made with respect to predicted tar yields and the OTC of LD-slag based on future CLG experiments with LD-slag. Although high carbon conversion is expected in CLG operations, the complete conversion of char assumed in this thesis may lead to slight overestimation in certain predicted values such as syngas composition and cold gas efficiency. At the same time, a relatively low OTC is specified in the model, that may lead to overestimation of the OC circulation mass flow rates to achieve an autothermal CLG operation. Therefore, the carbon conversion efficiency may also be updated in future, by specifying a certain carbon leakage to the air reactor in the CLG model and the OTC of LD-slag can also be modified with more available information regarding this. Although these suggested modifications to the model may have only a minor effect on the overall process, these changes can be made to minimize variation in the predictions from the current model. Different oxygen carriers suitable for CLG can also be tested in the model with their oxygen transport capacities, to further improve the model based on experimental results.

Finally, based on the heat integration study in this, the heat recovery steam cycle can be optimized, and plant-wide modelling can be performed with an efficient heat exchanger network. Further, a heat integration study for the integrated plant with other integration possibilities; for example, district heating can also be explored. A techno-economic analysis can be performed for the integrated CLG-FT plant that would enable identifying the various economic trade-off that exists with respect to certain technologies and operating conditions existing in the integrated process. To name a few optimization opportunities, increased CO conversion in the FT-reactor with higher catalyst amounts and thus higher FT reactor volumes, the type of fuel drier to be integrated, and different tar cleaning technologies can also be explored. A well-to-wheel analysis of the overall process chain, including transportation, FT-crude refining can be performed to estimate the final biofuel cost and the well-to-wheel GHG emissions.

References

[1] I. E. Agency, *CO2 Emissions from Fuel Combustion 2018*, ser. CO2 Emissions from Fuel Combustion. OECD, Oct. 2018, ISBN: 9789264056411. DOI: 10.1787/co2{_}fuel-2018-en. [Online]. Available: https://www.oecd-ilibrary.org/energy/co2-emissions-from-fuel-combustion-2018_co2_fuel-2018-en.

[2] IPCC, "Global Warming of 1.5°C. An IPCC Special Report on the impacts of global warming of 1.5°C above pre-industrial levels and related global greenhouse gas emission pathways, in the context of strengthening the global response to the threat of climate change," *Ipcc - Sr15*, 32 pp. 2018. [Online]. Available: http://www.ipcc.ch/report/sr15/.

[3] I. E. Agency, "Technology Roadmap: Biofuels for Transport", 2011. DOI: 10.1787/9789264118461-en. [Online]. Available: https://www.oecd-ilibrary.org/energy/technology-roadmap-biofuels-for-transport_9789264118461-en.

[4] Z. Szabó, "Reviewing the GHG savings of Ethanol", 2014. [Online]. Available: http://www.eerl.com/Uploads/Reviewing-the-GHG-savings-of-Ethanol-Nov-2014.pdf.

[5] T. Searchinger, R. Heimlich, R. A. Houghton, F. Dong, A. Elobeid, J. Fabiosa, S. Tokgoz, D. Hayes, and T.-H. Yu, "Use of U.S. Croplands for Biofuels Increases Greenhouse Gases Through Emissions from Land-Use Change", *Science*, vol. 319, no. 5867, Feb. 2008. DOI: 10.1126/science.1151861. [Online]. Available: http://science.sciencemag.org/content/319/5867/1238.abstract.

[6] W. Brussels, S. Francisco, and C. Malins, "Modelling of Indirect Land Use Change", pp. 1–14, 2011.

[7] S. Ahlgren and L. Di Lucia, "Indirect land use changes of biofuel production – a review of modelling efforts and policy developments in the European Union", *Biotechnology for Biofuels*, vol. 7, no. 1, p. 35, 2014, ISSN: 1754-6834. DOI: 10.1186/1754-6834-7-35. [Online]. Available: http://biotechnologyforbiofuels.biomedcentral.com/articles/10.1186/1754-6834-7-35.

[8] P. Basu, *Biomass Gasification and Pyrolysis - Practical Design and Theory*. Elsevier, 2010, ISBN: 9780123749888.

[9] H. Hofbauer, R. Rauch, and G. Veronik T Fleck, "Gasification of Organic material in a novel fluidized bed reactor", *1997*, 2554.

[10] H. Thunman, M. Seemann, T. Berdugo Vilches, J. Maric, D. Pallares, H. Ström, G. Berndes, P. Knutsson, A. Larsson, C. Breitholtz, and O. Santos, "Advanced biofuel production via gasification – lessons learned from 200 man-years of research activity with Chalmers' research gasifier and the GoBiGas demonstration plant", *Energy Science and Engineering*, vol. 6, no. 1, pp. 6–34, 2018, ISSN: 20500505. DOI: 10.1002/ese3.188.

[11] P. Moldenhauer, C. Linderholm, M. Rydén, and A. Lyngfelt, "Experimental investigation of chemical-looping combustion and chemical-looping gasification of biomass-based fuels using steel converter slag as oxygen carrier", in *Proceedings of the International Conference on Negative CO2 Emissions*, 2018, pp. 1–17.

[12] A. Lyngfelt and B. Leckner, "A 1000 MWth boiler for chemical-looping combustion of solid fuels – Discussion of design and costs", *Applied Energy*, vol. 157, pp. 475–487, 2015, ISSN: 03062619. DOI: 10.1016/j.apenergy.2015.04.057. [Online]. Available: http://dx.doi.org/10.1016/j.apenergy.2015.04.057.

[13] W. B. Association, "The Carbon Neutrality Of Biomass from Forests", no. November, 2012.

[14] World Bioenergy Association (WBA), "Global Biomass Potential Towards 2035", no. March, p. 6, 2016. [Online]. Available: http://www.worldbioenergy.org/sites/default/files/WBA%20Factsheet%20-%20Biomass%20potential_160303_Toprint.pdf.

[15] C. Wilen, M. Antero, and E. Kurkela, "Biomass feedstock analyses", Technical Research Centre of Finland, Espoo, Tech. Rep., 1996, 25p + app. 8p.

[16] F. Schipfer, R. Haas, I. Funcia, J. Gil, U. Bojner, J. Ströhle, F. Buschsieweke, W. Sarah, and C. Aichernig, "Deliverable D1.1: Analysis of Selected Feedstock", Chemical Looping Gasification for Sustainable Production of Biofuels, Tech. Rep. 817841, 2019, pp. 4056–4060.

[17] Elina Virtanen and S. Mannonen, "Forest of biofuels", *Biofuels International*, no. April, Apr. 2014.

[18] J. González-Montaña, A. Alonso Diez, M. Alonso de la Varga, and S. Avila Téllez, *Transportation sector energy consumption*. 2016, pp. 127–137. [Online]. Available: DOE/EIA-0484(2016).

[19] E. Johansson, T. Mattisson, A. Lyngfelt, and H. Thunman, "Combustion of Syngas and Natural Gas in a 300 W Chemical-Looping Combustor", *Chemical Engineering Research and Design*, vol. 84, no. 9, pp. 819–827, Sep. 2006, ISSN: 0263-8762. DOI: 10.1205/CHERD05024. [Online]. Available: https://www.sciencedirect.com/science/article/pii/S0263876206729628.

[20] M. Källén, M. Rydén, A. Lyngfelt, and T. Mattisson, "Chemical-looping combustion using combined iron/manganese/silicon oxygen carriers", *Applied Energy*, vol. 157, pp. 330–337, Nov. 2015, ISSN: 0306-2619. DOI: 10.1016/J.APENERGY.2015.03.136. [Online]. Available: https://www.sciencedirect.com/science/article/pii/S0306261915004389.

[21] C. L. Williams, T. L. Westover, R. M. Emerson, J. S. Tumuluru, and C. Li, "Sources of Biomass Feedstock Variability and the Potential Impact on Biofuels Production", *Bioenergy Research*, vol. 9, no. 1, pp. 1–14, 2016, ISSN: 19391242. DOI: 10.1007/s12155-015-9694-y.

[22] J. Isaksson, A. Åsblad, and T. Berntsson, "Pretreatment methods for gasification of biomass and Fischer-Tropsch crude production integrated with a pulp and paper mill", *Clean Technologies and Environmental Policy*, vol. 16, no. 7, pp. 1393–1402, 2014, ISSN: 16189558. DOI: 10.1007/s10098-014-0815-7.

[23] A. Alamia, S. Òsk Gardarsdòttir, A. Larsson, F. Normann, and H. Thunman, "Efficiency Comparison of Large-Scale Standalone, Centralized, and Distributed Thermochemical Biorefineries", *Energy Technology*, vol. 5, no. 8, pp. 1435–1448, 2017, ISSN: 21944296. DOI: 10.1002/ente.201600719.

[24] X. Zhao, H. Zhou, V. S. Sikarwar, M. Zhao, A. H. A. Park, P. S. Fennell, L. Shen, and L. S. Fan, "Biomass-based chemical looping technologies: The good, the bad and the future", *Energy and Environmental Science*, vol. 10, no. 9, pp. 1885–1910, 2017, ISSN: 17545706. DOI: 10.1039/c6ee03718f.

[25] J. Adánez, A. Abad, T. Mendiara, P. Gayán, L. F. de Diego, and F. García-Labiano, *Chemical looping combustion of solid fuels*. Elsevier, 2018, vol. 65, pp. 6–66, ISBN: 9780857092434. DOI: 10.1016/j.pecs.2017.07.005. [Online]. Available: http://dx.doi.org/10.1016/B978-0-85709-243-4.00014-8.

[26] H. Leion, T. Mattisson, and A. Lyngfelt, "Solid fuels in chemical-looping combustion", *International Journal of Greenhouse Gas Control*, vol. 2, no. 2, pp. 180–193, 2008, ISSN: 17505836. DOI: 10.1016/S1750-5836(07)00117-X.

[27] A. Lyngfelt, P. Markström, and C. Linderholm, "Chemical-Looping Combustion of Solid Fuels — Operational Experiences in 100 kW Dual Circulating Fluidized Bed System", *Energy Procedia*, vol. 37, pp. 608–617, Jan. 2013, ISSN: 1876-6102. DOI: 10.1016/J.EGYPRO.2013.05.148. [Online]. Available: https://www.sciencedirect.com/science/article/pii/S1876610213001586.

[28] T. Berdugo Vilches and H. Thunman, "Impact of oxygen transport on char conversion in dual fluidized bed systems", *Nordic flame days*, 2015.

[29] T. Mattisson, A. Lyngfelt, and H. Leion, "Chemical-looping with oxygen uncoupling for combustion of solid fuels", *International Journal of Greenhouse Gas Control*, vol. 3, no. 1, pp. 11–19, 2009, ISSN: 17505836. DOI: 10.1016/j.ijggc.2008.06.002.

[30] S. Pissot, T. B. Vilches, J. Maric, and M. Seemann, "Chemical looping gasification in a 2-4 MWth dual fluidized bed gasifier", in *23rd International Conference on Fluidized Bed Conversion*, 2018.

[31] J. Gil, J. Corella, M. P. Aznar, and M. A. Caballero, "Biomass gasification in atmospheric and bubbling fluidized bed: Effect of the type of gasifying agent on the product distribution", *Biomass and Bioenergy*, vol. 17, no. 5, pp. 389–403, 1999, ISSN: 09619534. DOI: 10.1016/S0961-9534(99)00055-0.

[32] H. Ge, W. Guo, L. Shen, T. Song, and J. Xiao, "Biomass gasification using chemical looping in a 25kWth reactor with natural hematite as oxygen carrier", *Chemical Engineering Journal*, vol. 286, pp. 174–183, 2016, ISSN: 13858947. DOI: 10.1016/j.cej.2015.10.092.

[33] J. Zeng, R. Xiao, D. Zeng, Y. Zhao, H. Zhang, and D. Shen, "High H2/CO Ratio Syngas Production from Chemical Looping Gasification of Sawdust in a Dual Fluidized Bed Gasifier", *Energy and Fuels*, vol. 30, no. 3, pp. 1764–1770, 2016, ISSN: 15205029. DOI: 10.1021/acs.energyfuels.5b02204.

[34] S. Huseyin, G.-q. Wei, H.-b. Li, F. He, and Z. Huang, "Chemical-looping gasification of biomass in a 10 kWth interconnected fluidized bed reactor using Fe2O3/Al2O3 oxygen carrier", *Journal of Fuel Chemistry and Technology*, vol. 42, no. 8, pp. 922–931, 2014, ISSN: 18725813. DOI: 10.1016/S1872-5813(14)60039-6. [Online]. Available: https://linkinghub.elsevier.com/retrieve/pii/S1872581314600396.

[35] M. Schmitz and C. Linderholm, "Chemical looping combustion of biomass in 10- and 100-kW pilots - Analysis of conversion and lifetime using a sintered manganese ore", *Fuel*, vol. 231, no. May, pp. 73–84, 2018, ISSN: 00162361. DOI: 10.1016/j.fuel.2018.05.071. [Online]. Available: https://doi.org/10.1016/j.fuel.2018.05.071.

[36] E. Jerndal, T. Mattisson, A. Lyngfelt, C.-l. Combustion, and O. After, "Thermal analysis of chemical-looping combustion", no. September, 2006.

[37] M. Rydén, M. Hanning, and F. Lind, "Oxygen Carrier Aided Combustion (OCAC) of Wood Chips in a 12 MWth Circulating Fluidized Bed Boiler Using Steel Converter Slag as Bed Material", *Applied Sciences*, vol. 8, no. 12, p. 2657, 2018. DOI: 10.3390/app8122657.

[38] F. Eliason, *Ash interactions with oxygen carriers Glödskal and LD-slag in biomass-CLC, Master's Thesis*. 2018.

[39] J. Lee, Y. Kim, W. Lee, and S. Kim, "Coal-gasification kinetics derived from pyrolysis in a fluidized-bed reactor", *Energy*, vol. 23, no. 6, pp. 475–488, Jun. 1998, ISSN: 03605442. DOI: 10.1016/S0360-5442(98)00011-5.

[40] Z. Huang, Y. Zhang, J. Fu, L. Yu, M. Chen, S. Liu, F. He, D. Chen, G. Wei, K. Zhao, A. Zheng, Z. Zhao, and H. Li, "Chemical looping gasification of biomass char using iron ore as an oxygen carrier", *International Journal of Hydrogen Energy*, vol. 41, no. 40, pp. 17 871–17 883, 2016, ISSN: 03603199. DOI: 10.1016/j.ijhydene.2016.07.089. [Online]. Available: http://dx.doi.org/10.1016/j.ijhydene.2016.07.089.

[41] N. Gao, A. Li, and C. Quan, "A novel reforming method for hydrogen production from biomass steam gasification", *Bioresource Technology*, vol. 100, no. 18, pp. 4271–4277, 2009, ISSN: 09608524. DOI: 10.1016/j.biortech.2009.03.045. [Online]. Available: http://dx.doi.org/10.1016/j.biortech.2009.03.045.

[42] H. Tian, R. Siriwardane, T. Simonyi, and J. Poston, "Natural ores as oxygen carriers in chemical looping combustion", *Energy and Fuels*, vol. 27, no. 8, pp. 4108–4118, 2013, ISSN: 08870624. DOI: 10.1021/ef301486n.

[43] M. Keller, H. Leion, and T. Mattisson, "Mechanisms of Solid Fuel Conversion by Chemical-Looping Combustion (CLC) using Manganese Ore: Catalytic Gasification by Potassium Compounds", *Energy Technology*, vol. 1, no. 4, pp. 273–282, 2013, ISSN: 21944296. DOI: 10.1002/ente.201200052.

[44] D. Chiche, C. Diverchy, A. Lucquin, F. Porcheron, F. Defoort, D. Chiche, C. Diverchy, A. Lucquin, F. Porcheron, F. D. Synthesis, and G. Purification, "Synthesis Gas Purification", *Oil & Gas Science and Technology*, vol. Revue d'IF, no. 68 (4), pp. 707–723, 2013.

[45] P. J. Woolcock and R. C. Brown, "A review of cleaning technologies for biomass-derived syngas", *Biomass and Bioenergy*, vol. 52, pp. 54–84, 2013, ISSN: 09619534. DOI: 10.1016/j.biombioe.2013.02.036. [Online]. Available: http://dx.doi.org/10.1016/j.biombioe.2013.02.036.

[46] N. Abdoulmoumine, S. Adhikari, A. Kulkarni, and S. Chattanathan, "A review on biomass gasification syngas cleanup", *Applied Energy*, vol. 155, pp. 294–307, 2015, ISSN: 03062619. DOI: 10.1016/j.apenergy.2015.05.095. [Online]. Available: http://dx.doi.org/10.1016/j.apenergy.2015.05.095.

[47] M. Bolhàr-Nordenkampf, R. Rauch, K. Bosch, C. Aichernig, and H. Hofbauer, "Biomass CHP Plant Güssing – Using Gasification for Power Generation", *Proceeding of the 2nd Regional Conference on Energy Technology Towards a Clean Environment 12-14 February 2003, Phuket Thailand*, vol. 3, no. February, pp. 566–572, 2003.

[48] C. Burgt MVD; Higman, *Gasification, Elsevier Science & Technology*. Oxford., 2008.

[49] M. D. André Steynberg, *Fischer-Tropsch Technology, Volume 152*, M. D. André Steynberg, Ed. Elsevier, 2004, 2004, ISBN: 044451354X, 9780444513540.

[50] W. Torres, S. S. Pansare, and J. G. Goodwin, "Hot gas removal of tars, ammonia, and hydrogen sulfide from biomass gasification gas", *Catalysis Reviews - Science and Engineering*, vol. 49, no. 4, pp. 407–456, 2007, ISSN: 01614940. DOI: 10.1080/01614940701375134.

[51] B. S. Turk, T. Merkel, R. P. Gupta, J. W. Portzer, G. N. Krishnan, B. D. Freeman, and G. K. Fleming, "Novel Technologies for Gaseous Contaminants Control", *US department for energy*, no. September, 2001.

[52] C. Ratnasamy and J. Wagner, "Water gas shift catalysis", *Catalysis Reviews - Science and Engineering*, vol. 51, no. 3, pp. 325–440, 2009, ISSN: 01614940. DOI: 10.1080/01614940903048661.

[53] M. Pondini and M. Ebert, *Process synthesis and design of low temperature Fischer-Tropsch crude production from biomass derived syngas, Master's Thesis*. 2013.

[54] I. Aspen Technology, "ASPEN PLUS® User Guide. Cambridge, MA.", Tech. Rep., 2019.

[55] M. Arvidsson, M. Morandin, and S. Harvey, "Biomass gasification-based syngas production for a conventional oxo synthesis plant-process modeling, integration opportunities, and thermodynamic performance", *Energy and Fuels*, vol. 28, no. 6, pp. 4075–4087, 2014, ISSN: 15205029. DOI: 10.1021/ef500366p.

[56] W. Doherty, A. Reynolds, and D. Kennedy, "Aspen plus simulation of biomass gasification in a steam blown dual fluidised bed", *Materials and processes for energy: Communicating current research and technological developments*, pp. 212–220, 2013. [Online]. Available: http://www.formatex.info/energymaterialsbook/.

[57] B. M. Halvorsen, U. Adhikari, and M. S. Eikeland, "Gasification of Biomass for Production of Syngas for Biofuel", *Proceedings of the 56th Conference on Simulation and Modelling (SIMS 56), October, 7-9, 2015, Linköping University, Sweden*, vol. 119, pp. 255–260, 2015. DOI: 10.3384/ecp15119255.

[58] I. Aspen Technology, "Physical Property Methods and Models 11.1", in, 2011, pp. 1–19.

[59] C. Koroneos and S. Lykidou, "Equilibrium modeling for a d wndraft biomass gasifier for cotton stalks biomass in comparison with experimental data", vol. 2, no. April, pp. 61–68, 2011.

[60] S. Ferreira, E. Monteiro, P. Brito, and C. Vilarinho, "A Holistic Review on Biomass Gasification Modified Equilibrium Models", *Energies*, vol. 12, no. 1, p. 160, 2019. DOI: 10.3390/en12010160.

[61] Z. Huang, F. He, A. Zheng, K. Zhao, S. Chang, Z. Zhao, and H. Li, "Synthesis gas production from biomass gasification using steam coupling with natural hematite as oxygen carrier", *Energy*, vol. 53, pp. 244–251, 2013, ISSN: 03605442. DOI: 10.1016/j.energy.2013.02.068. [Online]. Available: http://dx.doi.org/10.1016/j.energy.2013.02.068.

[62] A. Larsson, M. Israelsson, F. Lind, M. Seemann, and H. Thunman, "Using ilmenite to reduce the tar yield in a dual fluidized bed gasification system", *Energy and Fuels*, vol. 28, no. 4, pp. 2632–2644, 2014, ISSN: 15205029. DOI: 10.1021/ef500132p.

[63] Z. Yu, Y. Yang, S. Yang, Q. Zhang, J. Zhao, Y. Fang, X. Hao, and G. Guan, "Iron-based oxygen carriers in chemical looping conversions: A review", *Carbon Resources Conversion*, vol. 2, no. 1, pp. 23–34, 2019, ISSN: 25889133. DOI: 10.1016/j.crcon.2018.11.004. [Online]. Available: https://doi.org/10.1016/j.crcon.2018.11.004.

[64] H. Chen, Z. Zheng, Z. Chen, and X. T. Bi, "Reduction of hematite (Fe2O3) to metallic iron (Fe) by CO in a micro fluidized bed reaction analyzer: A multistep kinetics study", *Powder Technology*, vol. 316, pp. 410–420, 2017, ISSN: 1873328X. DOI: 10.1016/j.powtec.2017.02.067. [Online]. Available: http://dx.doi.org/10.1016/j.powtec.2017.02.067.

[65] L. P. R. Pala, Q. Wang, G. Kolb, and V. Hessel, "Steam gasification of biomass with subsequent syngas adjustment using shift reaction for syngas production: An Aspen Plus model", *Renewable Energy*, vol. 101, pp. 484–492, 2017, ISSN: 18790682. DOI: 10.1016/j.renene.2016.08.069. [Online]. Available: http://dx.doi.org/10.1016/j.renene.2016.08.069.

[66] D. Fiaschi and L. Lombardi, "Integrated gasifier combined cycle plant with integrated Co2 - H2S removal: Performance analysis, life cycle assessment and exergetic life cycle assessment", *International Journal of Applied Thermodynamics*, vol. 5, no. 1, pp. 13–24, 2002, ISSN: 13019724. DOI: 10.5541/ijot.83.

[67] S. Heyne, "Process Integration Opportunities for Synthetic Natural Gas (SNG) Production by Thermal Gasification of Biomass", no. June, 2010. [Online]. Available: http://publications.lib.chalmers.se/cpl/record/index.xsql?pubid=124695.

[68] Y. Jiang and D. Bhattacharyya, "Plant-wide modeling of an indirect coal-biomass to liquids (CBTL) plant with CO2 capture and storage (CCS)", *International Journal of Greenhouse Gas Control*, vol. 31, pp. 1–15, 2014, ISSN: 17505836. DOI: 10.1016/j.ijggc.2014.09.022. [Online]. Available: http://dx.doi.org/10.1016/j.ijggc.2014.09.022.

[69] L. Waldheim and T. Nilsson, "Heating value of gases from biomass gasification", TPS Termiska Processer AB, Tech. Rep. May, 2001.

[70] I. Kemp, *Pinch Analysis and Process Integration: A User Guide on Process Integration for the Efficient Use of Energy*, 2nd Editio. Elsevier Science & Technology, 2007, ISBN: 9780750682602.

[71] R. Smith, *Chemical Process Design and Integration*, Second, 11. Chichester, West Sussex, United Kingdom John Wiley & Sons, Inc 2016, 2014, vol. 68, pp. 1267–1270, ISBN: 0471486809.

[72] M. Götz, W. Köppel, R. Reimert, and F. Graf, "Potential to optimize scrubbers for biogas cleaning part 2. Chemical scrubbers", *Chemie Ingenieur Technik*, vol. 84, no. 1-2, pp. 81–87, Jan. 2012, ISSN: 0009286X. DOI: 10.1002/cite.201100129. [Online]. Available: http://doi.wiley.com/10.1002/cite.201100129.

[73] J. J. C. Karine Ballerat-Busserolles Ying Wu, *Cutting-Edge Technology for Carbon Capture, Utilization, and Storage Advances in Natural Gas Engineering*. John Wiley & Sons, 2018, 2018, ISBN: 1119363764, 9781119363767.

[74] I. Hannula and E. Kurkela, "Liquid transportation fuels bed gasification of lignocellulosic biomass", Tech. Rep., 2013, p. 126. [Online]. Available: http://www.vtt.fi/publications/index.jsp?lang=en.

[75] A. Alamia, A. Larsson, C. Breitholtz, and H. Thunman, "Performance of large-scale biomass gasifiers in a biorefinery, a state-of-the-art reference", *International Journal of Energy Research*, vol. 41, no. 14, pp. 2001–2019, Nov. 2017, ISSN: 0363907X. DOI: 10.1002/er.3758. [Online]. Available: http://doi.wiley.com/10.1002/er.3758.

[76] H. Ljungstedt, K. Pettersson, and S. Harvey, "Evaluation of opportunities for heat integration of biomass-based Fischer-Tropsch crude production at Scandinavian kraft pulp and paper mill sites", *Energy*, vol. 62, pp. 349–361, 2013, ISSN: 03605442. DOI: 10.1016/j.energy.2013.09.048.

[77] Deliverable 4.9. European best practice guidelines for assessment of CO2 capture technologies., "Project acronym: CAESAR. Carbon-free Electricity by SEWGS: Advanced materials, Reactor-, and process design.", *FP7 – ENERGY.2007.5.1.1.*, no. Project no: 213206.

A

Aspen Plus Data

A.1 Stream Summaries & Block IDs

Table A.1: Stream data of MIXED substreams in the CLG submodel

Stream-ID	DEC-OUT	2NON-EQ	2SEP2	ELEM2	ELEM3	2FR-SEP	RAWGAS	AIR	2-ARSEP
From	DECOMP	SEP1	SG	SEP2	SEP3	FR-RGIBB	MIX3	*Input*	AR
To	SEP1	NS	SEP2	MIX1	SG	FR-SEP	CL1	H2	AR-SEP
Total Stream - Mass Flows	5.000	2.820	8.980	8.979	2.800	353.899	11.097	9.006	351.829
Substream	MIXED	MIXED	MIXED	MIXED	MIXED	MIXED	MIXED	MIXED	MIXED
T (°C)	25.00	25.00	935.00	935.00	25.00	935.38	935.38	25.00	985.01
Pressure (bar)	1	1	1	1	1	1	1	1	1
Mass Flow (kg/sec)	2.763	2.763	8.412	8.412	2.743	11.021	11.041	9.006	6.909
Mole Flow (kmol/sec)	0.22512	0.22512	0.52334	0.52334	0.22337	0.52864	0.52964	0.31218	0.24662
Mole Fractions									
H_2O	0.185	0.185	0.216	0.216	0.186	0.464	0.463	0.000	0.000
CO	0.000	0.000	0.123	0.123	0.000	0.112	0.111	0.000	0.000
H_2	0.571	0.571	0.420	0.420	0.571	0.198	0.198	0.000	0.000
CO_2	0.000	0.000	0.082	0.082	0.000	0.188	0.188	0.000	0.000
O_2	0.241	0.241	0.104	0.104	0.243	0.000	0.000	0.210	0.000
N_2	0.003	0.003	0.000	0.000	0.000	0.000	0.000	0.790	1.000
CH_4	0.000	0.000	0.054	0.054	0.000	0.038	0.037	0.000	0.000
S	0.000	0.000	0.000	0.000	0.000	0.000	0.000	0.000	0.000
C_2H_6	0.000	0.000	0.000	0.000	0.000	0.000	0.000	0.000	0.000
C_2H_4	0.000	0.000	0.000	0.000	0.000	0.000	0.000	0.000	0.000
C_3H_8	0.000	0.000	0.000	0.000	0.000	0.000	0.000	0.000	0.000
C_6H_6	0.000	0.000	1.64E-04	0.000	0.000	1.62E-04	1.62E-04	0.000	0.000
C_7H_8	0.000	0.000	5.61E-04	0.000	0.000	5.55E-04	5.54E-04	0.000	0.000
$C_{10}H_8$	0.000	0.000	9.96E-05	0.000	0.000	9.86E-05	9.84E-05	0.000	0.000
NH_3	0.000	0.000	0.000	0.000	0.000	0.000	1.37E-03	0.000	0.000
H_2S	0.000	0.000	0.000	0.000	0.000	0.000	5.00E-05	0.000	0.000

Table A.2: Stream data of CISOLID substreams in the CLG submodel

Stream-ID	DEC-OUT	2SG1	2SEP2	OC-FR-IN	2FR	2FR-SEP	OC-RED	2-ARSEP	OC-2FR
From	DECOMP	SEP1	SG	*Input*	MIX1	FR-RGIBB	FR-SEP	AR	AR-SEP
To	SEP1	SG	SEP2	MIX1	FR-RGIBB	FR-SEP	MIX2	AR-SEP	-
Total Stream - Mass Flows	5.000	2.180	8.980	344.920	353.899	353.899	342.822	351.829	344.920
Substream	CISOLID	CISOLID	CISOLID	CISOLID	CISOLID	CISOLID	CISOLID	CISOLID	CISOLID
T (°C)	25.000	25.000	935.000	985.000	982.536	935.376	935.376	985.009	985.009
Pressure (bar)	1	1	1	1	1	1	1	1	1
Mass Flow (kg/sec)	2.180	2.180	0.511	344.920	345.431	342.822	342.822	344.920	344.920
Mole Flow (kmol/sec)	0.182	0.182	0.043	5.030	5.072	4.905	4.905	5.030	5.030
Mole Fractions									
C	1.000	1.000	1.000	0.000	0.008	0.000	0.000	0.000	0.000
SiO_2	0.000	0.000	0.000	0.161	0.160	0.165	0.165	0.161	0.161
Al_2O_3	0.000	0.000	0.000	0.008	0.008	0.008	0.008	0.008	0.008
Fe_2O_3	0.000	0.000	0.000	0.124	0.123	0.051	0.051	0.124	0.124
Mn_3O_4	0.000	0.000	0.000	0.000	0.000	0.000	0.000	0.000	0.000
TiO_2	0.000	0.000	0.000	0.011	0.011	0.011	0.011	0.011	0.011
MgO	0.000	0.000	0.000	0.155	0.154	0.159	0.159	0.155	0.155
CaO	0.000	0.000	0.000	0.514	0.510	0.527	0.527	0.514	0.514
K_2O	0.000	0.000	0.000	0.001	0.001	0.001	0.001	0.001	0.001
Fe_3O_4	0.000	0.000	0.000	0.000	0.000	0.051	0.051	0.000	0.000
Mn_2O_3	0.000	0.000	0.000	0.000	0.000	0.000	0.000	0.000	0.000
MnO	0.000	0.000	0.000	0.000	0.000	0.001	0.001	0.000	0.000
MnO_2	0.000	0.000	0.000	0.026	0.026	0.025	0.025	0.026	0.026

Table A.3: Stream data of MIXED substreams in the SYN-CLN submodel

Stream-ID	RG1	RG5	RG6	RG7	RG8	RG9	RG10
From	*Input from CLG*	CL3	RME-SCRB	SCRB	SG-CMPR	S-ABS	S-REM
To	ASHSEP	RME-SCRB	SCRB	SG-CMPR	S-ABS	S-REM	*Input to FTS*
Total Stream - Mass Flows	11.097	11.041	10.999	6.768	6.589	3.860	3.860
Substream	MIXED	MIXED	MIXED	MIXED	MIXED	MIXED	MIXED
T (°C)	210.000	110.000	108.290	30.000	40.000	39.934	39.885
Pressure (bar)	1.000	1.258	1.013	1.013	30.000	29.800	29.600
Mass Flow (kg/sec)	11.041	11.041	10.999	6.768	6.589	3.860	3.860
Mole Flow (kmol/sec)	0.530	0.530	0.529	0.294	0.284	0.222	0.222
Mole Fractions							
H_2O	0.463	0.463	0.463	0.036	0.003	0.003	0.003
CO	0.111	0.111	0.112	0.201	0.208	0.266	0.266
H_2	0.198	0.198	0.198	0.356	0.368	0.471	0.471
CO_2	0.188	0.188	0.188	0.338	0.350	0.170	0.170
O_2	0.000	0.000	0.000	0.000	0.000	0.000	0.000
N_2	4.58E-04	4.58E-04	4.59E-04	8.25E-04	8.54E-04	0.000	0.000
CH_4	0.037	0.037	0.037	0.067	0.070	0.089	0.089
NH_3	1.37E-03	1.37E-03	1.38E-03	1.49E-03	1.06E-03	0.000	0.000
H_2S	5.00E-05	5.00E-05	5.01E-05	9.00E-05	9.31E-05	4.77E-06	0.000
C_6H_5OH	1.62E-04	1.62E-04	0.000	0.000	0.000	0.000	0.000
C_7H_8	5.54E-04	5.54E-04	0.000	0.000	0.000	0.000	0.000
$C_{10}H_8$	9.84E-05	9.84E-05	0.000	0.000	0.000	0.000	0.000

Table A.4: Stream data of MIXED substreams in the FTS submodel

Stream-ID	S100	W104	S302	REC100	REC121	W204	FTV200
From	*Input from SYN-CLN*	*Input*	Rectisol	*FT- Recycle Stream*	ATR	*Input*	OPSEP
To	WGS	WGS	FTREA	ATR	Rectisol	ATR	*Output*
Substream	MIXED	MIXED	MIXED	MIXED	MIXED	MIXED	MIXED
T (°C)	39.88	350	220	29.79	0.00	250	29.79
Pressure (bar)	29.6	20.0	20.0	19.0	29.995	38.0	19.0
Mass Flow (kg/sec)	3.86	0.085	3.086	1.72	1.20	0.431	0.187
Mole Flow (kmol/sec)	0.22	0.0047	0.276	0.133	0.097	0.0239	0.0147
Mole Fractions							
H_2O	0.0034	1	0.0022	0.0053	0.005	1	0.0053
CO	0.265	0.000	0.307	0.287	0.283	0.000	0.289
H_2	0.471	0.000	0.614	0.520	0.635	0.000	0.523
CO_2	0.170	0.000	0.0016	0.003	0.063	0.000	0.003
CH_4	0.089	0.000	0.0738	0.168	0.0117	0.000	0.169

Table A.5: Block IDs of unit operators in the SYN-CLN submodel

Block-ID	Description
ASHSEP	Separation of ash components (NC)
CL3	Gas cooled to 144°C to compensate for the heat of compression in CMPR
CMPR	P set to 1.2576 bar to compensate for the pressure loss in RME-SCRB
CL4	Gas cooled to 110°C
RME-SCRB	Tar scrubber; RME flow input = 2.4% of energy rate (HHV) of the product gas
SCRB	MDEA-Scurbber; Flash unit at 30°
SG-CMPR	Multi-stage compressor; Gas compressed to 30 bar in 3 stages
S-ABS	Amine scrubber; SF based on [66], [67]
S-REM	Guard-bed; SF of S components set to 1

The majority of the block IDs in FTS submodel are left unchanged from the original FTS model in [53] and block IDs of only important blocks and blocks added to the original model are listed below in Table A.6.

Table A.6: Block IDs of unit operators in the FTS sub-model

Block-ID	**Description**
B1[1]	Transfer block; Transfers stream data from SYN-CLN to FTS submodel
SNH1[1]	Heater; T= 350°C, P=20 bar
WGS	Water-gas shift reactor; Q=0MW, ΔP= -0.05 bar
CO2REMOV	Rectisol Unit ®
FTREA	FT-reactor; Reactions specified in Excel sheet
ATR	Autothermal Reformer; Q=0MW, ΔP= -0.005 bar

[1] *blocks added*

Table A.7: Block IDs of unit operators in the CLG sub-model

Block-ID	**Inputs**	**Description**
DECOMP	T=25°C; P=1bar	Decomposition of biomass into its constituent elements
SG	T=935°; P=1bar	Char-steam gasification based on reaction X; α=1.1(*assumed*)
SEP1	C (CISOLID; SF=1; *2SG1*)	Separation of C from H,N,S elements
SEP2	C (CISOLID; SF=0.001; *UNCONV*	SF set assuming no carbon leakage to the FR
SEP3	N and S components (MIXED; SF=1; *1*)	Char-steam gasification based on reaction X
NS	T=25°; P=1bar	Xco = 0.6 and Xco = 1 assumed for N & S components
FR-RGIBB	Q=0 MW; P=1 bar Non-reacting feed components (CH_4=0.7, FE_2O_3=0.4, $Mn0_2$=0.95, Tar components = 1)	Volatiles combustion; Inert spec. specified to attain expected OTC and avoid complete conversion of CH4 and Tar components
AR	Q=0 MW; P=1 bar	100% oxidation of reduced OC particles assumed
MIX1	-	OC stream & volatile gases from SG mixed prior to FR-RGIBB
MIX2	-	Reduced OC particles mixed with incoming air prior to AR
MIX3	-	N & S impurities mixed with raw syngas from FR-SEP
FR-SEP	(MIXED & NC; SF=1; *FRSEP-O*)	Solid-gas separation after the fuel reactor
AR-SEP	(MIXED; SF=1; *DEP-AIR1*)	Solid-gas separation after the air reactor
H1	Q=0 MW;P=0 bar	Dummy heater used only for modelling purposes
GASMIX	T=935 MW;P=0 bar	Gas impurities heated prior to mixing with raw syngas
H2	Q=0 MW;P=0 bar	Dummy heater used only for modelling purposes
HX1	T=500°C; P=0 bar	Steam heater
HX2	T=450°C; P=0 bar	Air pre-heater
CL	Q=0 MW;P=0 bar	Dummy cooler used only for modelling purposes
CL1	T=210°C; P=0 bar	Raw syngas cooling prior to syngas cleaning processes
CL2	T=50°C; P=0 bar	Depleted air from AR-SEP cooled down to 50°C

A.1.1 Block Diagrams

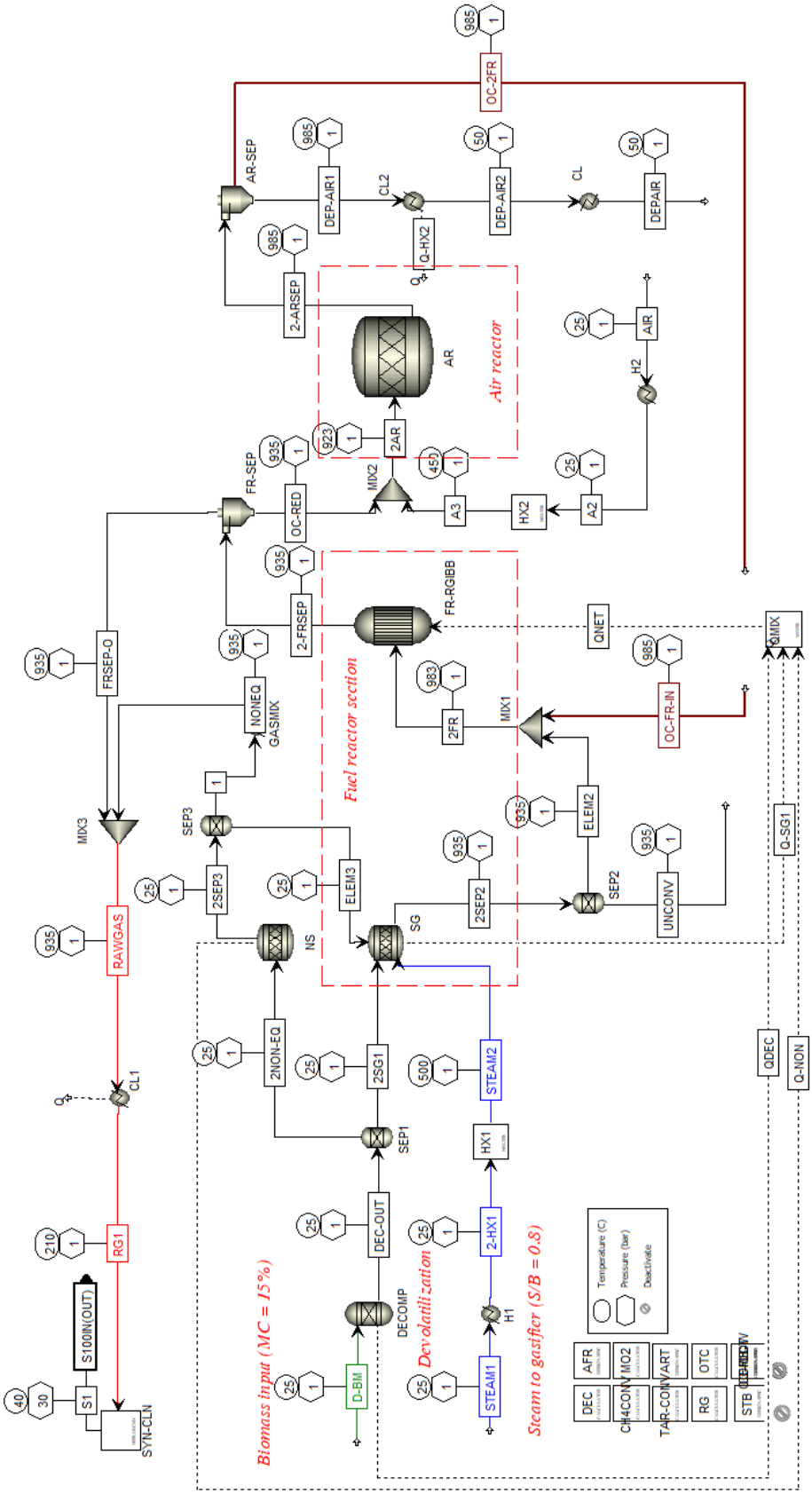

Figure A.1: Aspen Plus flowsheet diagram of the CLG submodel

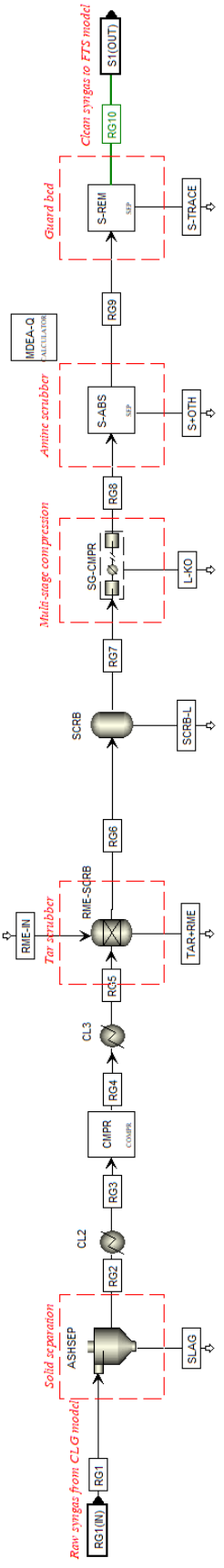

Figure A.2: Aspen Plus flowsheet diagram of the syngas cleaning model adapted from Arvidsson et al. [55]

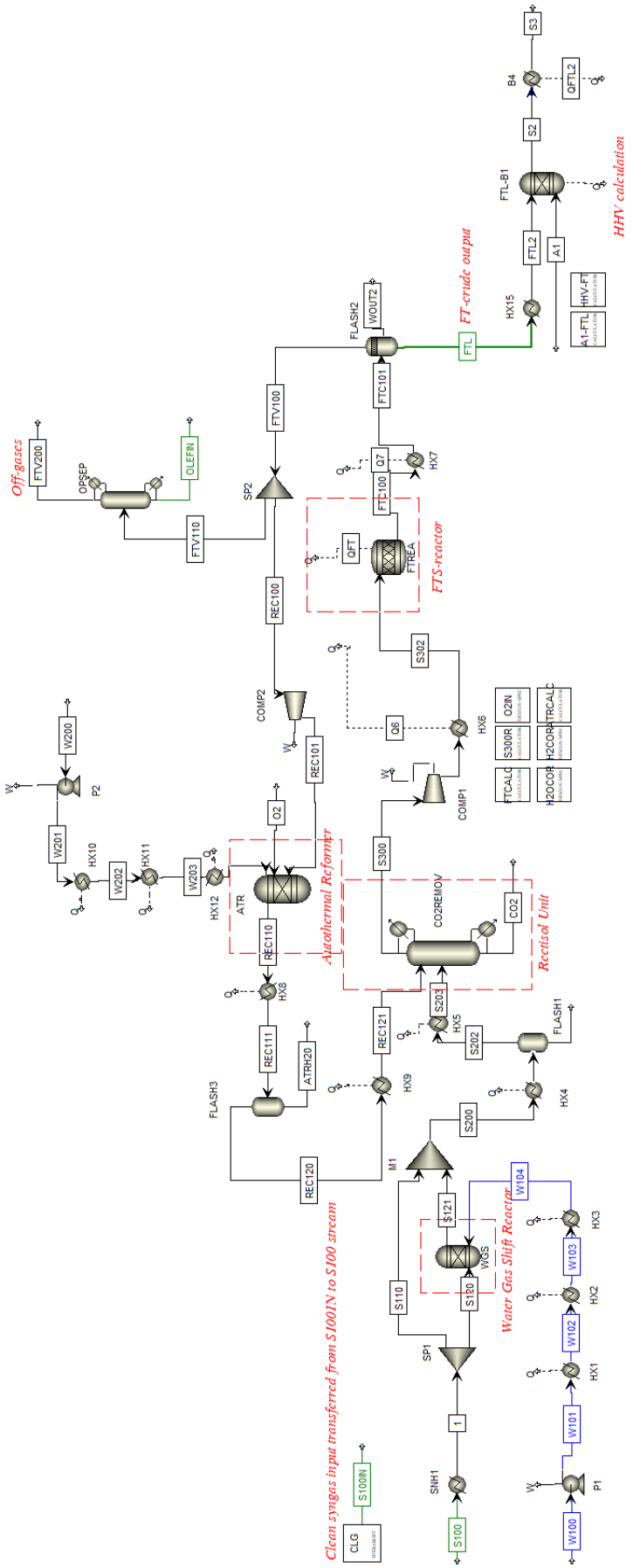

Figure A.3: Aspen Plus flowsheet of Fischer Tropsch Synthesis model adapted from [53]

A.2 Calculator blocks

A.2.1 Calculator blocks used in the CLG submodel

CALCULATOR: DEC

```
FACT = (100-WATER)/100
H2O = WATER/100
ASH = ULT (1)/100*FACT
C = ULT (2)/100*FACT
H2 = ULT (3)/100*FACT
C Chlorine excluded
N2 = ULT (4)/100*FACT
S = ULT (6)/100*FACT
O2 = ULT (7)/100*FACT
```

ULT and Water are the imported variables from the input stream DRY-BM. ULT imports ultimate analysis, biomass attributes. C, H_2, N_2, O_2, ASH are the exported variables, on mass-yield basis to the DECOMP block.

CALCULATOR: CH4CONV (Adapted from Arvidsson et al. [55])

```
C Manipulation of CH4-concentration in the product-/raw gas
C Set the desired dry product gas composition of CH4
C according to Figure in
C Hofbauer & Rauch (Vienna) - Stoichiometric water consumption of
C steam gasification by the FICFB-gasification process

MOLECOMP = 10

C MOLE FLOWS in kmol/hr
NCH4 = MOLECOMP*(MOLEFLOW - H2O)/100

C CONVERSIONS (EXPORT)
C Reaction 2: C + 2H2 -> CH4
CONVCH4 = NCH4/CMOLE
```

MOLECOMP - mol. fraction of CH_4 expected in syngas obtained from FICFB gasifier is taken. CONVCH4 variable is exported to block SG. CMOLE is the incoming mole flow of C to the SG block.

CALCULATOR: TAR-CONV (Adapted from Arvidsson et al. [55])

```
C Calculation: CONVERSION C -> TAR
C Gas constant in kJ/kmol-K
R = 8.3145
C Molar weights in kg/kmol
```

MW1 = 94.11304
MW2 = 128.17352
MW3 = 92.14052
C MW4 = 28.05

C SET THE TAR FORMATION in g/Nm3 dry
TARN = 6.49

C 2-4 g/Nm3 for Vienna DFB
C 6.49 g/Nm3 Huang et al. for BGLO(CLG/STBR 0.85/T 800/DRY)
C 25 g/kg-daf tar including BTX- CLG experiments with LDS-60 with STBR 0.63, 400 kg/hr fuel

C Conversion factor (Nm3/kmol)
FACT = 22.6831092524056

C VOLUME FLOW in Nm3 wet/hr (vs Nm3 dry/hr)
VFLOW = MOLEFLOW*FACT
VDRY = (MOLEFLOW-H2OMOLE) *FACT

C TAR COMPOSITION
C Linearization f(T), Milne et al 1998
C Modeled as: Secondary: Phenol (C6H6O),
C Tertiary-alkyl: Naphthalene (C10H8), Tertiary-PNA: Toluene (C7H8)
COMPA = -0.0039*T + 3.872
COMPB = -1E-5*T + 0.2
COMPC = 0.0037*T - 2.7833
C Adjust to a total composition of 1
ADJ = ((COMPA + COMPB + COMPC)-1)/3
COMP1 = COMPA - ADJ
COMP2 = COMPB - ADJ
COMP3 = COMPC - ADJ

C INDIVIDUAL TAR FORMATION
C kg/Nm3 dry
TAR1 = COMP1*TARN/1000
TAR2 = COMP2*TARN/1000
TAR3 = COMP3*TARN/1000

C MOLE FLOWS in kmol/hr (kg/Nm3 dry * Nm3 dry/hr / kg/kmol)
NFLOW1 = TAR1*VDRY/MW1
NFLOW2 = TAR2*VDRY/MW2
NFLOW3 = TAR3*VDRY/MW3

C CONVERSIONS (EXPORT)
C Reaction 5: 6C +3H2 + 0.5O2 -> C6H6O

C Reaction 6: 10C + 4H2 -> C10H8
C Reaction 7: 7C + 4H2 -> C7H8
CONVTAR1 = 6*NFLOW1/CMOLE
CONVTAR2 = 10*NFLOW2/CMOLE
CONVTAR3 = 7*NFLOW3/CMOLE

Here, TARN is the expected value of tars, which is taken as 6.49 g/Nm3, taken from the test results done by Huang et al. [61]. MOLEFLOW is the overall mole flow rate of gases from the FR, similarly H2OMOLE is the mole flow rate of steam from FR. T is the temperature of the stream 2FR-SEP. CMOLE is the total mole flow rate of C into the block SG. CONVTAR1, CONVTAR2, CONVTAR3 – are the export variables that sets the fractional conversion of C in block SG. This block could be modified based on the expected tar yields from a CLG operation.

CALCULATOR: OTC

R_o = ((OCIN-OCOUT)/(OCIN))*100

Here, the R_o is calculated based on the varied inert specification, specified in Block 5, see Figure 4.1. OCIN and OCOUT are the imported mass flows of OC in stream OC-FR-IN & 2-FRSEP, respectively.

CALCULATOR: RG

YCO2=(CO2)/(CO+CO2+CH4+(2*C2H4)+(10*C10H8)+(7*C7H8)+(6*C6H6O))
YCO=(CO)/(CO+CO2+CH4+(2*C2H4)+(10*C10H8)+(7*C7H8)+(6*C6H6O))
YCH4=(CH4)/(CO+CO2+CH4+(2*C2H4)+(10*C10H8)+(7*C7H8)+(6*C6H6O))
YCTOT= (2*C2H4)+(10*C10H8)+(7*C7H8)+(6*C6H6O)
YCT= (YCTOT)/(CO+CO2+CH4+YCTOT)

Here, carbon fractions of gas species in the syngas is calculated.

A.2.2 Calculator blocks used in the SYN-CLN & FTS submodel

CALCULATOR: MDEA-Q
TOT = H2S + CO2
Q = 3.33*TOT

C Q in MW
C Specific heat demand for H2S and CO2 separation, 3.33 MJ/kg of H2S and CO2 absorbed (44th Reference in Maria's paper)

The calculator blocks used in the FTS model are adapted from [53] and modified for compatibility with the upstream CLG and SYN-CLN submodels.

CALCULATOR: ATRCALC

CC12CC = FTVTOT*(FTVCH4 + FTVC2H6*2 + FTVC3H8*3 + FTVC4H10*4)

CALCULATOR: HHV-FT

MW=(QFT1+QFT2)
HHVFTL=(MW/FTFLO)

CALCULATOR: S300R

RATIO=H2S300/COS300
R=(H2O+H2OIN)/(CO)

CALCULATOR: A1-FTL

Stoichiometric air required (Stream-*A1*) to combust the FT-crude obtained in the FTL stream; done to estimate higher heating value (HHV) of the product stream, calculated in Calculator block *HHV-FT*.

CALCULATOR: FTCALC

FTS reactions in the FT reactor is calculated in a separate Excel file in [53] and has been left unchanged here. See [53] for more details.

A.3 Design Specification Blocks

Table A.8: Design specification blocks used in the CLG submodel

Block-ID	**AFR**	**ART**	**STB**
Manipulated Stream	AIR	OC-FR-IN	STEAM1
Manipulated variable	MASS-FLOW	MASS-FLOW	MASS-FLOW
Specification	OXIN	ART	STB
Spec. target	T	985	0.8
Spec. tolerance	0.001	0.01	0.01
Lower Bound	0	200	0
Upper Bound	30	600	10
Fortran staments	T=(FE3O4/4)+(MNO/2)	-	STB = ST/FFUEL
Comments	Here FE304 and MNO2 are mole flows in stream OC-RED	ART - Stream temperature of stream OC-2FR	ST and FFUEL - mass flow streams STEAM1 and D-BM respectively

A.4 Heat Integration Data

Table A.9: Design specification blocks used in the FTS model adapted from [53]

Block-ID	**H2COR**	**H2OCOR**	**O2IN**
Manipulated stream/block	SP1	W100	O2
Manipulated variable	Split fraction	MOLE-FLOW	MOLE-FLOW
Specification	MFH2/MFCO	(H2OIN+H2OSYN)/COSYN	ATRTEMP
Spec. target	2	3	1273.15
Spec. tolerance	0.1	0.01	5
Lower Bound	0	0	0
Upper Bound	1	2	2
Comments	Split friction in SP1 varied to achieve H_2/CO ratio of 2 in S300	H_2O input to WGS reactor varied to achieve H_2O/CO ratio of 3	O_2 inlet to ATR controlled to achieve ATR reactor temp. 1000°C

Table A.10: Electricity demand in the integrated CLG-FT model

Sub-models	**Units**	**Electricity Demand (kW)**
Gas Cleaning	Compressor 1	1.22
	Multi-stage compressor	4323.00
	CO2 compression	982.52
FTS	Pump W100	0.19
	Comp1 (20 bar)	4.05
	CO2 compression	720.55
	Recycle compression	209.01
	Pump W200	1.85
Total Demand (kW)	w/o refrigeration	6242.4
Refrigeration	Rectisol cooling	6200
	Mcompr-cooling	4456.16
Total Demand (kW)	w/ refrigeration	16898.5

Name		Inlet T [C]	Outlet T [C]	MCp [kJ/C-h]	Enthalpy [MW]	Segm.	HTC [kJ/h-m2-C]	Flowrate [kg/s]	Effective Cp [kJ/kg-C]	DT Cont. [C]
Raw syngas cooling - 2		209.6	110.0	6.672e+004	1.845		116.62	11.04	1.679	Global
Raw syngas cooling -3		209.9	144.0	6.707e+004	1.228		91.01	11.04	1.688	Global
Raw syngas cooling -1		935.4	210.0	---	15.40		----	11.04	----	Global
S301_To_S302		0.2	220.0	3.013e+004	1.840		412.54	3.086	2.713	Global
Steam to WGS reactor		25.0	350.0	---	0.2715		----	8.550e-002	----	Global
Steam to ATR		25.1	250.0	---	1.254		----	0.4310	----	Global
Depleted air cooling		985.0	50.0	---	7.240		----	6.909	----	Global
Clean syngas cooling prior to		49.1	0.0	---	0.4178		----	3.915	----	Global
Recycle stream cooling prior		53.7	0.0	---	0.1803		----	1.196	----	Global
ATR outlet cooling		999.3	50.0	---	8.543		----	2.612	----	Global
Air preheating		25.0	450.0	3.381e+004	3.992		24.16	9.006	1.043	Global
Clean syngas preheating pric		39.9	350.0	---	2.337		----	3.860	----	Global
FTC100_To_FTC101		220.0	30.0	---	3.317		----	3.086	----	Global
S200_To_S201		344.5	50.0	---	2.327		----	3.945	----	Global
Steam to Gasifier		25.0	500.0	---	13.92		----	4.000	----	Global
FT reactor cooling		220.0	219.5	5.064e+007	7.034		720.00	----	----	Global
CLG.SYN-CLN.SCRB_heat		108.3	30.0	5.547e+005	12.06		720.00	----	----	Global
Scrubber		119.9	120.0	3.226e+008	8.962		720.00	----	----	Global
Rectisol		178.9	179.0	1.139e+004	3.164e-004		720.00	----	----	Global

Figure A.4: Stream summary of process streams considered for heat integration